Design, Analysis and Testing of a Glazing Façade with Energy Dissipation Devices

José Augusto Carneiro Machado

Dissertation to obtain the Master of Science Degree in

Military Engineering

Supervisors: Prof. José Joaquim Costa Branco de Oliveira Pedro

Lt. Col. Eng. Pedro José da Silva Gonçalves Matias

Examination Committee

Chair Person: Prof. Mário Manuel Paisana dos Santos Lopes

Supervisor: Lt. Col. Eng. Pedro José da Silva Gonçalves Matias

Committee Member: Prof. Luís Manuel Coelho Guerreiro

Committee Member: Lt. Col. Eng. João Carlos Martins Rei

October 2022

“Strive for perfection in everything you do.
Take the best that exists and make it better.
When it does not exist, design it.”
Sir Henry Royce

Declaration

I declare that this document is an original work of my own authorship and that it fulfills all the requirements of the Code of Conduct and Good Practices of the University of Lisbon.

Acknowledgements

This MSc Dissertation could not be finished if it weren't for the tremendous support received by so many people.

To my girlfriend, Beatriz, for being there for me in times of need, and giving the motivation necessary to continue thriving. For keeping me focused and helping me improve and achieve the best work possible.

To my family, for the unbelievable support at all times, during this hard period and for pushing me for achieving and striving for perfection, my father, my mother and my sister, always keeping me focused and helping wherever it was necessary.

To my supervisor Professor José Oliveira Pedro, for the knowledge transmitted, the time spent on improvement of this work and the example of being a true professional in the engineering field. To my second supervisor Lt Col Eng Pedro Gonçalves Matias, for making possible the realization of the field experiments, for helping me when I needed the most, and for teaching me how to be resilient during all the period of the MSc Dissertation. Both supervisors were an excellent example of hard work professionals in their field.

To Maj Mat Luís Pratas Quinto for teaching me everything there is to know about 3D printing, and for helping print all the samples needed for the field experiments.

To Professor Hugo Bento Rebelo for helping me understand LS-Dyna, and helping me make the FE models even better.

To Chief Sargent Coelho for making possible to work with LS-Dyna trough the license activation as well as the ability to solve all the problems related to it.

To Cap Eng João Conceição, Lt Eng Luís Pires and Lt Eng Fátima Martins for helping begin this work, and the tutorials in LS-Dyna, as well as teach me how the work should be done, in time to finish it properly.

To my friend and partner in this MSc Dissertation, Tiago Oliveira, for being there in the fight every day, to help conclude this work.

To all my fellow engineers of the FOXTROT for helping with procrastination, and for helping making the time better, and to balance the hard every day work with some laughs.

To my friend from IST, Diogo Rebelo, for being present when the time required and for giving me support for finishing this MSc Dissertation.

To CORIFA, for making possible the experimental field tests, and for assembling and building the structure.

To all the team in CCPI, to Cap Eng Matos, to First Sargent Eng Silva, to First Corporal Dinis and to all the present team making possible also the experimental field tests.

To all the people mentioned above, as well the people that weren't mentioned by mistake, this MSc Dissertation was only possible to realize, because of the contribution of each one.

Thank you all!

Abstract

The primary objective of this MSc dissertation, which is part of ProFESEx (Protection Glass Façades Against Blast Loads), is to create a solution for a glass facade using 3D printable materials with an auxetic geometry and laminated glass made of two plies of blast-resistant tempered glass. The use of a dissipation system aims to reduce glass damage, improve its behavior, and increase its resistance to blast loads.

In comparison to a monolithic glass pane, which is to blame for the majority of victims inside a building when an explosion occurs due to the projection of the glass fragments, the damage to people can be lessened when a blast load is applied to laminated glass.

As a result of the complexity of its properties, laminated glass is a challenging material to model using the finite element method (FEM). To compare the FE solution and to better understand the behavior of a laminated glass with and without an energy dissipation system, it was searched to combine the FEM results with experimental field tests.

Although the field experiment results were insufficient to fully understand the behavior of the glass panel with the dissipation system under various blast loads, it was still concluded that the dissipation system affects the overall glass façade behavior under blast loads. When compared to the rigid support panel, the dissipation glass façade system is effective, but it is obviously in need of improvement if the glass panel is to benefit more from it.

Keywords: Blast Loads; Laminated Glass; Metamaterials; Energy Dissipation Device; Auxetic; LS-Dyna.

Resumo

A dissertação desenvolvida está incluída no projeto ProFESEx (Sistema de Proteção de Fachadas Envidraçadas Sujeitas a Explosões) em que o principal objetivo é desenvolver uma possível solução de fachada envidraçada utilizando metamateriais impressos em 3D com geometria auxética, e vidro laminado composto por duas lâminas de vidro temperado capazes de resistir a cargas explosivas. A utilização de um sistema de dissipação de energia proporcionará uma redução dos danos do vidro e melhorará o seu comportamento e resistência contra explosões.

Quando uma carga de explosiva é aplicada num vidro laminado, dependendo do tipo de vidro utilizado nas diferentes lâminas, os danos causados ao ser humano podem ser drasticamente reduzidos em comparação com um vidro monolítico que é responsável pela maioria das vítimas, devido à projeção dos fragmentos de vidro.

O vidro é um material difícil de modelar utilizando o método dos elementos finitos (MEF) devido ao facto das suas propriedades serem complexas de simular. Procurou-se combinar os resultados dos modelos de EF, para calibrar os modelos, e compreender o comportamento de um vidro laminado com e sem o sistema de dissipação de energia.

Concluiu-se que o sistema de dissipação funciona, embora os resultados obtidos nos ensaios de campo não sejam suficientes para compreender o comportamento completo do painel de vidro com o sistema de dissipação para diferentes cargas explosivas. O sistema de dissipação funciona devido à comparação com o painel de apoio rígido, mas necessita de melhorias para que o painel de vidro possa beneficiar mais da sua capacidade.

Palavras-Chave: Ação da Explosão; Vidro Laminado; Metamateriais; Dissipador de Energia; Auxético; LS-Dyna.

Contents

Declaration v

Acknowledgements vii

Abstract ix

Resumo x

Contents xii

List of Figures xvi

List of Tables xx

Abbreviations xxiii

Nomenclature xxiv

Chapter 1. Introduction 1

1.1. Proposed Problem and Motivation 1

1.2. Objectives and Methodology 3

1.3. Dissertation Outline 4

Chapter 2. Explosions and Blast Effects 5

2.1. Introduction 5

2.2. Definition 6

2.3. Classification 6

2.3.1. Origin of an explosion 6

2.3.2. Chemical Reaction 6

2.3.3. Confined and Unconfined Explosions 7

2.3.3.1. Confined Explosions 7

2.3.3.2. Unconfined Explosions 7

2.4. Shock Waves 8

2.4.1. TNT Equivalence Method 12

2.4.2. Scaled Distance 13

2.4.3. Peak Overpressure 13

2.4.4. Dynamic Pressure 13

2.4.5. Positive Phase Duration 14

2.4.6. Shock Wave Velocity 14

2.5. Shock Wave Reflection 15
2.5.1. Face-On Reflection 15
2.5.2. Regular Reflection 16
2.5.3. Mach Reflection 17
2.6. Structural Response to Blasting Loads 19
Chapter 3. Glazing Characterization 23
3.1. Glass Types and Fabrication 23
3.1.1. Annealed Glass 24
3.1.2. Heat Strengthened Glass 24
3.1.3. Tempered Glass 25
3.1.4. Laminated Glass 26
3.2. Laminated Glass Properties 26
3.2.1. Mechanical and Physical Properties 27
3.2.2. Thermal Properties 28
3.2.3. Interlayer 28
3.3. Fixing Systems 30
3.4. Energy-Dissipation Devices using Polymeric Materials 30
3.4.1. Characteristics 31
3.4.2. 3D Printing 31
3.4.3. Sample Printing 32
Chapter 4. Case Study Pre-Design 33
4.1. Case Study 33
4.2. Steel Structure Calculation 33
4.2.1. Elastic Bending Moment Resistance 33
4.2.2. Welding 37
4.2.3. Fixing Plates 38
4.2.4. Threaded Bolts 39
4.2.4.1 M24 Design Calculation 39
4.2.4.2. M12 Design Calculation 42
4.3. Glass Structure Calculation 42

4.3.1. Preliminary Design to Wind Resistance 43
4.3.1.1. Wind Pressure 43
4.3.1.2. Glazing Design 45
4.3.2. Preliminary Design to Blast Resistance 48
Chapter 5. Numerical Data Analysis 51
5.1. LS-Dyna Software Introduction 51
5.2. Modeling Base Characteristics 51
5.2.1. Generic Mesh Specifications 51
5.3. Energy Dissipation Device 51
5.3.1. Materials used and Mesh Specification 52
5.3.2. Replication Model 52
5.3.3. Static Load Experiment 54
5.3.4. Extrapolation to a Different Size Dissipator 55
5.3.5. Dynamic Response of the Dissipator to Blast Load Effects (Impulse Loading) 56
5.4. Obtained Results of the Glass Model 58
5.4.1. Materials Used and Mesh Specifications 58
5.4.2. Model Specifications 59
5.4.3. Comparison with Experimental tests described on “Hooper et al.” and “Zhang et. Al” 61
5.5. Experimental Set-Up Model 64
5.5.1. Materials Used and Mesh Specifications 65
5.5.2. Results and Dissipator Locations 66
Chapter 6. Experimental Tests 69
6.1. Experimental Set-Up 69
6.1.1. Sensor Settings 70
6.1.1.2. Reflected Pressure Sensors 70
6.1.1.3. Accelerometer 71
6.2. Measured Values 72
6.2.1. Incident and Reflect Pressure 72
6.2.2. Acceleration 74
6.3. Analysis of the Results 74

6.3.1. Glass Response Analysis with and without dissipation System 74
Chapter 7. Final Considerations 79
7.1. Main Conclusions 79
7.2. Further Work 80
References 81
Attachment A ..... A
Attachment B ..... B

List of Figures

Figure 1 - Beirut Explosion Damage (Source: [3]) 1
Figure 2 - Deaths caused by terrorism since 2007 (Source: [7]) 2
Figure 3 – Ten worst attacks committed by terrorists in 2021 (Adapted from [7]) 2
Figure 4 - Beirut victim due to glass laceration with limb amputation. Purposefully pixelized due to content in the image (Adapted from [8]) 3
Figure 5 - World Trade Center Lisbon Concept (Source: [9]) 3
Figure 6 - Oklahoma City explosion damage (Source: [17]) 5
Figure 7 - Confined Explosions (Adapted from [22]) 7
Figure 8 – Free air burst explosion (Adapted from [22]) 8
Figure 9 - Air burst with ground reflections (Adapted from [22]) 8
Figure 10 - Surface Burst (Adapted from [22]) 8
Figure 11 - Pressure variation of a blast load (Adapted from: [19]) 9
Figure 12 - Linear approximations of the pressure variation on time of a blast load (Adapted from: [19]) 10
Figure 13 - States for the passage of a shock wave (Adapted from [24]) 11
Figure 14 - Blast wave pressures in time (Adapted from [24]) 12
Figure 15 - Face-On Reflection (Adapted from [22]) 15
Figure 16 - Blast overpressure function for a face-on reflection (Adapted from [22]) 15
Figure 17 - Regular reflection of a blast wave (Adapted from [22]) 17
Figure 18 – Reflection coefficient variation with angle of incidence (Adapted from [23]) 18
Figure 19 - Mach Reflection (Adapted from [22]) 18
Figure 20 - Variation of the blast pressure with distance variation (Adapted from [21]) 19
Figure 21 - Shock wave interaction with a building (Adapted from [21]) 19
Figure 22 - Blast overpressure function acting on the front face of a building (Adapted from [22]) 20
Figure 23 - Simplification of a blast wave overpressure profile (Adapted from [22]) 20
Figure 24 - Simplified profile of the overpressure in the front face of a building (Adapted from [22]) 21
Figure 25 - Pressure-Impulse diagram (Adapted from [28]) 22
Figure 26 - Fabrication of Glass (Adapted from [30]) 23
Figure 27 - Types of fracture in glass. On the left annealed glass, on the center heat strengthened glass and on the right tempered glass (Adapted from [30]) 23
Figure 28 - Fractured annealed glass (Adapted from [31]) 24
Figure 29 - Stress-Strain function for glass (Adapted from [31]) 24
Figure 30 - Tension distribution in glass during heat treatment (Adapted from [30]) 24
Figure 31 - Comparison between annealed and tempered glass (Adapted from [30]) 25
Figure 32 - Tempered glass fracture behavior (Adapted from [31]) 25

Figure 33 - Laminated Glass Fabrication (Adapted from [33]) 26
Figure 34 - Laminated Glass behavior to fracture (Adapted from [30]) 26
Figure 35 - Typical resistance of a 7.52 mm laminated glass with annealed glass plies submitted to a blast load (Adapted from [12]) 27
Figure 36 - Laminated glass behavior depending on load time duration (Adapted from [31]) .. 28
Figure 37 - Shear Relaxation of PVB (Adapted from [37]) 29
Figure 38 - Shear Modulus Variation with Temperature (Adapted from [38]) 29
Figure 39 - Fixing Systems (Adapted from [39]) 30
Figure 40 – Energy Dissipator Geometry (Left), Auxetic Geometry Cell (Right) 30
Figure 41 – 3D Printing principles (Source: [42]) 31
Figure 42 – Original Prusa i3 MK3S printing two samples 32
Figure 43 – Experimental set-up 33
Figure 44 – SDOF approach (Adapted from [47]) 34
Figure 45 - Maximum deflection of elasto-plastic SDOF system to an impulse loading (Adapted from [23]) 35
Figure 46 - Interception of the calculation with the graphical solution 36
Figure 47 - Steel Structure 37
Figure 48 - Welding zones for Supporting Glass 38
Figure 49 – M12 Threaded bolts considered to be submitted to tension causing punching shear effects in the fixing plate 38
Figure 50 - M12 Threaded Bolts Supporting the Glass Panel 39
Figure 51 - Threaded Bolts Connecting the Wall and the Steel Structure 40
Figure 52 - Considered Influence Area for Calculation of M24 Threaded Bolts 41
Figure 53 - Considered Building for Glazing Design 42
Figure 54 - Wind Pressure variation with height (Adapted from [50]) 44
Figure 55 - Zone to take into consideration and Panel location (Adapted from [50]) 44
Figure 56 - Simple Supported Slab Values (Source: [52]) 47
Figure 57 - Pressure-Duration Line for a 19.05 mm thickness tempered glass with 1.07x2.14 m^2 (Adapted from [23]) 49
Figure 58 - Coutinho Model (Left) (Source: [14]), FE Model made (Middle), FE Model Made from perspective (Right) 53
Figure 59 - Displacement of 1st Series Experiments and FE Model comparison 53
Figure 60 - Force for 1st Series Experiments and FE Model Comparison 54
Figure 61 - FE Model of the Static Experiment 54
Figure 62 - Force - Displacement Comparison Graph 55
Figure 63 - Cellular organization difference between FE Model and Experiment 55
Figure 64 - FE Model of the dissipator (Left), Dissipator Glued to the Structure (Middle), Complete System of the structure (Right) 56
Figure 65 - Dynamic Response of the Energy Dissipation Device 57
Figure 66 – Stress-Strain equation obtained 57

Figure 67 - FE Model of Laminated Glass 59
Figure 68 - Overpressure differences between LBE and measurement of a real blast wave (adapted from [56]) 61
Figure 69 - Laminated Glass simplification and integration points location 61
Figure 70 - AutoCAD design of the System 64
Figure 71 - FE Model in comparison with the experimental Set-Up 64
Figure 72 - Free Displacement of the glass panel in the threaded bolt 65
Figure 73 - Final dissipator configuration after the analysis and the identification of the best performing dissipators 67
Figure 74 – SPOTWELD beams displacement measured 67
Figure 75 – SPOTWELD beams axial force measured 67
Figure 76 - Glass broken after a charge of 5kg@7m 68
Figure 77 - Front glass plie (Left) failing at 4.42 ms before the rear plie (Right) failure 68
Figure 78 - Accelerometer glued to the glass 69
Figure 79 - Computer used for data gathering and analysis 69
Figure 80 - Explosive Charge (5 kg of TNT) (Left), Blasting Machine (Middle), Detonator (Marked in red) (right) 69
Figure 81 - Incident Pressure Sensor (Blue) and Explosive Charge (Red) 70
Figure 82 - Reflected Pressure Sensor 71
Figure 83 - Reflected pressure Sensors Location (Red) (Not visible due to sensor size) 71
Figure 84 - Accelerometer location 72
Figure 85 - Experimental data and Friedlander equation for 5kg@9m 73
Figure 86 - Projectile impact on the glass with a charge of 5kg@9m 75
Figure 87 - Dissipator after charge of 5kg@9m (Red) and front glass plie broken (Green) 75
Figure 88 - Geotextile solution to prevent impacts on glass 75
Figure 89 - Glass rupture pattern comparison, on the left failure due to impact, on the right failure due to shock wave damage 75
Figure 90 - Dissipator response to charge of 5kg@7m 76
Figure 91 - Glass displacement (Left), Punctual damage of the top dissipators (Middle), Glass displacement and no damage on the side dissipators (Right), Charge: 5kg@5m 76
Figure 92 - Dissipator response to a charge of 5kg@6m 76
Figure 93 - Acceleration measurement differences 77

List of Tables

Table 1 - Equivalent Mass of TNT for different explosives (Adapted from [13], [22], [23]) 12
Table 2 - Pressure and Dynamic Pressure Values (Adapted from [22]) 14
Table 3 - Peak Reflected Pressures for different load values (Adapted from [20]) 16
Table 4 - Load Regimes differences (Adapted from [28]) 22
Table 5 - Glass Properties (Adapted from [31]) 28
Table 6 - Glass Thermal Properties (Adapted from [32]) 28
Table 7 - PVB Properties (Adapted from [31], [32]) 29
Table 8 – Printing Parameters 32
Table 9 – SHS 200x200x8 Parameters 33
Table 10 – Parameters for a simple supported beam submitted to a dynamic load (Adapted from [46], [47]) 34
Table 11 - Quantities in mass per meter of the steel structure 35
Table 12 - Peak Reflected Pressures for different explosions 36
Table 13 - F1 calculation for given Peak Reflected Pressures 36
Table 14 - Resistance of 100 mm welding (Adapted from [49]) 37
Table 15 - Minimum thickness of a plate for $B_{p,Rd} > F_{t,Rd}$ (Adapted from [49]) 39
Table 16 - Dynamic Increase Factors for Steel Structures (Adapted from [23]) 40
Table 17 - Parameters for a simple supported beam submitted to a dynamic load (Adapted from [46], [47]) 41
Table 18 - Wind multiplier coefficients (Adapted from [50]) 44
Table 19 - Values for k_{mod} according to an action (Adapted from [51]) 45
Table 20 - Values for k_{sp} (Adapted from [51]) 46
Table 21 - Values for $f_{b,k}$ (Adapted from [51]) 46
Table 22 - Values for k_v (Adapted from [51]) 46
Table 23 - Values for Ultimate Limit State resistance for glass (Adapted from [51]) 47
Table 24 - Pressure and Impulse values for different load combinations 48
Table 25 - Blast Resistance Response of UFC Tempered Glass 49
Table 26 - Values of charges the glass can withstand according to UFC [23] 50
Table 27 - MAT_003_PLASTIC_KINEMATIC Properties for Steel 52
Table 28 - Impulse Loads Applied 56
Table 29 - Values for DEFINE_CURVE 58
Table 30 – MAT_001_ELASTIC + ADD_MAT_EROSION Properties for Glass 60
Table 31 - MAT_098_SIMPLIFIED_JOHNSON_COOK Properties for PVB 60
Table 32 - Field Experiments Results from Hooper et al. [11] and Zhang et al. [12] 62
Table 33 - Overpressure values calculated by Kingery and Bulmash equations [45] 62
Table 34 - Values for transformation into an equivalent triangular load 63
Table 35 - Obtained Relative Error in the FE Model 63

Table 36 - MAT_100_SPOTWELD Properties for a M10 Threaded Bolt 65
Table 37 - MAT_100_SPOTWELD Properties for the Energy Dissipation Device 65
Table 38 - Comparison between FE Model and UFC [23] Values 66
Table 39 - Charges used and theoretical values used in the Field Experiment 70
Table 40 - ICP® Model 137B24B Pressure Sensor Measurement Values (Adapted from [67]) 70
Table 41 - ICP® Model 113B24 Pressure Sensor Measurement Values (Adapted from [68]) 70
Table 42 - ICP® Model 350D02 Shock Accelerometer Measurement Values (Adapted from [69]) 71
Table 43 - Values for Friedlander's fit equation 73
Table 44 - Pressure results and comparison 73
Table 45 - Impulse calculations and comparison 74
Table 46 - Acceleration measured results 74
Table 47 - Response Improvement Difference 78

Abbreviations

3D	3 Dimensions
AM	Addictive Manufacturing
ANFO	Ammonium Nitrate / Fuel Oil
ASCE	American Society of Civil Engineers
CCIP	Competence Center for Infrastructure Protection
CPU	Central Processing Unit
DIF	Dynamic Increase Factor
EN	European Norm
EVA	Ethylene Vinyl Acetate
FDM	Fused Deposition Modeling
FE	Finite Element
FEM	Finite Element Method
HST	Heat Soak Test
LBE	Load Blast Enhanced
LNS	Load Node Set
LOM	Laminated Objective Manufacturing
LSTC	Livermore Software Technology Corporation
MSc	Master of Science
NATO	North Atlantic Treaty Organization
PET	Polyethylene Terephthalate
PETG	Polyethylene Terephthalate modified with Glycol
prEN	Pre-European Norm
ProFESEx	Protection Glass Façades Against Blast Loads
PVB	Polyvinyl Butyral
SDOF	Single Degree of Freedom
SHS	Square Hollow Section
SLA	Stereolithography
SLS	Selective Laser Sintering
TNT	Trinitrotoluene
TPU	Thermoplastic polyurethane
UFC	Unified Facilities Criteria
ULS	Ultimate Limit State

Nomenclature

Latin Nomenclature

a	Welding diameter
A	Area
A_{proj}	Surface area taken into account
A_s	Tensile stress area of the bolt or of the anchor bolt
b	Decay rate of Friedlander's equation
$B_{p,Rd}$	Design punching shear resistance of the bolt head and the nut
c	Dynamic increase factor
c_0	Orography coefficient
c_{dir}	Direction coefficient
c_e	Exposure coefficient
c_{pe}	External pressure coefficient
c_r	Rugosity coefficient
c_{season}	Season coefficient
C_0	Sound speed on air
C_D	Drag coefficient
C_r	Reflection coefficient
d	Diameter
d_m	The mean of the across points and across flats dimensions of the bolt head or the nut, whichever is smaller
E	Young's modulus
$f_{b,k}$	Characteristic value of the bending strength of prestressed glass
f_{ds}	Dynamic yield strength
$f_{g,d}$	Allowable maximum stress for the surface of glass panes
$f_{g,k}$	Characteristic value of the bending strength of prestressed glass
f_t	Yield strength (PVB)
f_u	Ultimate yield strength
f_{ub}	Ultimate tensile strength for bolts
f_y	Yield strength
F_{blast}	Load caused by initial blast wave
$F_{dynamic}$	Load caused by the dynamic overpressures
$F_d(ELU)$	Ultimate limit state combination
F_{Ed}	Applied force
$F_E(t)$	Force applied in time
$F_{t,Rd}$	Design tension resistance per bolt
$F_{v,Rd}$	Design shear resistance per bolt
$F_{w,Rd}$	Welding Resistance to Shear

g	Gravitational acceleration
G	Distortion modulus
$G\ (PVB)$	Shear modulus
G	Permanent action
H_{EXP}^{d}	Heat of the Explosive in Study Detonation
H_{TNT}^{d}	Heat of the TNT Detonation
i_r	Specific reflected impulse
i_s	Positive specific impulse
i_s^-	Negative specific impulse
I	Inertia
$I_v(z)$	Wind turbulence intensity at height z
k	Spring constant
k_I	Turbulence factor
k_e	Spring stiffness
k_{mod}	Load duration factor
k_r	Roughness coefficient
k_{sp}	Factor for the glass surface profile
k_v	Factor for strengthening of prestressed glass
K_L	Load factor
K_M	Mass factor
l_w	Welding length
L	Length
m	Mass per meter
M	Mass
M_e	Body mass
$M_{Rd,El}$	Resistant elastic moment
N	Axial force
P_o	Atmospheric pressure
P_r	Peak reflected overpressure
P_s	Peak incident overpressure
P_{sf}	Overpressure Acting on the front face
P_{so}	Peak incident overpressure
q_b	Reference mean (basic) velocity pressure
$q_p(z)$	Peak velocity pressure
q_s	Peak dynamic Pressure
Q	Variable action
R	Distance between explosive charge and target
R_m	Maximum resistance to dynamic loading
R	Static reaction force

t	Time
$t_0{}^+$	Positive phase duration
$t_0{}^-$	Negative phase duration
t_a	Time of arrival
$t_{b,min}$	Minimum thickness of the steel plate
t_d	Equivalent time for triangular impulse simplification
t_p	Plate thickness
T	Period
T_n	Normal Period of a Structure
U	Sound speed in the reflected area
U_s	Shockwave velocity
v_b	Basic wind velocity
$v_{b,0}$	Fundamental value of the basic wind velocity
$v_m(z)$	Wind velocity at height z
V_{Ed}	Applied shear force
w_e	Wind pressure
W_{el}	Elastic section modulus
W_{EXP}	Weight of the Explosive in Study
W_{TNTe}	Equivalent TNT weight
$y(t)$	Displacement of the body in time
y_m	Maximum deflection
y_{el}	Elastic deflection
z	Height above ground
z_0	Roughness length
$z_{0.II}$	Roughness length for terrain category II
z_{max}	Maximum height
z_{min}	Minimum height
Z	Scaled distance

Greek Nomenclature

α	Thermal expansion coefficient
β_w	Correlation Factor between for steel grades
γ_G	Partial factor for permanent actions
γ_{M2}	Partial safety factor
$\gamma_{M,A}$	Material partial factor for annealed glass
$\gamma_{M,v}$	Material partial factor for surface prestress
γ_Q	Partial factor for variable actions
ΔT	Thermal shock resistance
ε	Strain

ε_t	Strain at Rupture
λ	Thermal conductivity
ν	Poisson's ratio
ρ	Mass density
σ	Stress
σ_v	Standard deviation of the turbulence
Ψ_0	Factor for combination value of a variable action

Chapter 1. Introduction

1.1. Proposed Problem and Motivation

Due to earlier explosions, such as the one in Beirut, Lebanon, infrastructure protection is crucial to ensuring that people are protected from the impacts of blasting. Witnesses report that following the explosion in Beirut, homes were destroyed 10 km away from the blast's epicenter, and seismic shock waves from the event traveled 160 km [1], [2].

Figure 1 - Beirut Explosion Damage (Source: [3])

Authorities in charge consider the explosion incident in Beirut to be a warning about the hazard in question and to emphasize the importance of exercising caution when handling and storing reactive materials as well as safeguarding existing infrastructures.

Sadly, explosions are not always accidental; periodically, terrorism is to blame. Following the French revolution in 1789, the term "terrorism" was first used in the globe in 1798 in France with the description "reign of terror" [4]. Due to its motivational intent or source - which may be political or even religious - terrorism can occasionally be difficult to understand, but the results are frequently the same. The true definition of terrorism is hard to find since it is volatile, as it can change trough time, the motivation, the objective and even the side effects of it can be different [4].

Terrorism has evolved since its appearance, being utilized as a weapon and a tool for hybrid war, the new concept of conflict, that North Atlantic Treaty Organization (NATO) is trying to fight. NATO's response to hybrid warfare is already on motion to fight this new spectrum of warfare that is difficult to respond to [5].

The ultimate aim of these terrorist acts is to create chaos by terrifying or killing the people. Due to the harm that may be done without a specialized individual being required to operate the explosive, as will be discussed later in this chapter [6], the idea of deploying terrorism as an operation enters the concept of hybrid war.

The terrorism evolution, in the last years is stabilizing, and the lethality of the attacks is also decreasing in developed countries. Africa is now becoming the center of terrorism, recording the highest values of terrorism since 2007 [7] (Figure 2). In Figure 3 shows the ten deadly events from terrorist action in 2021. Figure 3 shows that four out of ten deadliest attacks came from bombing, with one person, or needing only a small group of people, as in the other six, it can be concluded that it took groups of people to kill a huge number of civilians. It is possible to mention that the usage of explosions to produce a large number of casualties is a preferred method of terrorist organizations.

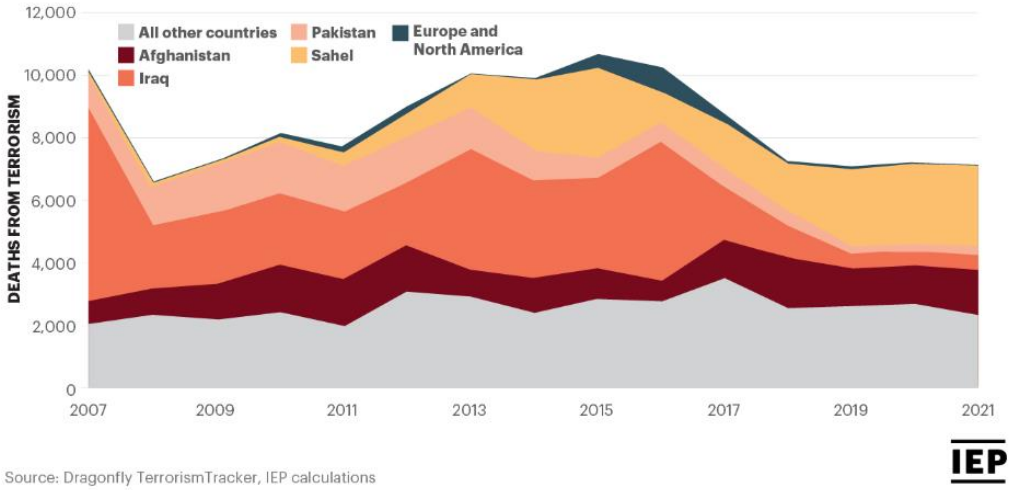

Figure 2 - Deaths caused by terrorism since 2007 (Source: [7])

							DESCRIPTION
1	COUNTRY	AFGHANISTAN	PROVINCE	KABUL	DEATHS	170	A suicide bomber killed at least 170 people and injured at least 200 others when he detonated his explosives at Kabul International Airport. The attack was followed by another suicide bomb nearby, with reports of gunfire. Islamic State - Khorasan Province claimed responsibility for the attack.
	DATE	26/8/21	GROUP	ISLAMIC STATE - KHORASAN PROVINCE			
2	COUNTRY	BURKINA FASO	PROVINCE	YAGHA	DEATHS	160	Gunmen killed at least 160 people and wounded at least 40 others in Solhan village in the Sahel region. The assailants first attacked members of a volunteer defence force militia before attacking civilians and burning down houses and a market. No group had claimed responsibility for the attack but jihadists operate in the area.
	DATE	5/6/21	GROUP	UNKNOWN			
3	COUNTRY	NIGER	REGION	TAHOUA	DEATHS	137	Gunmen killed 137 civilians in three coordinated attacks in the Tahoua region. Islamic State West in Africa (ISWA) claimed responsibility, saying they targeted pro-government militia members.
	DATE	21/3/21	GROUP	ISLAMIC STATE IN WEST AFRICA (ISWA)			
4	COUNTRY	AFGHANISTAN	PROVINCE	KANDAHAR	DEATHS	100	Gunmen killed at least 100 civilians they forced from their homes in Kandahar province. The Ministry of Interior Affairs said that at least another 200 people remained unaccounted for. The Ministry said the Taliban was responsible, although the group denied it had carried out the attack.
	DATE	22/7/21	GROUP	TALIBAN			
5	COUNTRY	AFGHANISTAN	PROVINCE	KABUL	DEATHS	86	A series of three bombs killed at least 86 civilians, most of them students, and wounded 150 others at a high school in Kabul province. A car bomb initially exploded, followed by two others of unspecified type that detonated as students fled outside. No group had claimed responsibility for the attack, but based on location and tactic jihadists were probably responsible. The Taliban issued a statement denying responsibility for the attack.
	DATE	8/5/21	GROUP	UNKNOWN			
6	COUNTRY	BURKINA FASO	REGION	SAHEL	DEATHS	80	Gunmen killed 59 civilians, 15 security forces personnel and six pro-government militiamen, and wounded 19 others, in an attack on a military convoy that was escorting civilians on the road between Arbinda and Gorgadji in the Sahel region. Jamaat Nusrat Al-Islam wal Muslimeen (JNIM) claimed responsibility for the attack.
	DATE	18/8/21	GROUP	JAMAAT NUSRAT AL-ISLAM WAL MUSLIMEEN (JNIM)			
7	COUNTRY	NIGER	REGION	TILLABERI	DEATHS	70	Gunmen on motorbikes killed around 70 civilians and wounded around 17 others in the village of Tchombangou. Islamic State in West Africa (ISWA) claimed responsibility, saying they targeted pro-government militia members.
	DATE	2/1/21	GROUP	ISLAMIC STATE IN WEST AFRICA (ISWA)			
8	COUNTRY	BURKINA FASO	REGION	SAHEL	DEATHS	53	Gunmen killed at least 49 police officers and four civilians at a police post near an abandoned mine in the Sahel region at around 0500hrs on 14 November. No group had claimed responsibility for the attack at the time of writing, but local media outlets reported that Jamaat Nusrat Al-Islam wal Muslimeen (JNIM) was probably responsible.
	DATE	14/11/21	GROUP	JAMAAT NUSRAT AL-ISLAM WAL MUSLIMEEN (JNIM)			
9	COUNTRY	AFGHANISTAN	PROVINCE	KUNDUZ	DEATHS	50	A suicide bomber detonated explosives during Friday prayers in a Shia mosque in the Kunduz province. Local officials reported that at least 50 civilians were killed and 140 more wounded. Islamic State - Khorasan Province claimed responsibility.
	DATE	8/10/21	GROUP	ISLAMIC STATE - KHORASAN PROVINCE			
10	COUNTRY	AFGHANISTAN	PROVINCE	KANDAHAR	DEATHS	47	Four suicide bombers killed at least 47 people and injured at least 80 others in an attack on a Shia mosque in Kandahar province. Two suicide bombers detonated explosives at the entrance to the mosque, followed by two further detonations inside the mosque. Islamic State - Khorasan Province claimed responsibility for the attack.
	DATE	15/10/21	GROUP	ISLAMIC STATE - KHORASAN PROVINCE			

Figure 3 – Ten worst attacks committed by terrorists in 2021 (Adapted from [7])

In this context, professionals from structural engineering develop studies evolving around designing advanced systems capable of protecting people from explosions. One of the main concerns, existing today, is related with the glazing utilization in buildings. In case of an explosion, they can cause hurt or even kill human beings. The blast phenomena in buildings with glazing façades can be problematic due to the projection of the glass, arising as a huge problem for the construction integrity. In Beirut explosion (mentioned before), most of the victims were not killed directly by the blast.

Figure 4 - Beirut victim due to glass laceration with limb amputation. Purposefully pixelized due to content in the image (Adapted from [8])

Figure 5 - World Trade Center Lisbon Concept (Source: [9])

Instead, they were injured or killed by glass projection. In Figure *4* it is shown the severe damage caused by glass projection in a human being. The Oklahoma City bombing was also an event were at least 80% of the victims were injured by glass laceration [8].

In the Portuguese Military Academy, the project “Protection Glass Façades Against Blast Loads” (ProFESEx) has, as main goals, designing and developing a solution for protection of the glazing facade using 3D printable metamaterials with the goal of developing and obtaining an energy dissipation device. This dissertation is integrated in ProFESEx with the main objective of studying a viable solution of energy dissipation in real sized glazing panels.

Nowadays, the glazing construction is used very often, as for instance, in the world trade center in Lisbon, which construction finished in the present year. Figure 5 shows the World Trade Center Concept, in Lisbon, as an example of the usage of the glass as a common practice in construction. This kind of approach has, as main objective, improving quality of life and health of the internal user due to the indirect contact with the exterior view, which is an important psychological factor [10]. There are several types of glass developed through history, namely: the float glass, used nowadays more than other types as its price is the lowest, heat-strengthened glass, and the most expensive, tempered glass, because of its more complex production.

With the appearance of several kinds of interlayers as the Poly Vinyl Butyral (PVB), Sentryglas®, Ethyl Vinyl Acetate (EVA) and others, the laminated glass also became a very performing technical solution. This kind of glass is the combination of glass panes bonded by the interlayer. The strongest known solution to blast loads is the laminated glass with tempered glass panels [11].

1.2. Objectives and Methodology

The major goal of this Master of Science (MSc) Dissertation is to contribute to the development of a protective solution to mitigate the glass damage caused by blast load events. This goal is intended to be attained my numerical studies and the design and execution of a test protocol and the collaboration in the execution of real scale field blast tests of glass panels facades.

The glazing solution includes the usage of a laminated glass with two tempered glass panes bonded with PVB. To help mitigating the damage on the glass, and reduce the damage caused by a

blast wave, it is taken advantage from 3D printed metamaterials to produce energy-dissipation devices of an auxetic geometry, due to good mechanical properties when submitted to blast loads. The final purpose is to understand if the proposed solution is reliable and which factors need to be changed to optimize the behavior of the glass panel subjected to a blast load.

The proposed methodology for this MSc Dissertation is as follows:

1) Finite Element (FE) model of a glass panel using field experiments from similar works as, for instance, Hooper et. Al. [11] and Zhang et. al. [12] and respective validation of the FE model;
2) FE model of the energy-dissipation device statically and dynamically analyzed and experimented in Martins [13], replication of the FE model used in Coutinho [14] and validation of the model;
3) Pre-Design of the glazing solution along with its structure;
4) FE model of the final glazing solution with and without the energy-dissipation device to understand the localization and number of energy-dissipation devices behind the glass panel;
5) Field experiments with and without energy-dissipation devices to understand the differences between the two solutions;
6) Finally, the analysis and discussion of the obtained results.

1.3. Dissertation Outline

This MSc Dissertation has seven chapters. The first chapter presents and explains the motivations of the dissertation along with its organization.

In the second chapter it is explained the explosion phenomena, as well as the complex state of the art around explosions characteristics.

The third chapter explains the different types of glasses, used nowadays, in the construction industry. Also, some aspects related with a possible solution for the fixation system used in the related studies of this MSc dissertation, along with a small introduction to 3D printing and the preparation of the used samples, for laboratory testing, developed by using Polyethylene Terephthalate modified with Glycol (PETG) material, are presented.

In chapter four the pre-design of the glazing panel is presented along with the design of the steel supporting structure.

The fifth chapter presents the FE models along with their detailed explanations. It is explained the glass model, the energy-dissipation device along with its dynamic behavior, and the final experimental testing set-up.

The sixth chapter details the experimental set-up, defines the sensors and accelerometers, and explains, in detail, the different setting of each sensor and accelerometer. Finally, this chapter shows some experimental results and the difference between the glazing solution with and without the energy-dissipation device.

In the last chapter there are presented the conclusions, of all the MSc work, along with proposals for possible future developments.

Chapter 2. Explosions and Blast Effects

2.1. Introduction

As presented in chapter one, the use of explosion, with the objective of causing mass killing, is one of the most preferred options of terrorist groups. This chapter explains the effect of explosions, along with some differences between its location and origin. Also, bombing is a choice, as a very used and common methodology, due to the low required expertise of operators for the success of the targeted operation. A simple and crude bomb, to be built, needs simple and cheap materials, it is easy to arm, and allows respective users being far away from the explosion site, does not requiring specialized skills. Another important issue is that only one person, or a small number of people, can produce serious damages to a huge number of civilian lives [15].

Also, it is from common knowledge that a dramatic and chaotic environment, after an explosion, is a key objective for the terrorist organizations. For achieving this purpose, the detonation of a large number of explosives is a natural alternative [15]. For instance, the Oklahoma City bombing, in 1995, is characterized by the scenario were a building collapsed after the usage of 2200 kg of Ammonium Nitrate/Fuel Oil (ANFO), seen in Figure *6* [16].

Figure 6 - Oklahoma City explosion damage (Source: [17])

In the context of structural engineering, it is important to consider the protection of buildings against explosions and, to do so, it is crucial to understand the main physical parameters that characterize an explosion and related environment.

2.2. Definition

An explosion happens when a chemical or physical reaction exists in the matter along with an impulsive liberation of large amount of energy and heat that can generate a blast wave capable of producing insane damage on buildings and surrounding environment, including people and goods [18].

Nowadays, there is a huge variety of materials that can generate or cause an explosion, but the most common are chemicals and nuclear materials because of its capacity to generate very intense reactions to maximize the damage, when properly mixed [18].

The sudden release of a large amount of energy, in a very short period, is what characterizes an explosion. After first moment of an explosion, the respective effect moves through the air, sometimes faster than sound, and respective particles are accelerated and deaccelerated by the passage of the shock front in its direction, creating positive and negative relative pressures [18].

2.3. Classification

2.3.1. Origin of an explosion

The origin of an explosion can be a physical, nuclear or chemical reaction. A physical reaction can consist, for instance, in a mixture of two liquids at very different temperatures together, or a discharge of a compressed gas [19], [20].

A nuclear reaction can also generate an explosion, like the atomic bombs that are an example of a fission reaction. In this case, the energy has its origin in a fission reaction happening in the core that breaks into smaller atoms. The fusion reaction is also an example of a nuclear reaction [19], [20].

A chemical explosion is related to the rapid oxidation of the element used as fuel. In this context, it is not required the presence of air. To be useful, the explosive should be stable under normal conditions, of pressure and temperature, meaning that it can only explode when it is intended to. To be possible this occurrence, the explosives are stored and used in two states: solid and liquid. When the chemical reaction is set, the violent decomposition of the fuel takes place and originates heat a production of gases, and along with its rapid expansion, comes the generation of shock pressures in any structure or material, that is in contact with the explosive, or the production of shock waves if the explosion is in the air environment. In this dissertation, it is focused the study of blast waves coming from an explosion in the air environment [19], [20].

2.3.2. Chemical Reaction

There are three types of chemical reactions related to their time: combustion, deflagration, and detonation. The slower one is the combustion that exists in every kind of oxidation, and the process is known as burning. In explosives, if they decompose in a rate below the sound speed of the material, it is called deflagration and it is propagated by the heat that is liberated during the reaction [19], [20].

From those mentioned above, the fastest one is the detonation, a form of reaction that produces an intense shock wave and intense heat along with an instantaneous generation of the front shock wave.

The normal velocity range of a detonation varies from 1500 to 9000 m/s which is faster than a deflagration [19], [20].

2.3.3. Confined and Unconfined Explosions

An explosion can be either confined or unconfined, and the response of the structure and the propagation of the blast waves are different in each individual situation.

2.3.3.1. Confined Explosions

When an explosion happens inside a building, the pressures and the response of the structure related to the shock wave is amplified because of the reflections happening multiple times. Along with the reflection of the shock waves, the temperature and the accumulation of gases will exert an additional pressure and increase the duration of the load within the structure. Depending on the degree of confinement the blasts can be classified as: fully vented, partially vented and fully confined as it is represented in Figure *7* [21], [22].

A fully vented confined explosion is produced when one or more surfaces of the building are open into the atmosphere and the blast wave is vented to the atmosphere [21]–[23].

A partially vented confined explosion is produced when the building has some openings in its surfaces and the blast wave takes a long time than a fully vented confined explosion to be vented to the atmosphere [21]–[23].

A fully confined explosion is produced when the building has no openings to the atmosphere and the explosion is totally contained inside [21]–[23].

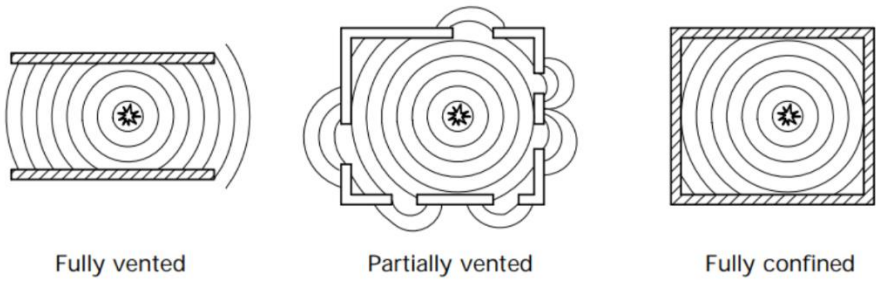

Figure 7 - Confined Explosions (Adapted from [22])

2.3.3.2. Unconfined Explosions

If the explosion is unconfined, it can be divided into free air burst, air burst and surface burst. A free air burst explosion occurs when the explosion happens high above from the ground and the building and the propagation of the blast wave is in free air until it reaches the surface of the building without having any reflections or intermediate amplifications as it can be seen in Figure 8 [22], [23].

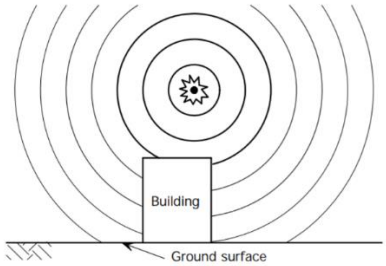

Figure 8 – Free air burst explosion (Adapted from [22])

An air burst explosion occurs when the explosive is above the ground, but can produce an intermediate amplification of the wave because of its reflection of the ground due to its rigidity, the wave propagates faster and when it is reflected creates a wave faster than the original shock wave, originating a Mach stem imaginary planar surface that hits the building as it is shown in Figure 9 [22], [23].

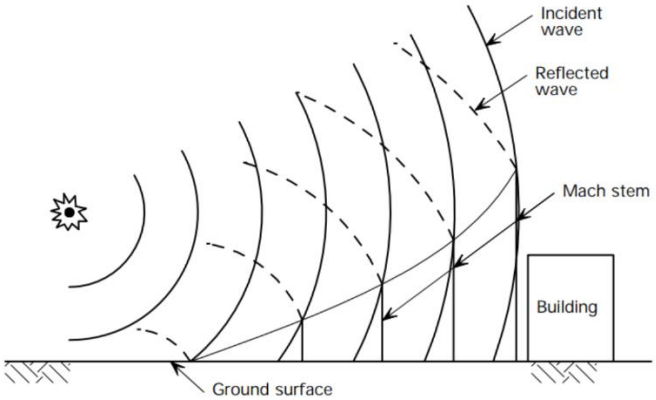

Figure 9 - Air burst with ground reflections (Adapted from [22])

A surface burst explosion happens when the detonation occurs near, or on the ground. The shock wave similarly to an air burst is also reflected by the ground and it is generated a wave that is faster than the one propagating in air, creating also a Mach stem, shown in Figure 10 [22], [23].

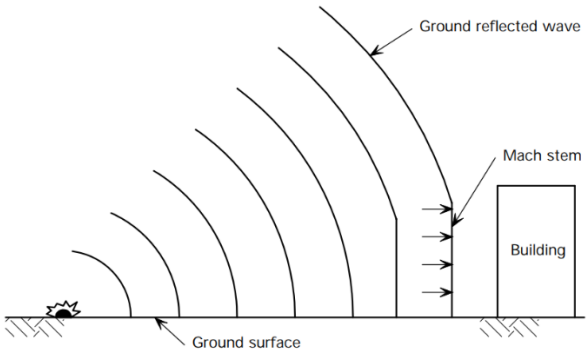

Figure 10 - Surface Burst (Adapted from [22])

2.4. Shock Waves

When an explosion occurs, it is verified, at first, a generation a hot gas which can be at pressures of 10 to 30 GPa and its temperature can reach from 3000 to 4000 ºC. The phenomena associated with this event is characterized by the surrounding air being forced to move out of place causing a

compressed layer of air that expands from the center of the explosion. This layer, the blast wave, is a form of pressure energy that is released from the explosion. The pressure of the wave decreases with the distance as the wave travels away from the explosion, and the momentum of the gas causes it to overexpand, resulting in a moment when the pressure is very high and then it decreases violently creating a suction, or negative phase, making the molecules of air flow in the direction of the center of the explosion, until the atmospheric pressure is restored [19]. This process can be divided in three different time periods. The first one occurs when the detonation of interior components of the charge is set but still inside; the second time period is the positive phase, when the total detonation of the charge occurs and the gases are released, almost instantaneously, creating the overexpansion, referred above, and the pressure is higher than the atmospheric pressure; the third and last time period happens when the wave passes, and creates a negative pressure due to the disturbance that occurred before in the positive phase as explained above. This negative phase is longer than the positive phase until balance is restored [19].

As illustration, in Figure 11 it is possible to see the pressure variation in time of an explosion, given a fixed point in a place, to a certain distance of a considered free air burst [23]–[25].

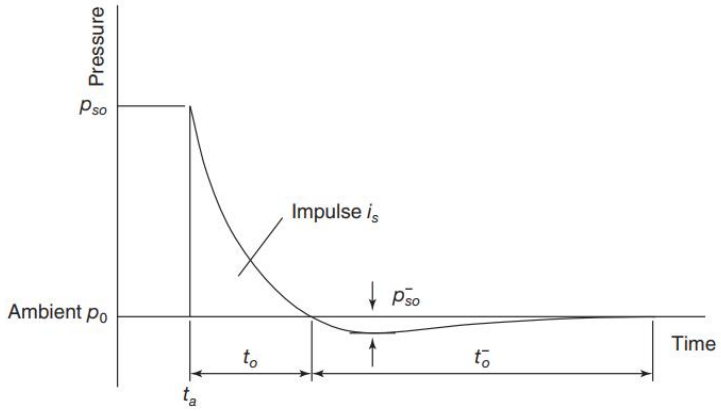

Figure 11 - Pressure variation of a blast load (Adapted from: [19])

In Figure 11 it can be observed that before the shock wave arrives the pressure is equal to the atmospheric pressure, P_0. It is assumed that after the wave arrives, t_a, the pressure instantaneously increases to a maximum value, P_{so}, and it is followed by a rapid decay in pressure to a value below the atmospheric pressure to a minimum pressure, P_{so}^-, until it starts rising again to its normal value of environmental pressure. As it is possible to see, t_0 or t_0^+, is the positive phase duration, as the pressure stays above P_0, and t_0^- is the negative phase, as the pressure stays below p_0. The duration of t_0^- is longer than t_0 but it is considered less important for the design of a building, as the positive phase is the one that results in most damage to the structure [23]–[25]. Along with the overpressures there are the specific impulse of each phase. This impulse is the integration of the overpressure curve, this impulse is calculated starting at the time of arrival, t_a [23]–[25].

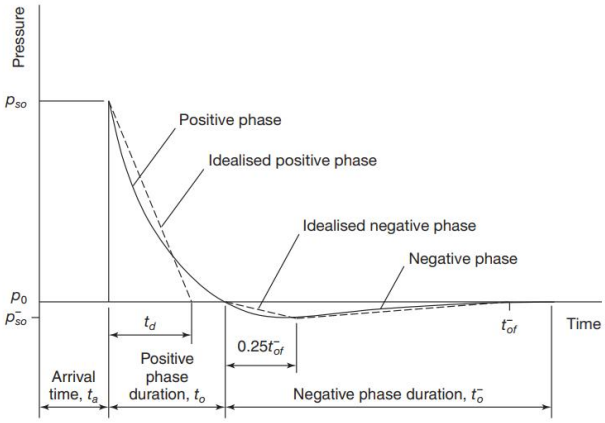

Figure 12 - Linear approximations of the pressure variation on time of a blast load (Adapted from: [19])

The Friedlander equation can describe the behavior of the overpressure over time, and it can be written as [25]:

$$P_s(t) = P_0 + P_{so}\left(1 - \frac{t}{t_0^+}\right)e^{-bt/t_0^+} \tag{2.1}$$

Considering P_0 that as the atmospheric pressure, equal to zero, to simplify the calculations, the Friedlander equation is [25]:

$$P_s(t) = P_{so}\left(1 - \frac{t}{t_0^+}\right)e^{-bt/t_0^+} \tag{2.2}$$

Where, P_{so} (kPa) is the peak incident overpressure, t_0^+ is the positive phase duration and b is the decay rate of the curve.

As referred before, the specific impulse is the integration of the Friedlander equation on each phase, positive or negative. For the MSc dissertation, it is only considered the positive phase duration due to the damage on the evaluated structure. For the positive phase duration, the equation of the positive impulse is [19]:

$$i_s = \int_{t_a}^{t_a+t_0^+} P_s(t)dt = \frac{P_{so} \times t_0^+}{b} \times \left[1 - \left(\frac{1 - e^{-b}}{b}\right)\right] \tag{2.3}$$

For the negative phase a similar equation can be described as:

$$i_s^- = \int_{t_a+t_0^+}^{t_a+t_0^++t_0^-} P_s(t)dt = -\frac{P_{so} \times t_0^+}{b^2} \times e^{-b} \tag{2.4}$$

However, frequently, it is common to use a simplification. This simplification is a triangular equivalent approach with a positive phase duration of t_d, and with the specific impulse of equal value to the original Friedlander equation. The specific impulse can be calculated as [19]:

$$i_s = \frac{1}{2} t_d P_{so} \tag{2.5}$$

And therefore, the instant, t_d, can be obtained by [19]:

$$t_d = \frac{2i_s}{P_{so}} \tag{2.6}$$

As we use this approximation to calculate the specific impulse, the overpressure-time equation can be described now as [22]:

$$P_s(t) = P_{so}\left(1 - \frac{t}{t_d}\right) \tag{2.7}$$

The graphic representation of this approximation is shown above in Figure 12.

Another way of assessing the specific impulse was developed by Kinney and Graham [24], who developed the following equation [24]:

$$i_s\,[\mathrm{MPa.ms}] = \frac{0.0067 \times \sqrt{1 + \left(\frac{Z}{0.23}\right)^4}}{Z^2 \times \sqrt[3]{1 + \left(\frac{Z}{1.55}\right)^3}} \tag{2.8}$$

Where Z (m/kg$^{1/3}$) is the scaled distance, which will be presented further in this MSc dissertation.

The shock wave propagates faster than sound, and given this fact, the effect and damage of this shock wave is felt without any warning whatsoever. In Figure 13 it is possible to see the instants when the shock wave passes through a building [24].

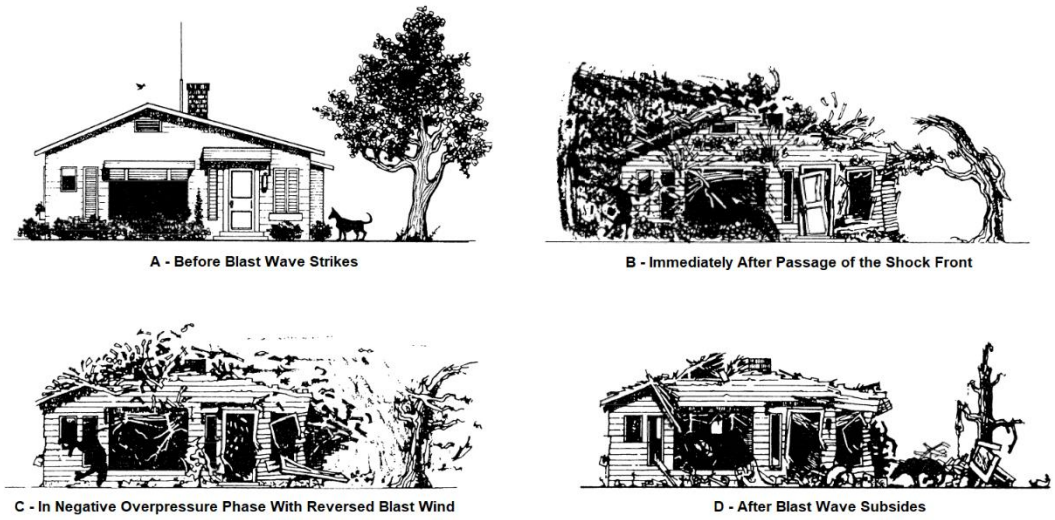

Figure 13 - States for the passage of a shock wave (Adapted from [24])

On the first stage, A, it can be observed the building and the atmosphere untouched yet by the shock wave. On B it is illustrated the instant where the shock front reaches the building and causes instant damage to it due to overpressures that rise almost instantly and then decay to a value of the atmospheric pressure, corresponding to the positive phase duration. The instant represented in C, is the instant where the negative phase is taking place and the building is pulled inwards to the center of the blast, because of the negative overpressures starting from the ending of the positive phase duration, passing through the lowest value of pressure and ending at atmospheric pressure. Finally in D, it is shown the final result of the blast wave effect on the building [24]. The following graph represents the overpressure-time curve as well as the instants represented in Figure 14.

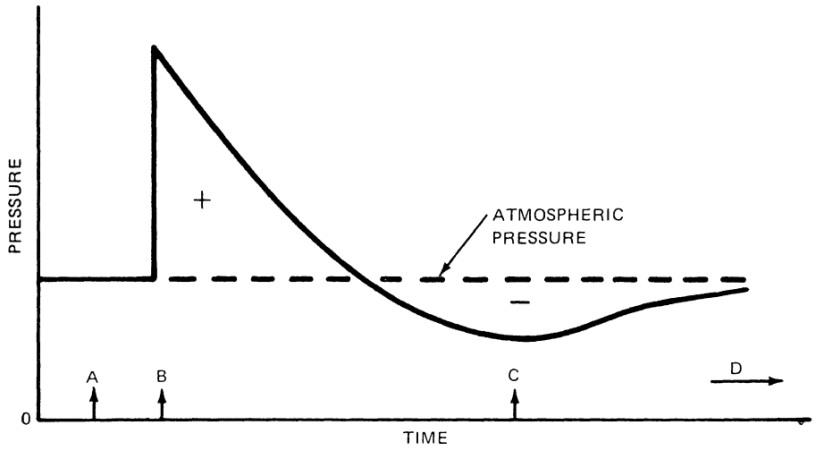

Figure 14 - Blast wave pressures in time (Adapted from [24])

2.4.1. TNT Equivalence Method

Nowadays there are many explosives around the world like gunpowder to home-made explosives, and every one of them has a single behavior in terms of blast wave, but to simplify the analysis it was verified that Trinitrotoluene (TNT) was the best explosive to give repeatability of experimental results. Due to this fact, it was chosen to represent the great majority of studies, becoming the standard value for measuring the specific energy released and the pressure output on a structure [22].

The best way to convert the explosive effect into equivalent mass of TNT is based on the ratio of the specific energy of the used explosive and the specific energy of TNT [22].

This can be expressed in the following expression [23]:

$$W_{TNTe} = \frac{H^{d}_{EXP}}{H^{d}_{TNT}} \times W_{EXP} \tag{2.9}$$

Where W_{TNTe} is the effective charge weight, H^{d}_{EXP} is the heat of detonation of explosive in question, H^{d}_{TNT} is the heat of detonation of TNT and W_{EXP} is the weight of the explosive in question [23]. Table 1 shows the equivalent mass of TNT of some commonly used explosives.

Table 1 - Equivalent Mass of TNT for different explosives (Adapted from [13], [22], [23])

Explosive	Equivalent Mass of TNT
Compound B (60% RDX, 40% TNT)	1.1
RDX	1.2
HMX	1.3
Nytro-glycerin	1.5
Semtex	1.3
PETN	1.66
PE4-A	1.4
Home-Made Generic	0.4 – 1.0

2.4.2. Scaled Distance

A common way to compare the results of two different explosions, is to use their scaled distance. The scaled distance is a measure that can correlate explosions, and estimate its values of pressure of the respective shock wave, based on distance and the weight of the explosive. It is a common practice to use this method because it saves money giving the fact that a real scale explosion can be reproduced in a small scale if the scaled distance of the small explosive is the same as the real one [18].

Initially Hopkinson (1915) and later Cranz (1926) came up with a principle that it is possible to reproduce similar shock waves if the scaled distances of two explosions are the same, giving that the explosive has the same geometric values, the same compound, the same atmosphere but only with different weight [25]. The equation that explains what was written follows as:

$$Z = \frac{R}{W^{\frac{1}{3}}} \tag{2.10}$$

Being Z (m/(kg$^{1/3}$)) the scaled distance, R (m) the distance between the structure and the center of the explosive charge and W (kg) the weight of the explosive charge [24], [25].

2.4.3. Peak Overpressure

One way of calculating the peak overpressure, as in P_{so} (MPa), to chemical explosions as written by Kinney and Graham [24] is:

$$P_{so}\,[\mathrm{MPa}] = \frac{808 \times \left[1 + \left(\frac{Z}{4.5}\right)^2\right] \times P_0}{\sqrt{1 + \left(\frac{Z}{0.048}\right)^2} \times \sqrt{1 + \left(\frac{Z}{0.32}\right)^2} \times \sqrt{1 + \left(\frac{Z}{1.35}\right)^2}} \tag{2.11}$$

As an alternative, Newmark and Hansen (1961) developed an easier way to obtain the peak overpressure of a detonation of a high intensity explosive [21], [26]:

$$P_{so}\,[\mathrm{bar}] = 6784 \times \frac{W}{R^3} + 93 \times \left(\frac{W}{R^3}\right)^{\frac{1}{2}} \tag{2.12}$$

Considering that:

$$1\ \mathrm{bar} = 100\ \mathrm{kPa} \tag{2.13}$$

Mills in 1987 also proposed a different way of calculating the peak overpressure [26]:

$$P_{so}\,[\mathrm{kPa}] = \frac{1772}{Z^3} - \frac{114}{Z^2} + \frac{108}{Z} \tag{2.14}$$

2.4.4. Dynamic Pressure

After the initial blast hits the structure of the first shock wave passes, an additional blast-induced effect, which consists of air, combustion products and gases, causes dynamic pressures to occur. This dynamic pressure cause, what it is called, drag loads to the structure [22]. These drag loads, q_s, depending on the peak overpressure and are neglectable and can eventually be greater as shown in Table 2.

Table 2 - Pressure and Dynamic Pressure Values (Adapted from [22])

p_s (kPa)	q_s (kPa)
100	31
300	225
500	518
700	875

This phenomenon is explained as the effect of the passage of the shock wave that causes a disturbance on air particles that move after the shock wave passage in its direction. The particles do not move because of the passage of the shock wave directly but move because of the pressure variance created by it [26].

The first analytical solution defined for the shock wave parameters were obtained by Rankine in 1870 and later on by Hugoniot in 1887, and define the drag load, q_s, based on the peak side-on overpressure of the explosion, in which P_0 corresponds to the atmospheric pressure [26]:

$$q_s = \frac{5P_{so}^2}{2(P_{so} + 7P_0)} \tag{2.15}$$

In alternative it can be used for low pressures and sea level atmospheric conditions the following equation [27]:

$$q_s = 0.022 \times (P_{so})^2 \tag{2.16}$$

2.4.5. Positive Phase Duration

The positive Phase duration is directly related to the damage caused to the building. Generally, this is the phase that causes the most damage to a building, and to simplify the calculations, it can be considered only the duration of this phase, t_0^+.

Kinney and Graham [24] came up with an equation that can give the duration of the positive phase time based on the scaled distance, Z, of the explosion and the weight of the explosive, W.

$$t_0^+[\text{ms}] = \frac{980 \times \left[1 + \left(\frac{Z}{0.54}\right)^{10}\right] \times \sqrt[3]{W}}{\left[1 + \left(\frac{Z}{0.02}\right)^{3}\right] \times \left[1 + \left(\frac{Z}{0.74}\right)^{6}\right] \times \sqrt{1 + \left(\frac{Z}{6.9}\right)^{2}}} \tag{2.17}$$

2.4.6. Shock Wave Velocity

According to Rankine-Hugoniot, the velocity of the shock wave can be obtained by [23]:

$$U_s = C_0 \times \left(1 + \frac{6 \times P_{so}}{7 \times P_0}\right)^{1/2} \tag{2.18}$$

Where C_0 is the sound speed on air, P_{so} (bar) is the peak overpressure and P_0 is the atmospheric pressure.

2.5. Shock Wave Reflection

After the shock wave encounters an object or a solid surface denser than the wave, it will get reflected and depending on the surface geometry and size, will also diffract from it. When the explosion happens, around many buildings, this reflection process can lead to complex loading conditions and sometimes, it can generate shock waves of higher magnitude that were amplified by the reflection process. This process can be divided into three different types of reflection: face-on reflection, regular reflection and Mach reflection [22], [28].

2.5.1. Face-On Reflection

This reflection occurs when the wave front hits the structure perpendicular to its direction of propagation as shown in Figure *15*.

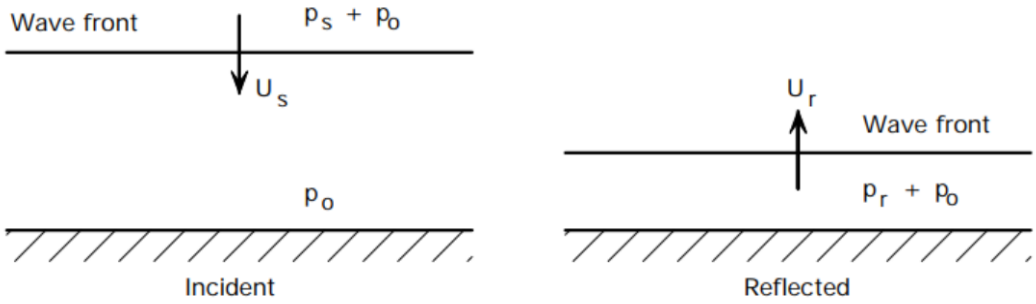

Figure 15 - Face-On Reflection (Adapted from [22])

This event causes the particles of air to stop abruptly when they encounter the surface generating a compression of this molecules which creates a reflected pressure of higher magnitude than the incident pressure. Although the pressure increases, the duration time of the respective phases remain the same [22], [28]. The pressure-time graph is the following for a face-on reflection.

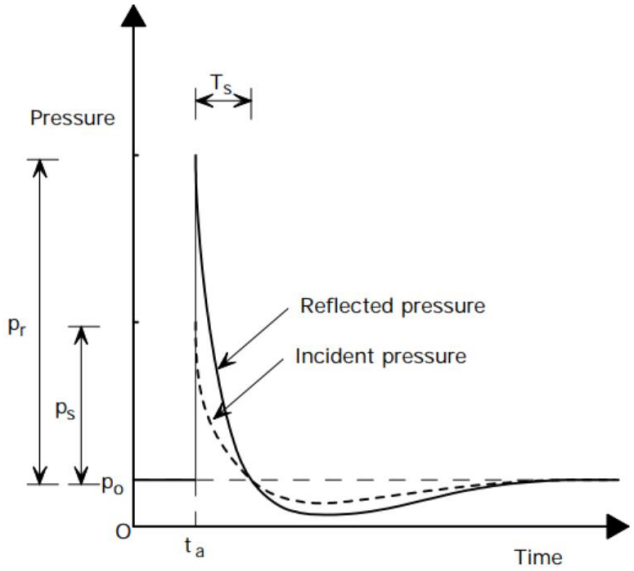

Figure 16 - Blast overpressure function for a face-on reflection (Adapted from [22])

Rankine and Hugoniot developed an equation for the calculation of the peak reflected overpressure. This method has assumptions as: the explosion is at standard sea level conditions and the specific heat ratios are the equal to 1.4 [20], [26], [28].

$$P_r\,[\mathrm{MPa}] = 2 \times P_{so} \times \frac{4 \times P_{so} + 7 \times P_o}{P_{so} + 7 \times P_o} \tag{2.19}$$

Where P_{so} is the peak overpressure and P_0 is the atmospheric pressure.

In Table 3 there are presented some values of reflected overpressure with different distance-mass combinations.

Table 3 - Peak Reflected Pressures for different load values (Adapted from [20])

R \ W_{TNT}	**100 kg**	**500 kg**	**1000 kg**	**2000 kg**
1 m	165.8	354.5	464.5	602.9
2.5 m	34.2	89.4	130.8	188.4
5 m	6.65	24.8	39.5	60.19
10 m	0.85	4.25	8.15	14.7
15 m	0.27	1.25	2.53	5.01
20 m	0.14	0.54	1.06	2.13
25 m	0.09	0.29	0.55	1.08
30 m	0.06	0.19	0.33	0.63

For design purposes, it is possible to use an equivalent triangular impulse with the values of the peak reflected overpressure with the goal of achieving a simplified calculation to get the same results. The impulse calculation follows as [26]:

$$i_r = \frac{1}{2} \times P_r \times t_d \tag{2.20}$$

Where i_r is the reflected impulse, P_r is peak reflected overpressure and t_d is the equivalent positive phase duration.

If, for any valuable reason, a precise measure cannot be applied to the experiment, it is also possible to achieve the reflected impulse by assuming a correlation between the peak overpressure and the peak reflected overpressure as follows [25]:

$$\frac{i_r}{i_s} \approx \frac{P_r}{P_{so}} \tag{2.21}$$

2.5.2. Regular Reflection

When the blast wave reaches the building with an oblique direction and the angles, α, lies between 0 and 40 degrees, regular reflection occurs [22] [28].

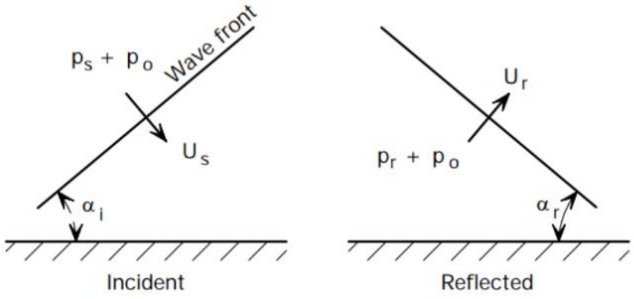

Figure 17 - Regular reflection of a blast wave (Adapted from [22])

The reflected pressure in this situation is greater than the reflected pressure caused by a face-on reflection. Also, the angle of incidence will not be same of the reflected angle.

For the calculation of the reflected overpressure of the wave front, the assessment of the value is obtained by [22]:

$$P_r = P_{so} \times C_r \tag{2.22}$$

with C_r the reflection coefficient (Figure 18).

The peak reflected pressure, for cases where α lies between 0 and 40 degrees, can reach from two to thirteen times the value of incident overpressure.

2.5.3. Mach Reflection

When the angle of incidence is superior to 40 degrees, the domain changes and the Mach reflection takes place instead regular reflection. In air, the approximating limiting angle is 40 degrees [22], [23].

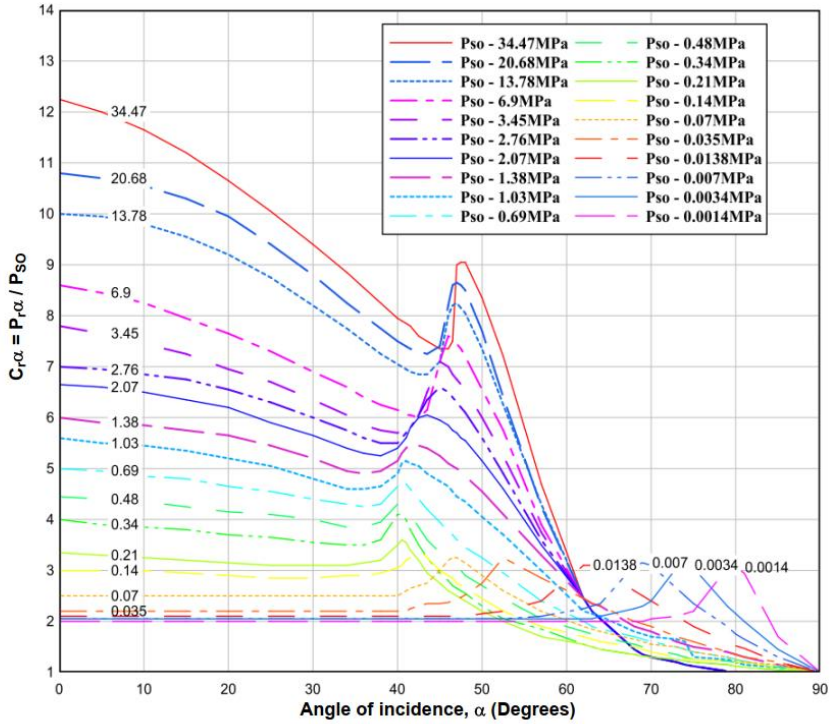

Figure 18 – Reflection coefficient variation with angle of incidence (Adapted from [23])

This Mach stem reflection is a result of the reflected wave intercepting the incident wave in a way where neither one of them can overtake the other creating a zone of higher pressure. This higher-pressure zone generates a Mach stem that propagates as a plane front shock wave. The interception between the Mach stem and the incident shock wave and the reflected wave is an imaginary point is called the triple point [22]. In Figure *19* it is explained how the Mach Reflection process along time.

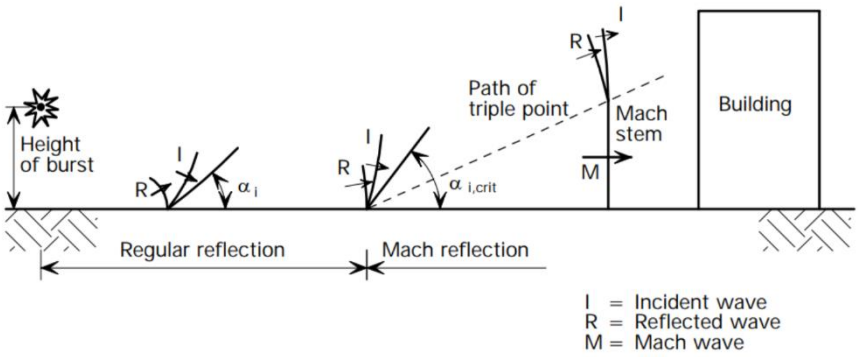

Figure 19 - Mach Reflection (Adapted from [22])

The Mach reflection is the worst-case scenario because it causes a substantial increase in the reflected overpressure. This can result in a much higher overpressure than the predicted if the blast wave is assumed to be regularly reflected. The extent of this amplification of pressure depends on the initial peak overpressure [22].

2.6. Structural Response to Blasting Loads

The blast wave effect on building is directly related to the explosion magnitude, the location of the blast and its origin. The geometric configuration of the surroundings has also influence on the blast wave, and the explosive distance to the ground level (above, at ground level or even underground) [23].

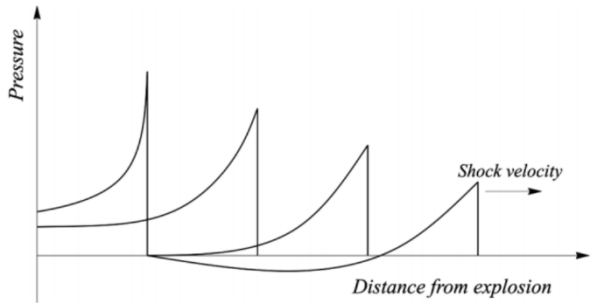

Figure 20 - Variation of the blast pressure with distance variation (Adapted from [21])

As referred, the shock wave overpressure and speed reduce both as the wave gains distance from the center of the detonation [21]. Considering now a rectangular shape building of finite dimensions, and only one side facing the shock front. The phenomenon of overpressures around all the four faces of the building has a complex formulation even more than the simpler procedures explained above. The values of overpressure in the respective faces are related to the peak reflected overpressure, the peak overpressure, the drag loads as well as the size, either in length and in high, and even the surroundings of this building are important for possible calculations [22].

A simple approach for understanding this phenomenon is explained in Figure 21.

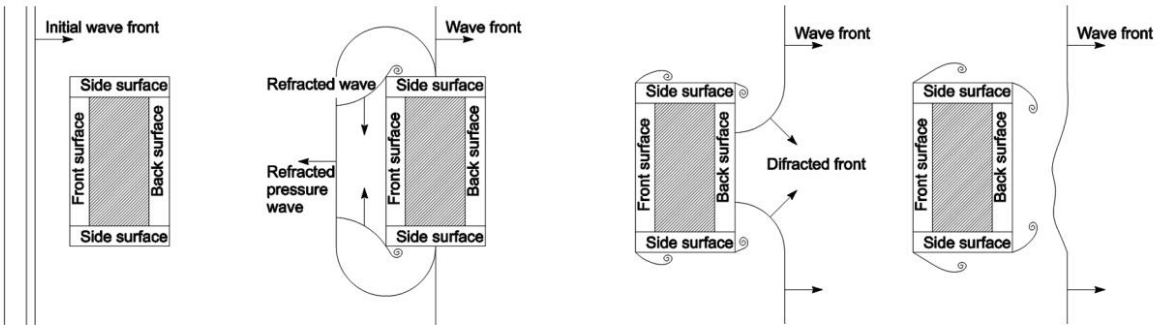

Figure 21 - Shock wave interaction with a building (Adapted from [21])

For this dissertation, the detonation is considered near ground level and with regular reflection and then Mach reflection. As expected for most situations, the greater damage happens in the front face. When the shock front reaches the structure, there is an instantaneous increase of the overpressure to the value of the peak reflected overpressure, P_r, and after that the dynamic pressure after the passage of the shock wave. In Figure 22 it can be seen how the overpressure varies through time in the front surface of a building. This front face will experience and enhanced effect of the overpressure due to

reflections of the incident wave. The side faces will receive a peak reflected overpressure lower than the front face [22], [23].

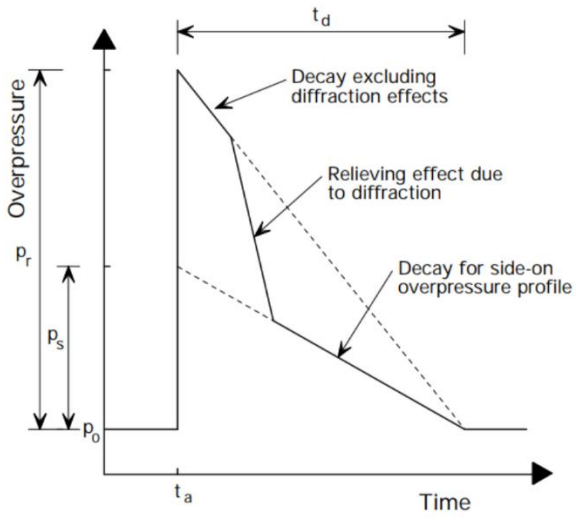

Figure 22 - Blast overpressure function acting on the front face of a building (Adapted from [22])

After the front surface receives the shock wave, as it passes from the front surface to the sides, the front surface will experience a relieving effect on the overpressure, which causes the rate of decay of the overpressure to increase. After this phenomenon the decay rate of the overpressure in the front face is similar to the side faces, and the gradient of the line changes again as we can see in Figure *22* [22].

To simplify either de dynamic overpressure and the peak overpressure we can use an equivalent triangular impulse. For the blast overpressure we can simplify the impulse as in Figure 23, giving that the impulse stays the same as the initial equation [22], [23].

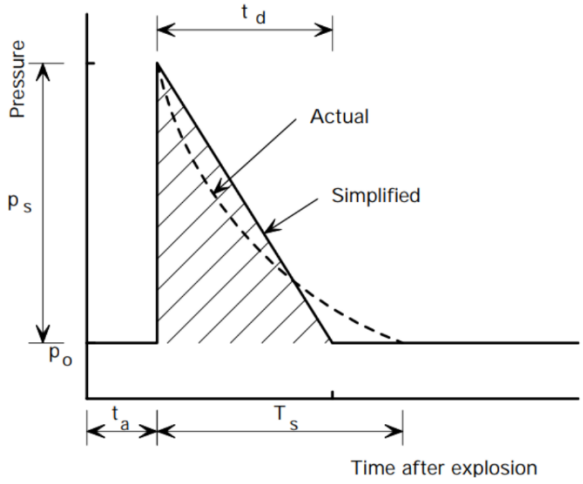

Figure 23 - Simplification of a blast wave overpressure profile (Adapted from [22])

For the dynamic overpressure felt in the front face of the building the simplification is the same as long as we maintain the value of the impulse.

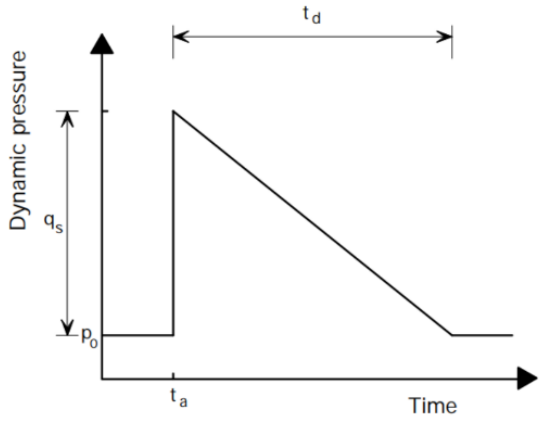

Figure 24 - Simplified profile of the overpressure in the front face of a building (Adapted from [22])

According to Kinney and Graham [24], the necessary time for the overpressure to reach the value of 0, t_c, can be obtained by:

$$t_c = \frac{3 \times s}{U} \tag{2.23}$$

Where s (m) is the smaller value between the height and half the length, and U (m/s) is the sound speed inside the reflected area.

Therefore, the overpressure acting the front face, P_{sf}, after the time, t_c, is the algebraic sum of the peak incident overpressure, P_{so}, with the drag overpressure, C_d x q_s, as in the following equation [23]:

$$P_{sf} = P_{so} + C_d q_s \tag{2.24}$$

The drag coefficient, C_d, gives the relationship between the translational pressure in the wind direction generated by the dynamic overpressures and the dynamic overpressure itself and varies with the value of the Mach number and the related geometry of the building [23]. As it is written in the United Facilities Criteria (UFC) [23], it is considered adequate to take C_d=1 for the front face. Given the facts, to obtain the total load from an explosion in an area or structural element, we should add the two components that appear in the following equation [22]:

$$F(t) = F_{blast}(t) + F_{dynamic}(t) \tag{2.25}$$

F_{blast} is the load caused by the initial blast wave and $F_{dynamic}$ is the load caused by the dynamic overpressures as a result of the airflow due to the process explained above.

The two components can be calculated as follows [22]:

$$F_{blast} = p \times A_{proj} \tag{2.26}$$

$$F_{dynamic} = q_s \times C_d \times A_{proj} \tag{2.27}$$

Where p is the overpressure of the shock wave, A_{proj} is the area of surface taken into consideration, q_s is the dynamic overpressure and C_d is the drag coefficient.

As mentioned before, the structural response to a blast load depends on several factors, but one factor that is very important to take into account is the normal period of the structure, T_n, and its relation to the positive phase duration of the overpressure, t_0 [28]. If the t_0 is much greater than T_n, we have what we

call a quasi-static load, and in this regime, the deflections happen as the load is applied. If t_0 is much lower than T_n, we enter the impulse regime, and force is so quick that the structure does not have time to respond to it. If the relation of t_0 and T_n is in-between we have a dynamic response of the structure, where the deflection happens after the load is applied but still in action and about to cease, like for example, the response of a building to a seismic load.

To better explain and visualize the different regimes, it is common to use an iso-response curve in a diagram called Pressure-Impulse (P-I) (Figure 25).

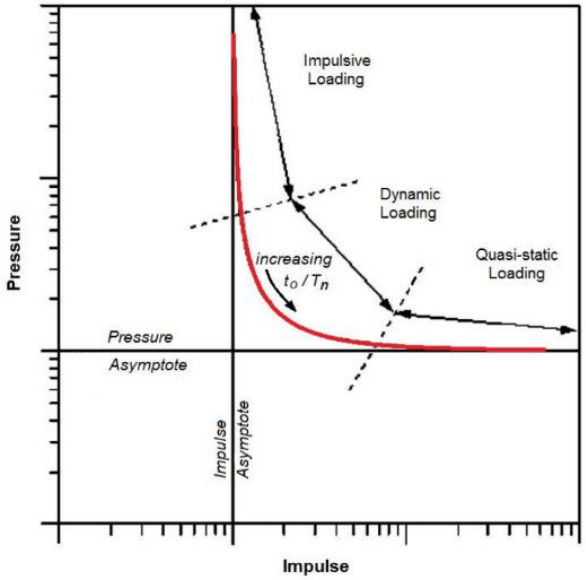

Figure 25 - Pressure-Impulse diagram (Adapted from [28])

Gough and Yandzio [22] limit in their work the values from which the structure starts to respond to a quasi-static loading or to impulsive-loading.

Table 4 - Load Regimes differences (Adapted from [28])

Loading Regime	**t_0/T_n Relationship**
Impulsive	$t_0/T_n < 0.4$
Dynamic	$0.4 < t_0/T_n < 2$
Quasi-static	$t_0/T_n > 2$

Due to experimental results in bibliography, we know that the T_n for the buildings is much superior when compared to a positive phase time of a blast wave, as T_n is normally is seconds and t_0 is in milliseconds. In these situations, the deflection of the building takes place only after the passage of all the blast wave. In this context, it can be considered an impulsive loading on the structure. This phenomenon allows possible to consider the structure during the duration of the blast as rigid, which allows the analysis of the structural response without considering the interaction between the load and the deflection of the structure due to the blast [28].

Chapter 3. Glazing Characterization

3.1. Glass Types and Fabrication

Nowadays in the modern construction the glazing solutions are increasing due to its translucid glass properties, color, and transparence [29]. This factor makes possible the creating of wide spaces illuminated with natural light, as it is an important factor for the human being as an office worker [10].

The fabrication of the glass appeared 4000 years ago, and until today the manufacturing has been improving to produce better material, with better properties for thermal behavior, impact resistance and durability [10], [29]. In manufacturing glass, it is known a wide variety of techniques, but all include as basic ingredient the silica (present in sand). With the addiction of sodium and calcium the most basic form of glass is produced, also called float glass, that currently represent about 90% of the glass fabricated worldwide. The float glass production starts by melting the raw materials in a furnace at temperatures up to 1500 ºC, then the molten glass is poured, at approximately 1000 ºC, continuously on a pool of melted tin where the oxidation is prevented by an inert atmosphere of hydrogen and nitrogen. Tin is a material with a wide temperature range maintaining the liquid state that reach from 230 ºC to 2200 ºC and it is heavier than the glass, which makes the molten glass float in it, after entering the pool, creating a smooth flat surface, like ice in water at lower temperatures, of equal thickness. After, the glass slides into the Lehr hoven where it is slowly cooled to prevent residual tensions of being induced into the glass due to rapid cooling. This process is called annealing, and after this process the glass is inspected and then cut [30] (Figure 26). After this process, the glass can be submitted to thermal treatment to increase its mechanical properties to achieve a higher resistance and better behavior to the applied loads [29].

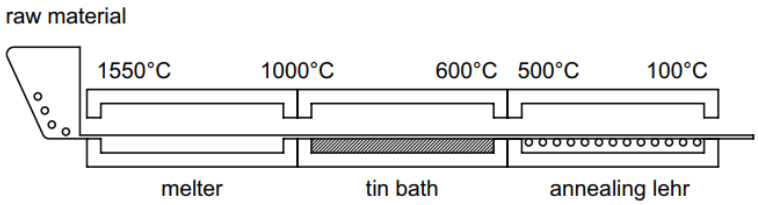

Figure 26 - Fabrication of Glass (Adapted from [30])

The most used types of glass nowadays are the annealed glass, the heat-strengthened glass and tempered glass. Also, the combination between two or more glass panes of the same or different types of glass through one or more interlayers is called laminated glass. The breaking pattern of such glass are shown in Figure 27.

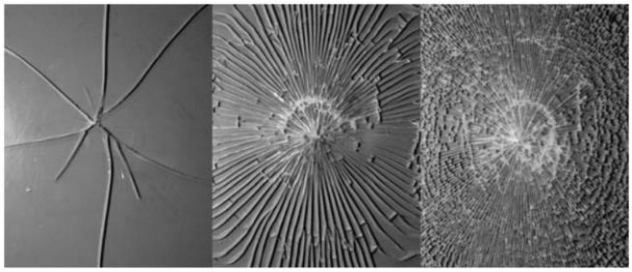

Figure 27 - Types of fracture in glass. On the left annealed glass, on the center heat strengthened glass and on the right tempered glass (Adapted from [30])

3.1.1. Annealed Glass

The annealed Glass is the basic type of glass that comes from the annealing process on the fabrication of the Glass. The characteristic resistance to pure bending is 45 MPa. It has a clean surface and his sensibility to thermal variations is high but has no retentions or creep effects as Gy described in 1999 during a one-year experiment [31]. The annealed glass when it brakes originates large pieces with sharp edges, that are dangerous for the human being and do not qualify for applications as a monolithic panel (Figure 28).

Figure 28 - Fractured annealed glass (Adapted from [31])

The mechanical behavior of an annealed glass is totally elastic as is shown in Figure 29 and the fracture is extremely brittle, even thought, the annealed glass has some capacity to still hold some very light load if the glass breaks but does not detach from the fixing system, since there is still a way through the unbroke areas to withstand the load [10], [30], [31].

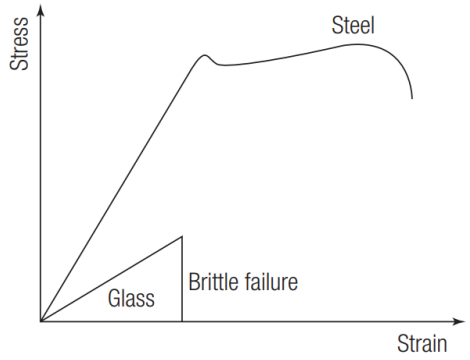

Figure 29 - Stress-Strain function for glass (Adapted from [31])

3.1.2. Heat Strengthened Glass

The heat strengthened glass is thermally treated, but not to a degree that it becomes tempered glass. This process makes the glass behave better than the annealed glass but worse than tempered glass [31].

The process of thermal treating the glass is based on a heating of the glass to a temperature of approximately 600 ºC, and then quenched by cooled air in the surface. The interior part of the glass will cool slower than the surface creating a tension of compression in the glass as it is shown in Figure *30* [10], [30], [31].

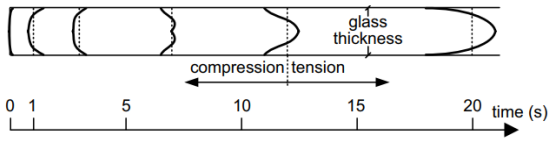

Figure 30 - Tension distribution in glass during heat treatment (Adapted from [30])

Due to the tempering process, the yield fracture can reach to values of 80 MPa. The thermal resistance of this type of glass is significantly higher than the annealed glass, and the thermal shock resistance will not induce fractures in the glass. To perforate or apply a cut in the glass, it must be done earlier, since, after the compression is generated, such alteration will cause the rupture of the glass [30], [31].

When the heat strengthened glass breaks it will originate, similar to annealed glass, large pieces with sharp edges, but the load to break the glass is higher [31].

3.1.3. Tempered Glass

The fully tempered glass is made by doing the same process as the heat strengthened glass but the temperature to which the glass is heated is almost the same, but the quenching made by cooled air, has the objective of being even faster than the cooling of the heat strengthened glass, creating a range even greater of tensions. The bending resistance of a fully tempered glass can be considered 120 MPa [10], [31].

Also, there is one detail that is important when proceeding with the heat treatment, that is the existence of small impurities inside the glass, that during the cooling process after the heating, the expansion and retention of the impurities is different from the glass, causing the glass to break sometimes with no apparent reason [31]. To improve the quality of the panels, quality test was developed, the Heat Soak Test (HST) that consists into raising the temperature on the glass panel during a time period to see if the glass breaks or not. If the glass passes the test, then it is ready to commercialize [32]. Figure 31 shows the difference between annealed glass and tempered glass with the generic values from tension components in the surface of the glass and on its core.

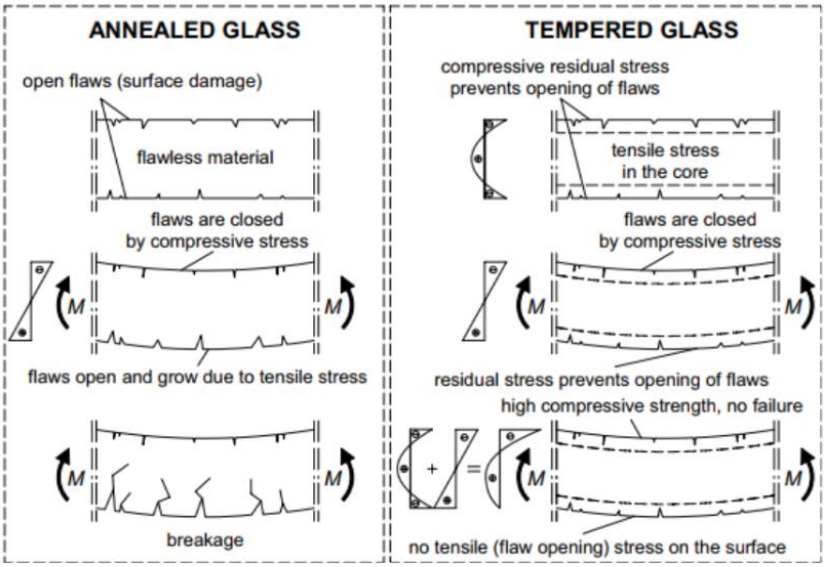

Figure 31 - Comparison between annealed and tempered glass (Adapted from [30])

Figure 32 - Tempered glass fracture behavior (Adapted from [31])

The high resistance achieved by this treatment, in a tempered glass, the thermal resistance is higher than the other two types of glass. Along with that property, when the glass breaks the tension is released through the glass creating small fragments along all the panel. The fragments do not detach completely from one another, they are together still in blocks then the glass breaks as Figure 32 illustrates [10], [31].

Due to this phenomenon the tempered glass is considered for “safety glass” even though, if a large mass of glass fall into a person, can create serious injuries.

3.1.4. Laminated Glass

The laminated glass consists in at least two panes of glass bonded by an interlayer [33]. Laminated glass was invented with the final goal of improving the mechanical properties of the glass, to better compensate its brittle behavior. For that reason, most of the times, the laminated glass is considered as “safety glass” [29].

Today, the interlayer for laminated glass can be chosen from a wide variety of interlayers, each one with its properties. The most used are Polyvinyl Butyral (PVB), thermoplastic polyurethane (TPU), ethyl vinyl acetate (EVA), Polyethylene terephthalate which is a type of polyester (PET) and Sentriglas® which is an ionoplast interlayer. The most common is PVB, and its thickness range goes from 0.38 mm to 6.08 mm, and every foil of PVB has a thickness number multiple of 0.38 mm [31].

The process of laminating glass is divided into two parts. The first part consists into the cleansing of the panels and the interlayer is placed between the glass and then heated and compressed. Then, it is created the autoclaving through high pressures and temperature of around 140 ºC as represented in Figure *33*. The glass used to produce laminated glass can be annealed, tempered, or heat strengthened [33].

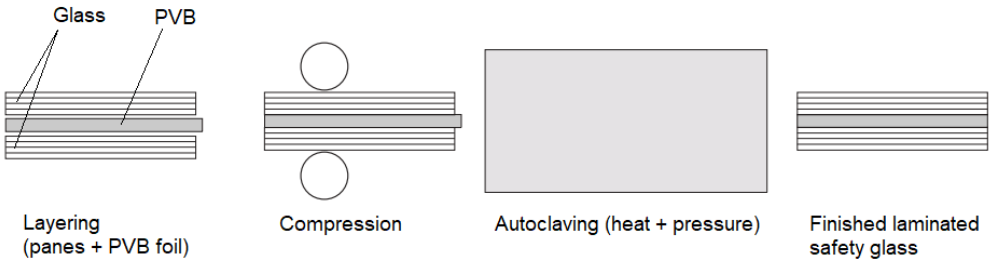

Figure 33 - Laminated Glass Fabrication (Adapted from [33])

3.2. Laminated Glass Properties

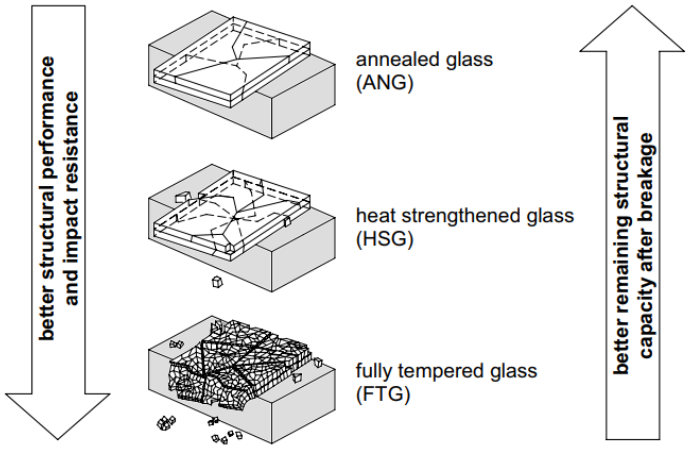

Figure 34 - Laminated Glass behavior to fracture (Adapted from [30])

Laminated glass as it is written in the previous subchapter, was invented to improve the properties of the glass, mechanical, physical and thermal [29].

The term safety glass was applied to laminated glass for the fact that, when it breaks, the damage is controlled. It is controlled because of its capacity to retain the broken glass attached to the interlayer, event thought, the laminated glass could

be pulled out of the fixing frame if the load is too large and still creating deadly injuries if it falls onto someone. The damage is still significantly lower than if a monolithic glass pane was used [30], [31].

The fragment patterns still remain the same for each pane of glass, but the projection of the fragments its drastically reduced since they stay connected to the interlayer. As it is shown in Figure 34, the patterns and different behavior of different types of laminated glass made from annealed glass, heat strengthened glass and fully tempered glass [30].

The behavior of the laminated glass to failure also depends on the interlayer used, and for the load duration, also, the laminated glass has a complex behavior which is explained further, and depends on the interlayer used as well [10].

3.2.1. Mechanical and Physical Properties

The glass density is the same as the concrete, meaning that the mass density of the glass is around 2500 kg/m^3. The atomic organization in glass does not have a proper order, and the atoms are distributed randomly meaning that there are zones where the density is lower, and zones where it is higher not detected by human eye [34].

The young's modulus for glass is 70 GPa, the same value for aluminum, with bending resistance values that differ from 45 MPa to 120MPa depending on the type of glass used. The compression value for the glass is higher than the tension, which means that the tension will dictate the type of glass to use. When in bending, the compressive strength of the glass is ten times higher than the tension originated because the impurities present in the glass do not affect the compressive behavior, but in the other hand, it can reduce drastically the tension resistance. The practical value for compression resistance when a permanent load is applied is around 170 MPa, a very low value compared to the theoretical value of 500 MPa as given in literature [32].

The behavior of the laminated glass submitted to a load is explained in Figure 35, where we have the failure of the first pane, then the second pane almost at the same time and only then, the PVB that works as a membrane until rupture [10], [12], [32], [35].

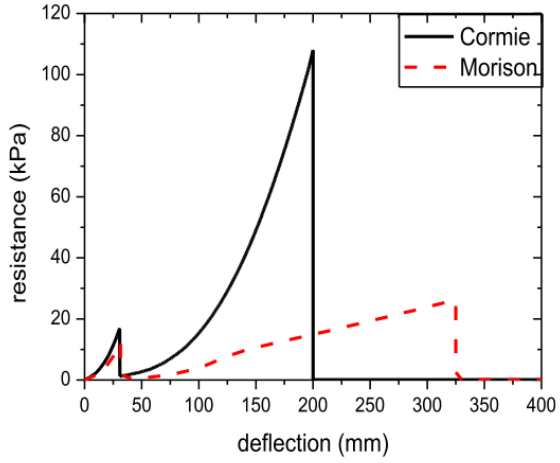

Figure 35 - Typical resistance of a 7.52 mm laminated glass with annealed glass plies submitted to a blast load (Adapted from [12])

When the laminated glass is submitted to a load, the reaction may depend on the duration of the load. For long-term durations the glass plies on the laminated glass behave almost totally disconnected from each other due to creep effects on the interlayer, and the total resistance is the sum of the individual resistances of each glass plie, which will be lower than for a short-term duration load. For short-term duration loads, the laminated glass will behave as a monolithic glass of the same thickness, since the interlayer can

transfer the load between the glass plies increasing the resistance of the laminated glass compared to the long-term duration loads [11], [31].

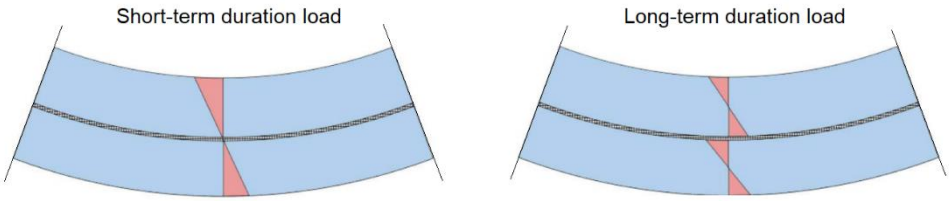

Figure 36 - Laminated glass behavior depending on load time duration (Adapted from [31])

When the interlayer is an ionoplast interlayer, the approach is not totally valid as for long-term duration loads as the creep effects on the ionoplast are reduced and the total behavior is composed since there is still a percentage of transferred load between the glass plies trough the interlayer [31]. Table 5 shows the values for different coefficients and properties of glass [31], [34].

Table 5 - Glass Properties (Adapted from [31])

Properties	Glass Type		
	Annealed Glass	Heat-Strengthened Glass	Fully Tempered glass
Mass Density, ρ [kg/m^3]	2500		
Young's Modulus, E [GPa]	70		
Distortion Modulus, G [GPa]	28.7		
Poisson's Coefficient, v	0.22		
Bending Resistance [MPa]	45	70	120

3.2.2. Thermal Properties

The thermal properties of a laminated glass are dependent from the glass plies individually. The glass has a coefficient of thermal expansion, α [32]. The thermal shock resistance of glass, ΔT, is equal to a variation of nearly 40 Kelvin without breaking, but for the heat-strengthened glass and tempered glass this value is higher due to the prestress of the heat treatment [32]. The thermal conductivity of the glass, λ, has a value of 1 [W/(mK)] which is a high value, meaning that, to explore thermal insulation, the use of a thermal insulating glass to improve the behavior to temperature variation [32].Table 6 shows the resumed thermal properties of glass.

Table 6 - Glass Thermal Properties (Adapted from [32])

Properties	Value	Units
Thermal Expansion Coefficient, α	9 x 10^{-6}	1/K
Thermal Shock Resistance, ΔT	40	K
Thermal Conductivity, λ	1	W/(mK)

3.2.3. Interlayer

The most used interlayer in the market is PVB. PVB is polymer characterized by excellent mechanical properties as well as his clarity which combined with glass make a clean material [36].

The principal purpose of using PVB is to keep the fragments of the glass attached to it after the glass breaks. This is possible due to the excellent ductility as well as excellent adhesive properties that make possible the safe behavior of a laminated glass [36].

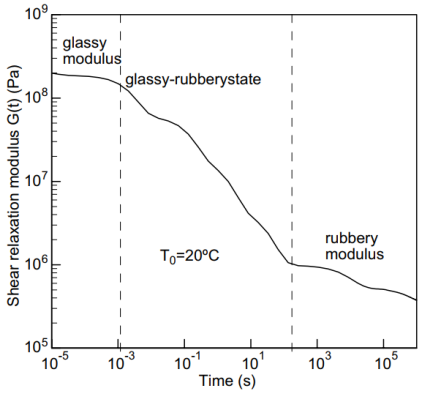

Figure 37 - Shear Relaxation of PVB (Adapted from [37])

The behavior of the PVB changes highly with temperature, in which the flexibility and capacity for tension transference between glass plies vary. In higher temperatures, PVB reduces the capability of transferring tensions between glass plies. In lower temperatures the capacity from transferring the tensions between glass plies is almost total, but the total extension before rupture is lower. In ambient temperature, the PVB is extremely flexible, and the maximum extension considered before rupture is 200%, even though it can reach higher strain rates [30]. Also, PVB has a stress-strain rate that depends on the time duration of a load, having a behavior of a viscoelastic material. The shear modulus of the PVB decreases with higher load time durations and increases when the load duration is lower. This is usually called shear relaxation. In Figure 37 it is shown the variation of the shear relaxation modulus with the time duration of a load with PVB at 20 ºC [11], [37].

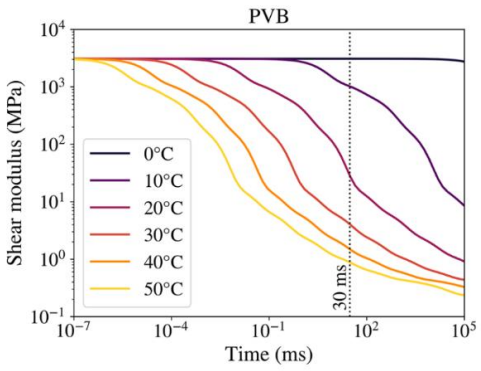

Figure 38 - Shear Modulus Variation with Temperature (Adapted from [38])

Also, the temperature variation in PVB induces variations in the Shear Modulus, making it important to know the temperature in which the experiments are made. As verified in Zemanová et al. [38], the shear modulus variation for different temperatures is clearly visible as shown in Figure 38.

For construction purposes, the PVB is affected by humidity, and one consequence of it is the loss of adherence to the glass, making it lose properties. This phenomenon is called the delamination of PVB. To prevent delamination, the recommended method is to protect the surroundings of the laminated glass panel, making it almost impossible for water to have contact with the PVB [33]. In Table 7 it is shown some characteristically values for PVB.

Table 7 - PVB Properties (Adapted from [31], [32])

Properties	Value	Units
Mass Density, ρ	1070	kg/m^3
Shear Modulus, G	Variable	GPa
Poisson's Coefficient, v	0.485	-
Thermal Expansion Coefficient, α	80 x 10^{-6}	1/K
Yield Strength, f_t	28	MPa
Strain at rupture, ε_t	2	-
Young's Modulus, E	530	MPa

3.3. Fixing Systems

The fixing systems choices used in the glazing systems are wide, and used according to necessity, and today the fixing systems can be divided into different categories. The objective of the fixing systems is to hold the glass and provide the distance between the glass and the steel or other structural element, so that the glass does not make contact with it, to prevent damage and breaking possibility [33].

The diagram presented in Figure 39 shows the different types of fixing systems used nowadays in glazing solutions. To glazing façades, one fixing system that is used to better make use of glass is the continuous clamped solution, as it is commonly seen in windows.

For the MSc Dissertation it was decided to use a fixing system with continuous fixing solution, to maximize the capacity of the glass to withstand a blast load.

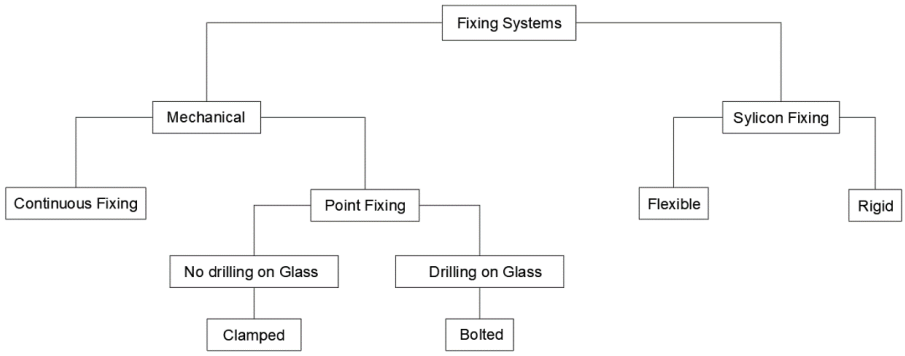

Figure 39 - Fixing Systems (Adapted from [39])

3.4. Energy-Dissipation Devices using Polymeric Materials

For a better response of the glazing panel, its used in this MSc Dissertation the concept of using a device that could dissipate some of the total energy transmitted from the blast to the glass and consequently the structure. As it is concluded in Martins [13] after the experiments using the Explosive Driven Shock Tube, the usage of an Energy-Dissipation can improve the behavior and resistance of a glazing solution to a blast wave. These devices are made from PETG and have an auxetic geometry with the 125x50x42 mm as showed in the schema below.

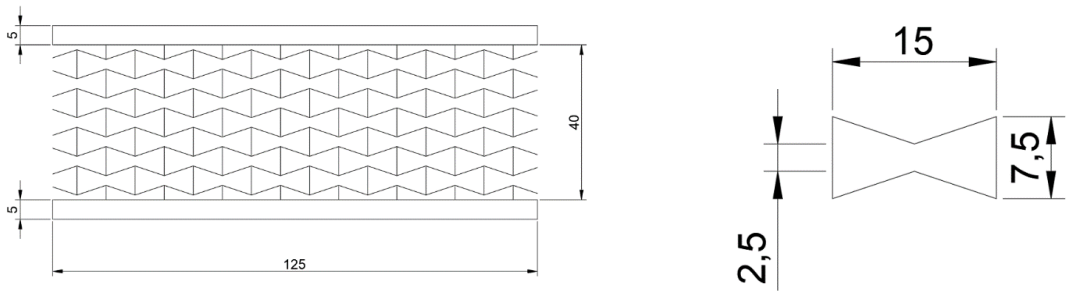

Figure 40 – Energy Dissipator Geometry (Left), Auxetic Geometry Cell (Right)

The geometry is divided between two parts, the solid part, which has a 5 mm thickness, and the auxetic cellular geometry which has 0.8 mm thickness as it can be seen in Figure 40.

3.4.1. Characteristics

A metamaterial is an artificial material, where it is possible to change its physical or chemical formulation to get better mechanical, electrical, thermal or even acoustic properties [40]. The mechanical metamaterials are a little bit different from other metamaterials where a change their chemical elements is possible to obtain the results needed. Mechanical metamaterials are made from current conventional materials, as for example PETG used in this MSc Dissertation, and then, these materials are made into different shapes and geometries than give much better results as an all piece, that the material could not offer if by itself [40].

The resort to 3D printing is a consequence of its evolution, and today it is possible to 3D print a wide number of materials, given certain properties. This technology makes possible to print complex designs to a certain limitation, where the result gives a good solution without any material loss, fast and easy to compute.

In this MSc Dissertation, the objective is to use an auxetic geometry, represented in Figure 40, to get advantage from negative Poisson's coefficient as verified in Coutinho [14], so the response to dissipate energy is better due to experimental results [14]. PETG is the combination between PET (Polyethylene terephthalate) used commonly in water bottles for example, with glycol. This combination was made to better help the 3D printing of the material itself due to extrusion temperatures [14].

3.4.2. 3D Printing

3D printing has been evolving since it was first invented by Charles Hull in 1986. Today, it can be seen a variety of different methods to produce what is necessary. Some different processes like Stereolithography Apparatus (SLA), Laminated Object Manufacturing (LOM), Selective Laser Sintering (SLS) and Fused Deposition Modelling (FDM) are used nowadays out a wide range of many more.
Regarding FDM, it is an Addictive Manufacturing (AM) process that involves material extrusion. FDM builds layer by layer by deposing material in a determined path. The process is based on the principle of melting a thermoplastic in a certain temperature, and then extruding it through a proper nozzle, at a certain speed, at a certain quantity [41]. This principle can be seen in Figure 41.

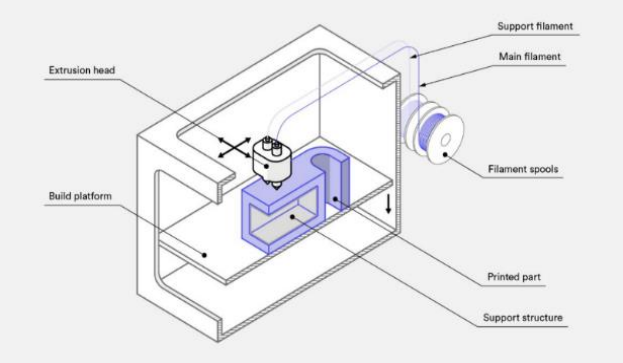

Figure 41 – 3D Printing principles (Source: [42])

The thermoplastic usually is in a filament that is connected to an extrusion head. In this extrusion head it is heated to the melting temperature, and then extruded through the nozzle while this extrusion head is moving in the X and Y axis. When the filament is deposed, it cools, and it returns to its original solid state. Layer by layer in Z axis, the filament is deposed to a final state, according to the digital file uploaded in the printer.

3.4.3. Sample Printing

To fabricate the Energy-Dissipation Devices, the process used was the FDM resorting to a Original Prusa i3 MK3S 3D printer (Figure *42*). It is important to note that the printed material, does not have the same characteristics has the filament used, as there is a difference when the material is printed at a 0-degree angle with the X or Y axis, or at a different angle for instance 45-degree angle or even more. Also, the direction of the load is important, meaning that it is possible to have a different behavior from the printed sample than the filament, as the load is applied differently to each one and the geometric configuration [43].

For the auxetic energy-dissipation device the filament of PETG used had 1.75 mm diameter and extruded at 0.4 mm diameter from the nozzle, with layers of 0.2 mm thickness. To ensure the minimum amount of printing errors, the temperature of the nozzle and the bed where constant during all the printing except for the first layer. The printing speed during the first layer is lower to minimize the probability of the non-adherence of the material to the bed, and the normal speed of 60 mm/s is almost constant during all the printing.

Figure 42 – Original Prusa i3 MK3S printing two samples

Table 8 – Printing Parameters

Parameter	Value
Nozzle Temperature (1st Layer)	240 ºC
Nozzle Temperature	250 ºC
Bed Temperature (1st Layer)	85 ºC
Bed Temperature	90 ºC
Layer Thickness	0.2 mm
1st Layer Printing Speed	20 mm/s
Average Printing Speed	60 mm/s
Maximum Printing Speed	200 mm/s

Chapter 4. Case Study Pre-Design

4.1. Case Study

The case study is a glazing façade of 2x1 m^2 of laminated tempered glass. Each pane of tempered glass has 10 mm thickness, and the PVB interlayer has 1.52 mm. The laminated glass is fixed with a continuous clamped solution with two 15x100 mm steel plates, and behind it, the energy-dissipation devices. The final set-up is supported by SHS 200x200x8 beams, along with threaded bolts and the respective nut. The energy-dissipation devices are place between a steel plate, to better support the compression forces from the impulse of a blast load.

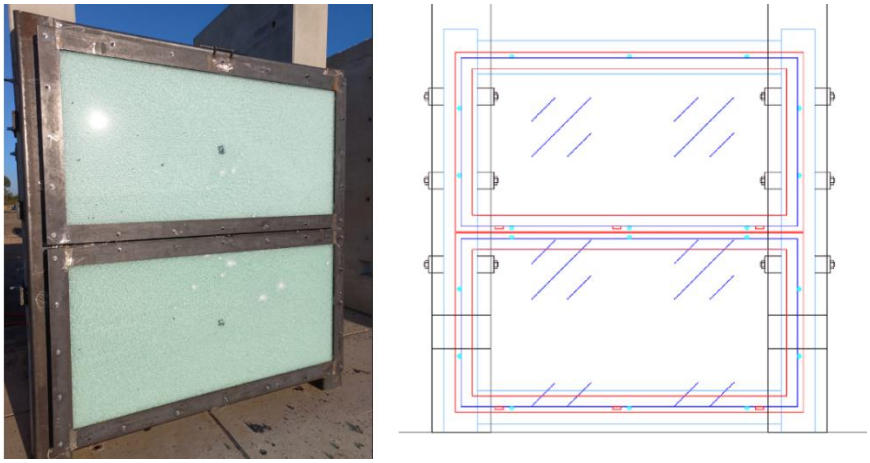

Figure 43 – Experimental set-up

4.2. Steel Structure Calculation

The case study is supported by a steel structure that is connected to a concrete wall considered as rigid, due to its size compared to the applied load. The design load applied on the steel structure can be obtained by a simple calculation considering a simply supported beam of 2 m, as it is the worst-case scenario for the situation.

4.2.1. Elastic Bending Moment Resistance

The profile chosen was a Square Hollow Section SHS 200x200x8 with S355 J2H steel with the following characteristics:

Table 9 – SHS 200x200x8 Parameters

Variable	Value
Elastic Modulus, W_{el}	371 cm^3
Young's Modulus, E	210 Gpa
Mass per meter	47.7 kg/m
Moment of Inertia, I	3709 cm^4
Length, L	2 m

The elastic bending moment resistance of a steel SHS 200x200x8 is given by [EC3-1-1] [44]:

$$M_{Rd,El} = W_{el} \times f_y = 371 \times 10^{-6} \times 355 \times 10^3 = 131.71\ \text{kNm} \quad (4.1)$$

The applied load in the SHS is not static, but an impulse load, which implies that the resistance of the SHS profile will be higher, since the time that the structure is submitted to the load is around 5ms, which is approximately the time of an impulse load of 10kg@10m [45]. The calculation of the resistance to a blast load is written in Biggs [46] as a simple approach of a Single Degree of Freedom (SDOF) analysis of a beam.

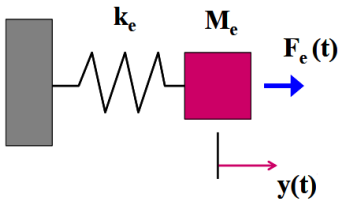

Figure 44 – SDOF approach (Adapted from [47])

being k_e the spring stiffness; M_e the Mass of the body; $F_e(t)$ the force applied in time and y(t) the response of the body to the force in time. The relation between the elastic deflection and the maximum deflection is taken as $y_m = y_{el}$.

When an elastic response is chosen, it is important to take into account several factors such as the Uniform Mass Factor, K_M, and the Load Factor, K_L, and the spring constant, k. The values are given in Table 10.

Table 10 – Parameters for a simple supported beam submitted to a dynamic load (Adapted from [46], [47])

Loading diagram	Strain range	Load Factor, K_L	Uniform Mass Factor, K_M	Maximum Resistance, R_m	Spring constant, k
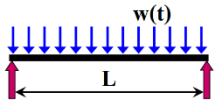	Elastic	0.64	0.50	$\frac{8 \times M_{Rd.El}}{L}$	$\frac{384 \times EI}{5 \times L^3}$

The maximum resistance for a simply supported beam submitted to an equivalent triangular load is calculated as:

$$R_m = \frac{8 \times M_{Rd.\ El}}{L} = \frac{8 \times 131.71}{2} = 526.82\ \text{kN} \quad (4.2)$$

The spring constant, k, can be obtained by:

$$k = \frac{384 \times EI}{5 \times L^3} = \frac{384 \times 210 \times 10^6 \times 3709 \times 10^{-8}}{5 \times 2^3} = 74773.44\ \text{kN/m} \quad (4.3)$$

The mass of the body considers also the associated mass of the structure that is connected to the beam. The glass and the steel structure are taken into consideration. The mass density of every material as well as the considered quantity is shown in Table 11. From Table 9 it is known directly the value of mass per meter.

The total mass can be calculated as:

$$M = L \times m = 2 \times (11.8 + 50 + 47.7) = 219\ \text{kg} \quad (4.4)$$

Table 11 - Quantities in mass per meter of the steel structure

Material	Mass Density (kg/m^3)	Dimension (mm^2/m)	Quantity per meter (m/m)	Mass per meter, m (kg/m)
Steel Plates	7850	15x100	3	11.8
Laminated Glass	2500	1000x20	1	50
SHS 200x200x8	7850	-	1	47.7

The period of the structural beam in a SDOF analysis submitted to a blast load is defined in Biggs [46] as:

$$T = 2\pi\sqrt{\frac{M_e}{k_e}} = 2\pi\sqrt{\frac{K_M \times M}{K_L \times k}} = 2\pi\sqrt{\frac{0.5 \times 219}{0.64 \times 74773.44}} = 0.30s \quad (4.5)$$

It is possible to use a graphical solution from UFC charts:

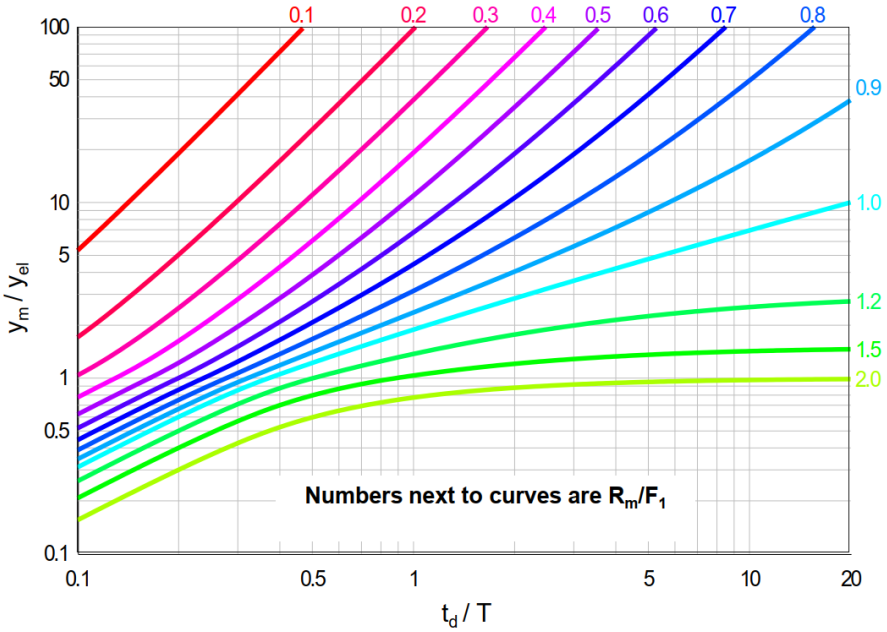

Figure 45 - Maximum deflection of elasto-plastic SDOF system to an impulse loading (Adapted from [23])

The value of t_d is taken as 5 ms which is the reference value for the duration of a blast load. Therefore:

$$\frac{t_d}{T} = \frac{0.005}{0.30} = 0.017 \quad (4.6)$$

And from the initial assumption:

$$\frac{y_m}{y_{el}} = 1 \quad (4.7)$$

The interception can be given as follows:

$$\frac{R_m}{F_1} = 0.3 \tag{4.8}$$

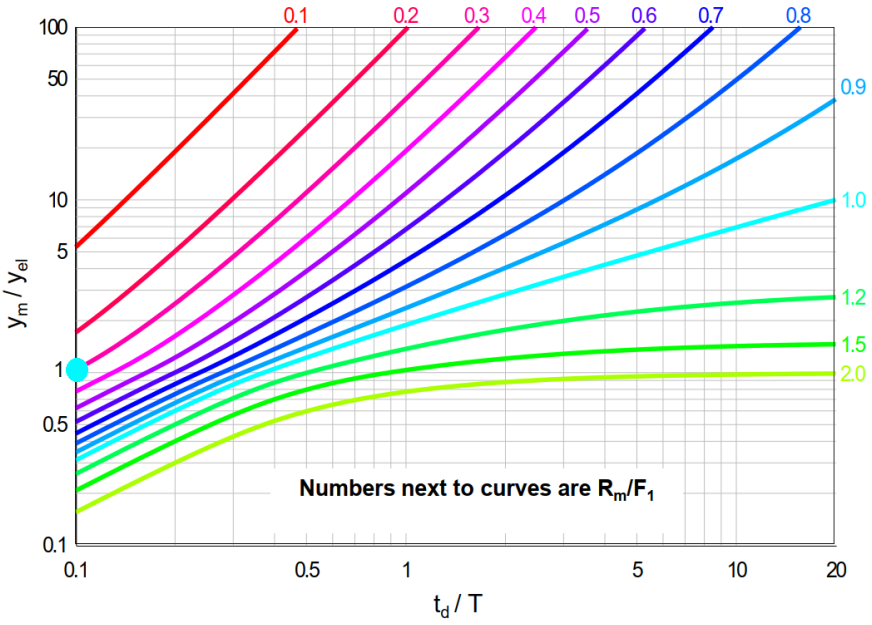

Figure 46 - Interception of the calculation with the graphical solution

Which means that:

$$F_1 = \frac{R_m}{0.3} = \frac{526.82}{0.3} = 1756.1 \text{ kN} \tag{4.9}$$

For different blast pressures at different stand-off distances, the pressures are shown in Table 12.

Table 12 - Peak Reflected Pressures for different explosions

Weight (kg of TNT)	Stand-off Distance (m)	Peak Reflected Pressure (kPa)
5	5	354.2
5	7	153.9
5	9	91.0
10	10	117.2

Considering that the glass is rigid, as well as the rest of the structure, we can see can multiplying the pressure by the area on influence of 2 m^2, the obtained values are presented in Table 13.

Table 13 - F1 calculation for given Peak Reflected Pressures

Peak Reflected Pressure (kPa)	F1 Equivalent
354.2	708.2
153.9	307.8
91.0	182
117.2	234.4

As it can be seen, the bending resistance to a blast load of a SHS 200x200x8 beam is more than enough to withstand blast pressures caused by a detonation of 5 kg of TNT at a stand-off distance of 5 meters. For this reason, the Steel Structure represented in Figure *47* will resist the blast loading of the same order.

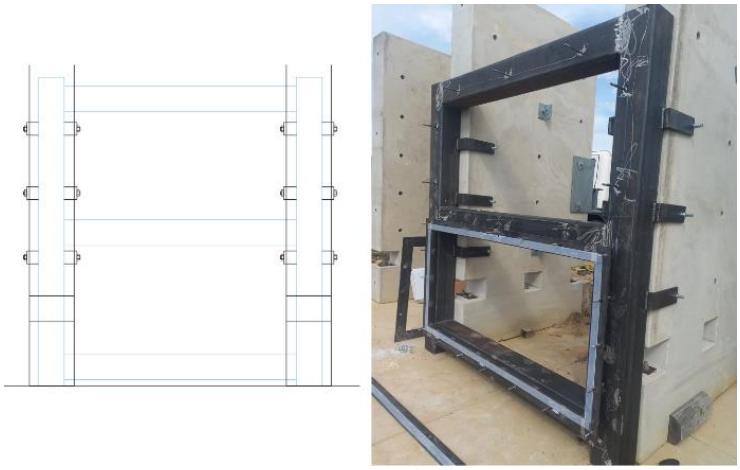

Figure 47 - Steel Structure

4.2.2. Welding

The welding resistance ($F_{w,Rd}$) it is obtained by [48]:

$$F_{w,Rd} = \frac{f_u/\sqrt{3}}{\beta_w \gamma_{M2}} a\, l_w \tag{4.10}$$

The safety factor given by EC3-1-8 [48], γ_{M2} is equal to 1.25. The welding objective is to support the laminated glass, that has a mass density of 2500 kg/m^3. The weight of the glass is transmitted to the welding almost by pure transversal force.

$$V_{Ed} = 9.8 \times 2500 \times 2 \times 1 \times 0.020 = 980\ N \tag{4.11}$$

For a 3 mm welding diameter and a S355 steel, it is possible to use a table to simplify the calculations [49].

Table 14 - Resistance of 100 mm welding (Adapted from [49])

S355	**l_w = 100 mm**		
a (mm)	3	4	5
$F_{w.Rd}$ (kN)	72.4	96.5	120.6

As it can be seen in Table 14, for l_w of 100 mm, a 3 mm diameter in welding can resist 72.4 kN, which is safe by a large margin since l_w is taken as 150 mm.

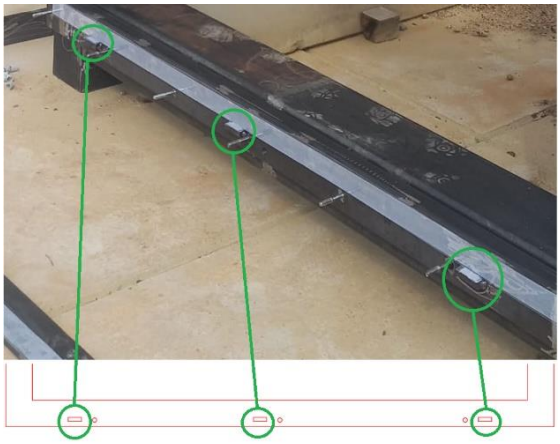

Figure 48 - Welding zones for Supporting Glass

4.2.3. Fixing Plates

For the proposed objective, the glazing solution as a continuous clamped fixing system, therefore, steel plates were chosen to clamp the glass. The dimensions of the cross section for the steel plates were 0.1x0.015 mm^2 and the hole diameter for the threaded bolt was designed to 16 mm.

To hold the plates and the glass attached to the structure, M12 Cl8.8 threaded bolts were used. The considered threaded bolts were the M12 ones, since those are the one that will resist the tension force if, eventually, the negative pressure is high enough to pull the glass panel in the opposite direction that it is supposed to move.

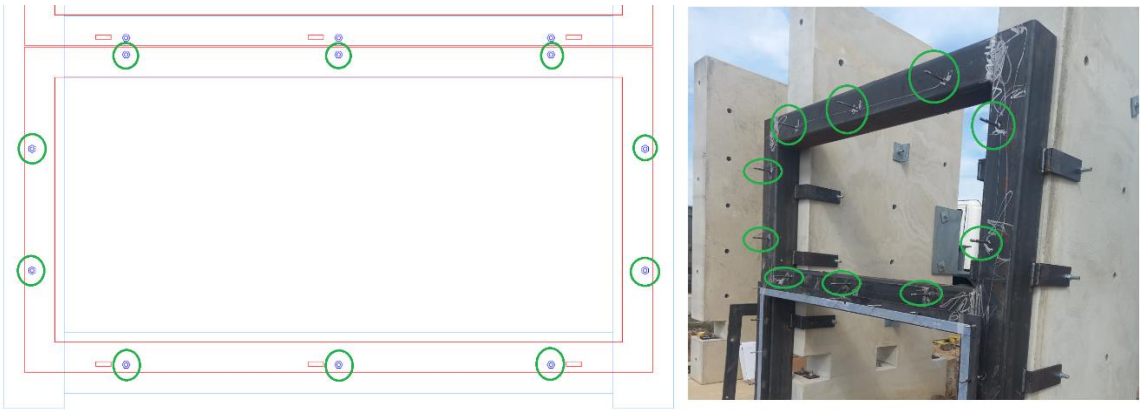

Figure 49 – M12 Threaded bolts considered to be submitted to tension causing punching shear effects in the fixing plate

To ensure its safety from the punching shear effect of the threaded bolt on the steel plate was considered as [48]:

$$B_{p,Rd} = \frac{0.6 \times \pi \times d_m \times t_p \times f_{ub}}{\gamma_{M2}} \quad (4.12)$$

According to [49], the table presented shows the minimum thickness of a plate to which the resistance of the tension of the bolt or threaded bolt, $F_{t,Rd}$, starts to be the conditioning force.

Table 15 - Minimum thickness of a plate for $B_{p,Rd} > F_{t,Rd}$ (Adapted from [49])

	Steel	Class	M12	M24
Punching Shear – $t_{Bp,min}$ (mm)	S355	5.6	2.3	5.1
		8.8	3.7	8.2
		10.6	**4.6**	10.2

The designed value for the plates with M12 Cl 8.8 threaded bolts was 15 mm, and for this reason, the tension resistance of the threaded bolt is the design force, and it will be used further in this Chapter.

4.2.4. Threaded Bolts

4.2.4.1 M24 Design Calculation

The threaded bolts were designed to support the metal plates and the glazing solution.

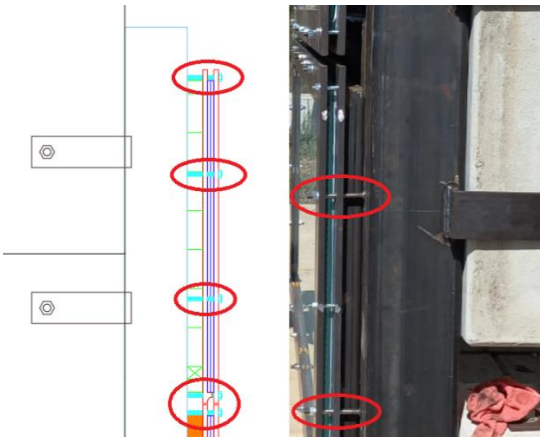

Figure 50 - M12 Threaded Bolts Supporting the Glass Panel

The resistance of one M12 Cl 8.8 to shear load in the threaded zone is given by [EC3-1-8] [48]:

$$F_{v,Rd} = \frac{a_v \, f_{ub} \, A_s}{\gamma_{M2}} \tag{4.13}$$

where a_v = 0.6 for 8.8 Class, γ_{M2} = 1.25 and f_{ub} is 800 MPa. A_s is the area of the cross section of the bolt.

$$F_{v.Rd} = \frac{0.6 \times 800 \times 10^3 \times 113.1 \times 10^{-6}}{1.25} = 43.43 \text{ kN} \tag{4.14}$$

To evaluate the design resistance the weight of the glass and the glazing solution was taken into account. As so, it was noted that the load was static. The steel plates weight was calculated as:

$$\begin{gathered} M = 2 \times (\text{Perimeter} \times \text{Cross Section} \times \text{Steel Mass Density}) \\ M = 2 \times (4 \times 0.1 \times 0.015 \times 7850) = 94.2 \text{ kg} \end{gathered} \tag{4.15}$$

The glass weight was calculated as:

$$\begin{gathered} M = \text{Volume} \times \text{Mass Density} \\ M = 2 \times 1 \times 0.02 \times 2500 = 100 \text{ kg} \end{gathered} \tag{4.16}$$

The total load in the threaded bolts is assessed by:

$$F_{Ed} = (M_{Steel\ Plates} + M_{Glass}) \times g = (94.2 + 100) \times 9.8 = 1.903\ kN \quad (4.17)$$

The load applied into the threaded bolts is much lower that its shear resistance meaning that, theoretically, it was only needed one bolt to support the shear load of the panel, therefore safety is maintained, since there are 10 threaded bolts. For the connection between the structure and the concrete wall, the threaded bolts used were M24 Cl 8.8 (Figure *51*).

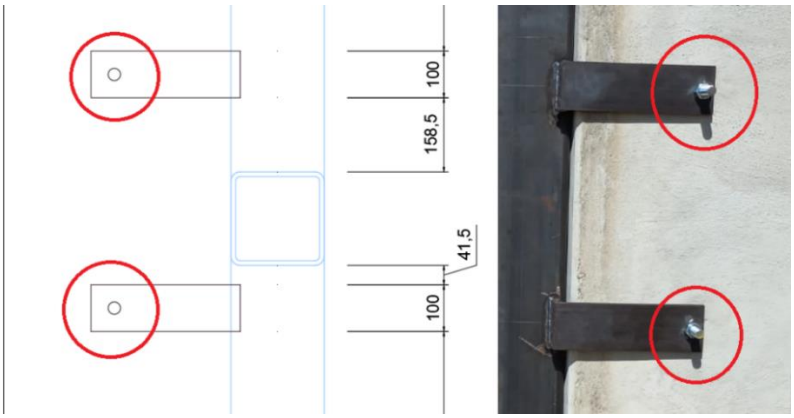

Figure 51 - Threaded Bolts Connecting the Wall and the Steel Structure

The calculations needed for the assessment of the shear resistance were the same as an M12 Cl 8.8 threaded bolt, therefore:

$$F_{v.Rd} = \frac{a_v\, f_{ub}\, A_s}{\gamma_{M2}} = \frac{0.6 \times 800 \times 10^3 \times 452.4 \times 10^{-6}}{1.25} = 173.72\ kN \quad (4.18)$$

Since the threaded bolt is resisting shear in both ends, the resistance is multiplied by 2, which equals a value of 347.44 kN.

According to UFC [23] and the America Society of Civil Engineers (ASCE), the resistance of a structural steel element can be increased since the load applied is dynamic. The presented table shows the Dynamic Increase Factors for different structural steel elements.

Table 16 - Dynamic Increase Factors for Steel Structures (Adapted from [23])

Steel (American Standard)	**Steel (European Standard)**	**Bending/Shear**		**Tension/Compression**	
		Low Pressure (Strain Rate = 2.54 mm/mm/s)	**High Pressure (Strain Rate = 7.62 mm/mm/s)**	**Low Pressure (Strain Rate = 0.51 mm/mm/s)**	**High Pressure (Strain Rate = 1.27 mm/mm/s)**
A36	Equivalent to S235	1.29	1.36	1.19	1.24
A588	Equivalent to S355	1.19	1.24	1.12	1.15
A514	**Equivalent to Yield strength of 700 MPa**	1.09	**1.12**	1.05	1.07

It is assumed that the threaded bolt acts as a structural steel element. The dynamic increase factor chosen was based on a high pressure, where the strain rate is high, to ensure the safety of the system, and so, the value of the Dynamic Increase Factor (DIF) is 1.12 for being the closest value of

the threaded bolt design resistance which is 800 MPa. For the dynamic yield strength calculation, it was considered as [23]:

$$f_{ds} = f_{dy} = c \times a \times f_y \tag{4.19}$$

where, f_{dy} is dynamic yield strength; c is the dynamic increase factor on the yield strength, chosen as 1.12; a is an average strength increase factor (1.1 for steels with a specified minimum yield strength of an S355 Steel or less or 1.0 if otherwise) and f_y is the static yield strength. The yield strength of a threaded bolt can be calculated as:

$$f_{dy} = 1.12 \times 1 \times 800 = 896 \text{ MPa} \tag{4.20}$$

$$F_{v.Rd} = 2 \times \frac{0.6 \times 896 \times 10^3 \times 452.4 \times 10^{-6}}{1.25} = 2 \times 194.57 \text{ kN} = 389 \text{ kN} \tag{4.21}$$

For the next calculation it was assumed that all the structure is disconnected from the concrete wall and the applied load will move all the structure backwards, applying all the force on the threaded bolts that will resist through shear. The influence area considered for the threaded bolt in the worst-case scenario is presented in Figure *52***Erro! A origem da referência não foi encontrada.**.

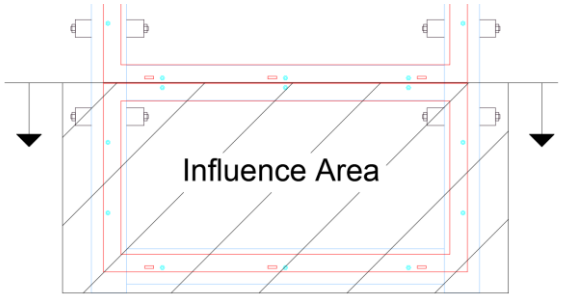

Figure 52 - Considered Influence Area for Calculation of M24 Threaded Bolts

The applied load was assumed to be a consideration of the calculations made previously considering that the reaction loads are multiplied by the influence area and then calculate the applied load in the worst-case scenario threaded bolt. In Table *17* are presented the values used for threaded bolts resistance to a dynamic load [46], [47].

Table 17 - Parameters for a simple supported beam submitted to a dynamic load (Adapted from [46], [47])

Loading diagram	Strain range	Load Factor, K_L	Uniform Mass Factor, K_M	Dynamic Reaction, V
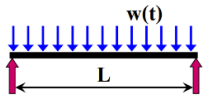	Elastic	0.64	0.50	0.39R + 0.11F

In which R is the static reaction force. And F was considered as the pressure of a blast load of 5kg@5m which is 708.2. [46] Meaning that V was calculated as:

$$V = 0.39 \times \frac{708.2 \times 2}{2} + 0.11 \times 708.2 = 354.1 \text{ kN} \tag{4.22}$$

As it is shown by the calculations, even the worst-case scenario considered is not enough to yield the threaded bolt.

4.2.4.2. M12 Design Calculation

The approximation taken for the tension of the threaded bolts was gross because the value of the positive impulse of an explosion will never be lower than the negative impulse, first, because it is an impulse load, and second because the negative impulse of an explosion is never higher than the positive impulse, but if the design can resist the load, therefore, it is safe to use in every situation.

The load considered was the value for an explosive charge of 5kg@5m, which is 708.2 kN, divided by 10 threaded bolts, which is:

$$F_{Ed} = \frac{708.2}{10} = 71\ \text{kN} \tag{4.23}$$

For tension resistance of a threaded bolt according to EC3-1-8 [48] the calculation follows as:

$$F_{t,Rd} = \frac{0.9 \times A_s \times f_{ub}}{\gamma_{M2}} \tag{4.24}$$

The applied load in each threaded bolt is 71 kN as seen before and shown in Figure 49, and the dynamic resistance can be calculated as:

$$F_{t.Rd} = \frac{0.9 \times 113.1 \times 10^{-6} \times 896 \times 10^{3}}{1.25} = 72.96\ \text{kN} \tag{4.25}$$

As it can be seen, the value for $F_{t,Rd}$ is enough to resist the same load as tension, even though it is known that is not possible to have the same order of values for negative force as for positive force.

4.3. Glass Structure Calculation

For the design of the glazing solution, it was considered that, the solution could resist the wind action at a 50-meter-high building with a full glazing façade using continuous clamped fixing system. The considered panel was the cornered one because it is according to EN 1991-1-4 [50] the worst-case scenario to wind loads.

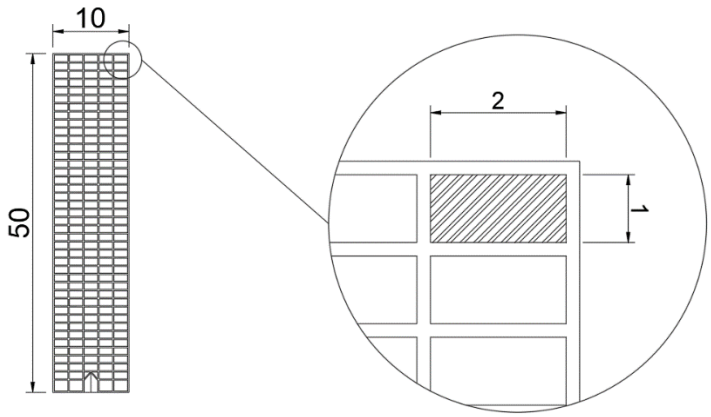

Figure 53 - Considered Building for Glazing Design

4.3.1. Preliminary Design to Wind Resistance

4.3.1.1. Wind Pressure

It is considered for the wind resistance calculation that the building is located in Cascais, Lisbon, near seacoast, without surrounding buildings, which according to the National Annex the Zone is B and the terrain category is chosen to be I. For Zone B the basic wind speed, $v_{b,0}$, is 30 m/s, and for category I, Z_0 is 0.005 m and Z_{min} is 1 m. The reference value according to EC1-1-4 [50] can be obtained by:

$$v_b = c_{dir} \times c_{season} \times v_{b,0} \tag{4.26}$$

The recommended values for the direction coefficient, c_{dir}, and season coefficient, c_{season} by the national annex are 1 for both parameters.

$$v_b = v_{b,0} = 30\ m/s \tag{4.27}$$

The wind speed changes with heigh, meaning that a tall building will have more pressure from wind than a small building. The calculation is:

$$v_m(z) = c_r(z) \times c_0(z) \times v_b \tag{4.28}$$

being $c_0(z)$ the orography coefficient that according to the national annex can be taken as 1 and the $c_r(z)$ the rugosity coefficient, obtained according to the Portuguese National Annex as:

$$\begin{cases} c_r(z) = k_r \times \ln\left(\dfrac{z}{z_0}\right) & \text{for } z_{min} \le z \le z_{max} \\ c_r(z) = c_r(z_{min}) & \text{for } z \le z_{min} \end{cases} \tag{4.29}$$

where Z_0 is the roughness length and k_r is the roughness coefficient that depends on the roughness length, Z_0, obtain by:

$$k_r = 0.19 \times \left(\frac{z_0}{z_{0.II}}\right)^{0.07} \tag{4.30}$$

And Z_0 is 0.003 m, $Z_{0,II}$ is 0.05 m, Z_{max} is 200 m and Z_{min} is the minimum height defined as 1 according to the national annex.

$$k_r = 0.19 \times \left(\frac{0.003}{0.05}\right)^{0.07} = 0.156 \tag{4.31}$$

$$c_r(z) = 0.156 \times \ln\left(\frac{50}{0.003}\right) = 1.517 \tag{4.32}$$

$$v_m(z) = 1.517 \times 1 \times 30 = 45.5\ m/s \tag{4.33}$$

Another fact to take into consideration is the turbulence, calculated as:

$$\begin{cases} I_v(z) = \dfrac{\sigma_v}{v_m(z)} = \dfrac{k_I}{c_0 \times \ln(z/z_0)} & \text{for } z_{min} \le z \le z_{max} \\ I_v(z) = I_v(z_{min}) & \text{for } z \le z_{min} \end{cases} \tag{4.34}$$

k_I is 1 by recommendation of EC1-1-4 [50].

$$I_v(z) = \frac{1}{1 \times \ln(50/0.005)} = 0.109 \tag{4.35}$$

To obtain the dynamic peak pressure for wind the following equation was solved:

$$q_p(z) = [1 + 7 \times I_v(z)] \times \frac{1}{2} \times \rho \times v_m^2(z) = c_e(z) \times q_b \tag{4.36}$$

The parameter ρ is the mass density of air, that depends on the height, temperature and atmospheric pressure of the region during intense wind situations according to EC1-1-4 [50]. The recommended value is 1.25 kg/m^3.

The exposure coefficient, $c_e(z)$ is calculated as:

$$c_e(z) = \frac{q_p(z)}{q_b} \tag{4.37}$$

And the dynamic pressure reference for wind, q_b can be obtained by:

$$q_b = \frac{1}{2} \times \rho \times v_b^2 \tag{4.38}$$

$$q_p(z) = [1 + 7 \times 0.109] \times \frac{1}{2} \times 1.25 \times 45.5^2 = 2281.16\ \mathrm{N/m2} = 2.28\ \mathrm{kN/m^2} \tag{4.39}$$

To calculate the pressure that a wind causes in a surface at a specific height, it is important to consider the dimensions of the building as well as certain parameters.

The wind pressure in a surface follows as:

$$w_e = q_p(z_e) \times c_{pe} \tag{4.40}$$

The dimensions of the building are 50 meters of height with a square configuration from the ground to the top with a 10 meters width. For higher buildings, one important thing to consider is that, the higher the building, the higher the wind pressures become. The difference between pressures is written in EN 1991-1-4 [50] as in Figure 54.

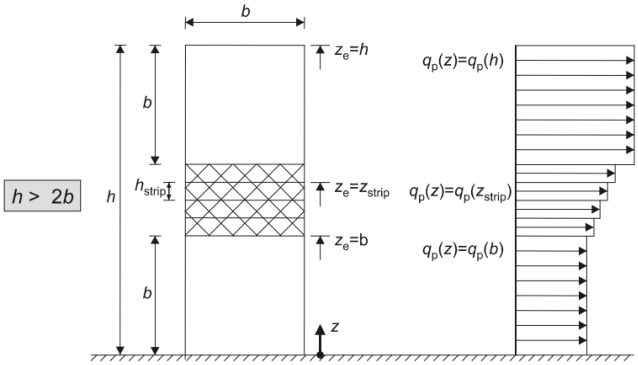

Figure 54 - Wind Pressure variation with height (Adapted from [50])

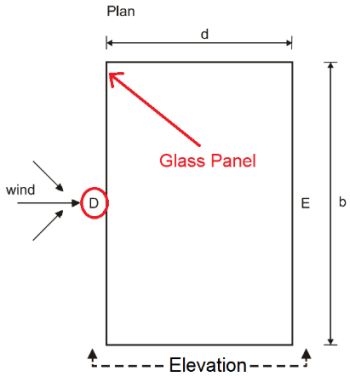

Figure 55 - Zone to take into consideration and Panel location (Adapted from [50])

According to EN 1991-1-4 [50], the situation varies with the geometry. To the chosen geometry the elevation, e, is greater than two times the width. In Figure 55 it is shown the areas of influence of the wind pressure associated with the problem being $h = b = 50\ \mathrm{m}, d = 10\ \mathrm{m}$.

Table 18 - Wind multiplier coefficients (Adapted from [50])

Zone	A		B		C		**D**		E	
h/d	$c_{pe.10}$	$c_{pe.1}$	$c_{pe.10}$	$c_{pe.1}$	$c_{pe.10}$	$c_{pe.1}$	$c_{pe.10}$	**$c_{pe.1}$**	$c_{pe.10}$	$c_{pe.1}$
5	-1.2	-1.4	-0.8	-1.1	-0.5		+0.8	**+1.0**	-0.7	
1	-1.2	-1.4	-0.8	-1.1	-0.5		+0.8	+1.0	-0.5	
≤ 0.25	-1.2	-1.4	-0.8	-1.1	-0.5		+0.7	+1.0	-0.3	

To maximize the load in the glazing panel, it was chosen the highest number of the table giving the design conditions, which is $c_{pe,1}$ of Zone D, the windward side.

$$w_e = q_p(h) \times c_{pe} = 2.28 \times 1 = 2.28\ kN/m^2 \quad (4.41)$$

4.3.1.2. Glazing Design

The Glass resistance to a wind load was designed according to the Pre-European Norm [51] for glass resistance calculation and testing. The chosen glass was a laminated glass with two tempered glass panes with a total of 20 mm thickness.

The resistance of a prestressed glass according to the norm [51] is as follows, which is independent from its composition:

$$f_{g,d} = \frac{k_{mod} k_{sp} f_{g,k}}{\gamma_{M,A}} + \frac{k_v (f_{b,k} - f_{g,k})}{\gamma_{M,v}} \quad (4.42)$$

Where, k_{mod} is the factor for the load duration in hours; k_{sp} is the factor for the glass surface profile; $f_{g,k}$ is the characteristic value of the bending strength; k_v is the factor for strengthening of prestressed glass; $f_{b,k}$ is the characteristic value of the bending strength of prestressed glass; $\gamma_{M,A}$ is the material partial factor for annealed glass and $\gamma_{M,v}$ is the material partial factor for surface prestress.

And k_{mod} can be calculated as:

$$k_{mod} = 0.663\ t^{-\frac{1}{16}} \quad (4.43)$$

This formulation is valid for values of time higher than 20 ms. For normal buildings, the minimum value recommended is 0.25 and the maximum is 1 as it is the value for dimensioning resistance against peak wind pressure. Table 19 shows different values for k_{mod}.

Table 19 - Values for k_{mod} according to an action (Adapted from [51])

Action	Load Duration	k_{mod}
Personnel loads	Short. Single	0.89
Wind	Single Gust	1
Wind	Short. Multiple	0.74
Snow	Intermediate	0.44
Daily temperature variation (eleven hours extreme peak duration)	Intermediate	0.57
Barometric pressure variation	Intermediate	0.50
Yearly temperature variation (six-month extreme mean value duration)	Intermediate	0.39
Dead load, self-weight	Permanent	0.29

The k_{mod} considered was 1, as it is the worst-case scenario for the glazing solution. Some values presented by the pre-norm for the glass surface profile are:

Table 20 - Values for k_{sp} (Adapted from [51])

Glass Material (whichever glass composition)	Factor for glass surface profile. k_{sp}	
	As produced	Sandblasted
Float glass	1.0	0.6
Drawn sheet glass	1.0	0.6
Enameled float or drawn sheet glass	1.0	0.6
Patterned glass	0.75	0.45
Enameled patterned glass	0.75	0.45
Polished wired glass	0.75	0.45
Patterned wired glass	0.6	0.36

The value of the glass surface profile, k_{sp}, chosen was float glass as produced that is 1. In Table 21 is presented the characteristic strength for prestressed glass.

Table 21 - Values for $f_{b,k}$ (Adapted from [51])

Glass material per product (whichever composition)	Values for characteristic bending strength, $f_{b,k}$, for prestressed glass processed from:		
	Thermally toughened safety glass to EN 12150, and heat soaked thermally toughened safety glass to EN 14179	Heat strengthened glass to EN 1863	Chemically strengthened glass to EN 12337
Float glass or drawn sheet glass	**120**	70	150
Patterned glass	90	55	100
Enamelled float or drawn sheet glass	75	45	
Enamelled patterned glass	75	45	

The laminated glass chosen for the case of study was composed by thermally strengthened safety glass panes and according to the Pre-Norm [51] the value of $f_{b,k}$ is 120 N/mm^2.

Table 22 - Values for k_v (Adapted from [51])

Manufacturing Process	Strengthening factor, k_v
Horizontal toughening (or other process without the use of tongs or other devices to hold the glass)	1.0
Vertical toughening (or other process using tongs or other devices to hold the glass)	0.6

For k_v the recommended value is 1. The $\gamma_{M,A}$ value is taken was 1.8 and the $\gamma_{M,v}$ was 1.2 as shown in Table 23 for the Ultimate Limit State.

Table 23 - Values for Ultimate Limit State resistance for glass (Adapted from [51])

	Ultimate Limit State
Annealed Glass	$\gamma_{M,A} = 1.8$
Surface Prestress	$\gamma_{M,v} = 1.2$

The final calculation taking into consideration the values that were taken, was:

$$f_{g.d} = \frac{1.0 \times 1.0 \times 45}{1.8} + \frac{1.0 \times (120 - 45)}{1.2} = 87.5 \text{ MPa} \quad (4.44)$$

As an approximation, for the resistance of the laminated glass submitted to a static load, it was used a simple calculation considering a simply supported slab in the sides [52]. The load applied was calculated by:

$$F_d(ELU) = \gamma_G \times G + \gamma_Q \times Q + \gamma_Q \times \Psi_0 \times Q \quad (4.45)$$

where G is not considered because the load is perpendicular to the panel and the panel is vertically oriented, meaning that the self-weight is supported by another structure that is not evaluated by this calculation. Q is the value for the wind pressure, w_e, Ψ_0 is taken as 0.6 as recommendation from the Pre-Norm [51] and γ_Q is 1.5 according to EC0 [53] for ultimate limit state.

$$F_d(ELU) = 1.5 \times 2.28 + 1.5 \times 0.6 \times 2.28 = 5.47 \text{ kN/m}^2 \quad (4.46)$$

Tabla 1.13

$\mu = 0,25$

$\gamma = \frac{a}{b}$

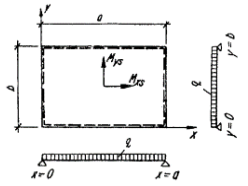

γ	w_s	M_{xs}	M_{ys}	T_{xs}	T_{ys}	R_{xs}	R_{ys}	R_0
1,00	0,0457	0,0460	0,0460	±0,338	±0,338	0,426	0,426	−0,070
1,10	0,0373	0,0389	0,0535	±0,314	±0,360	0,405	0,445	−0,065
1,20	0,0306	0,0330	0,0609	±0,293	±0,379	0,383	0,460	−0,068
1,30	0,0251	0,0281	0,0677	±0,274	±0,396	0,363	0,473	−0,066
1,40	0,0206	0,0240	0,0739	±0,257	±0,411	0,343	0,483	−0,064
1,50	0,0171	0,0205	0,0796	±0,242	±0,424	0,325	0,490	−0,061
1,60	0,0142	0,0177	0,0848	±0,228	±0,435	0,308	0,495	−0,059
1,70	0,0119	0,0154	0,0895	±0,215	±0,444	0,292	0,500	−0,056
1,80	0,0100	0,0134	0,0937	±0,204	±0,452	0,278	0,502	−0,054
1,90	0,0084	0,0118	0,0975	±0,194	±0,459	0,265	0,505	−0,052
2,00	0,0071	0,0104	0,1008	±0,185	±0,465	0,252	0,506	−0,049
Fact. de mult.	$\frac{qa^4}{Eh^3}$	qa^2	qb^2	qa	qb	qa	qb	qab

Figure 56 - Simple Supported Slab Values (Source: [52])

In Figure 56, it is shown the values for the calculation of the bending moments at the center of the slab. The a/b ratio is 2 and the maximum bending moments were calculated as:

$$M_{xs} = 0.0104 \times 5.47 \times 2^2 = 0.228 \text{ kNm} \quad (4.47)$$

$$M_{ys} = 0.1008 \times 5.47 \times 1^2 = 0.551 \text{ kNm} \quad (4.48)$$

To assess the tension of the glass the inertia of the glass panel was calculated as:

$$I_y = \frac{b \times h^3}{12} = \frac{1 \times 0.02^3}{12} = 6.66(7) \times 10^{-7} \text{ m}^4 \quad (4.49)$$

The final tension can be calculated as:

$$\sigma = \frac{N}{A} + \frac{M_y \times z}{I_y} - \frac{M_z \times z}{I_z} \quad (4.50)$$

Where z is equal to 0.01 m because of the consideration that the neutral axis is in the middle of the section.

$$\sigma = \frac{0.551 \times 0.01}{6.66(7) \times 10^{-7}} = 8265 \text{ kPa} = 8.27 \text{ MPa} \quad (4.51)$$

According to the Pre-Norm [51], the resistance of the laminated glass was calculated as 87.5 MPa, meaning that the resistance is much higher than the applied load.

4.3.2. Preliminary Design to Blast Resistance

Since the objective of the MSc Dissertation is to design a glazing façade capable of resisting a blast load. To do so, the glass resistance to a blast load can be assessed by the same method as the wind resistance, but the k_{mod} value changes because of the duration of the load. Note that, the adoption of k_{mod} for the design against a blast load contains errors, since, according to the Pre-Norm [51], the formula must only be used to values of duration down to 20 ms and the blast load duration is shorter. There are no other formulations in literature that predict the resistance of the glass to a blast load, therefore, k_{mod} was used, knowing that a certain error is implied. Depending on the blast load, the time can change between a large number of values. Table 24 holds different values of time regarding different detonations.

Table 24 - Pressure and Impulse values for different load combinations

Weight (kg of TNT)	Stand-off Distance (m)	Time (ms)	Peak Reflected Pressure (kPa)	Reflected Impulse (kPa.ms)
5	5	4.73	354.2	395.2
5	9	6.6	91.0	202.9
5	12	7.30	54.5	148.2
10	17	9.55	45.1	164.5

The value taken for the time of an explosion is 5 ms which is 0.005 s.

For this value, k_{mod} was calculated as:

$$k_{mod} = 0.663\, t^{-\frac{1}{16}} = 0.663 \times \left(\frac{0.005}{3600}\right)^{-\frac{1}{16}} = 1.54 \quad (4.52)$$

And the final calculation for the resistance of the glass submitted to a blast load was made as:

$$f_{g.d} = \frac{1.54 \times 1.0 \times 45}{1.8} + \frac{1.0 \times (120 - 45)}{1.2} = 101 \text{ MPa} \quad (4.53)$$

To obtain the resistance of the glass pane, a simply supported slab approximation could not be done because of the fact that, for a load like a blast, the behavior enters the non-linear analysis domain, and one possible way to calculate the tension and behavior of the glazing solution is to use a Finite Element (FE) program which is explained further.

Since k_{mod} is only a viable answer for load durations superior to 20 ms, and the duration of the positive phase of a blast load is less than 20 ms, it was chosen to use the United Facilities Criteria (UFC)

[23] tables that predict a response of a monolithic tempered glass pane response to an explosion. These tables can be used since, the laminated glass behaves like a monolithic pane of glass of the same thickness if subjected to a very short-term duration load.

In the graphic presented, the relationship of pressure and duration of the blast according to UFC [23], using a full tempered glass of 19,05 mm, and with the dimension of 1.07 x 2.14 m is:

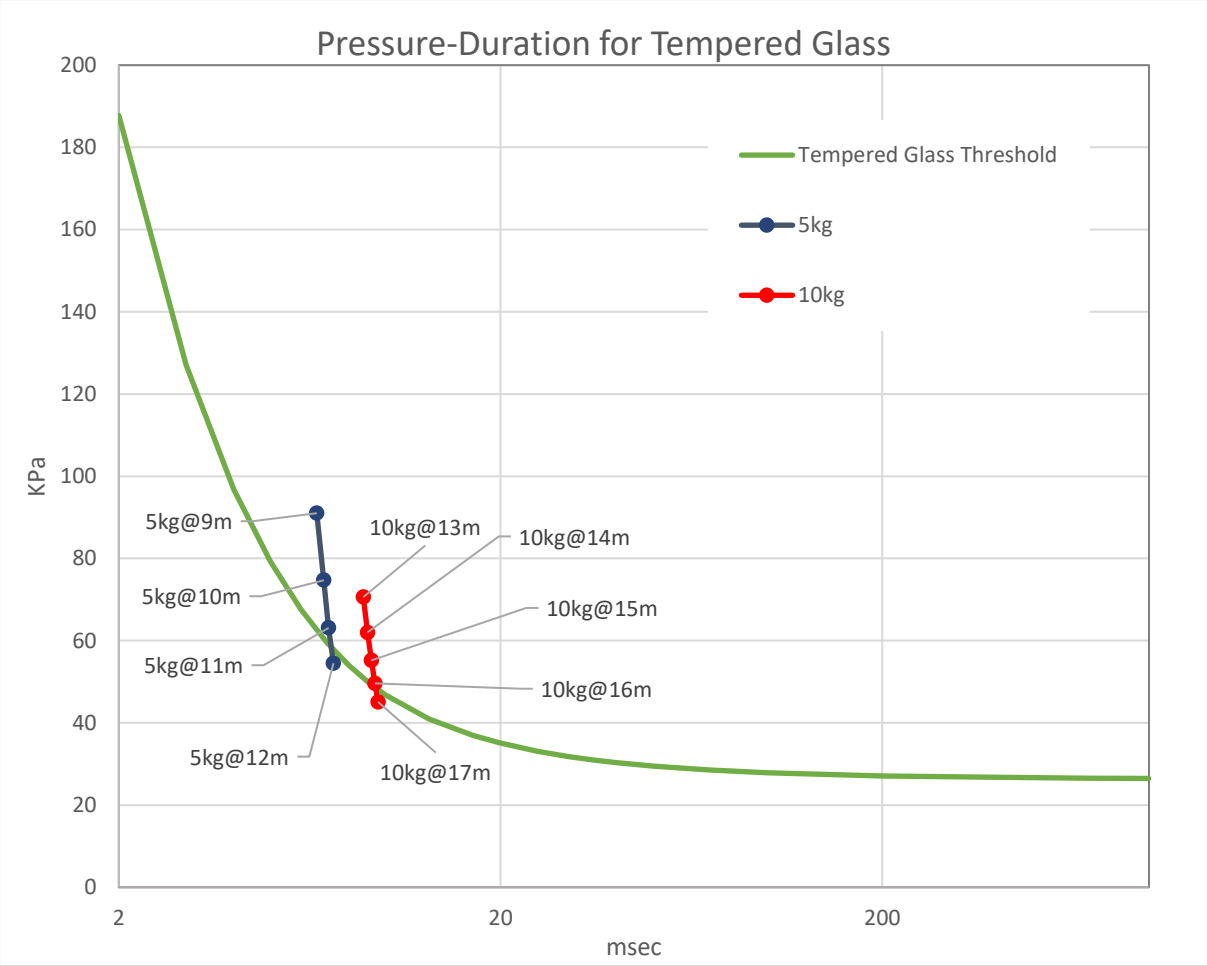

Figure 57 - Pressure-Duration Line for a 19.05 mm thickness tempered glass with 1.07x2.14 m^2 (Adapted from [23])

The graphic presented shows the threshold in which the tempered glass can withstand the blast load without breaking. If the pressure is above the line, the tempered glass will break.

Table 25 - Blast Resistance Response of UFC Tempered Glass

Charge	Scaled Distance, Z ($m/(kg^{1/3})$)	Positive Phase Duration, t_0^+ (ms)	Peak Reflected Overpressure, P_{so} (kPa)	Reflected Impulse, I_r (kPa.ms)	Glass Response
5kg@12m	7.02	7.30	54.5	148.2	Doesn't Fail
5kg@11m	6.43	7.09	63.1	162.8	Fails
5kg@10m	5.85	6.89	74.7	180.7	Fails
5kg@9m	5.26	6.60	91.0	202.9	Fails
10kg@17m	7.89	9.55	45.1	164.5	Doesn't Fail
10kg@16m	7.43	9.37	49.6	175.6	Fails
10kg@15m	6.96	9.17	55.2	188.3	Fails
10kg@14m	6.49	8.96	62.0	202.9	Fails

In Table 25 it can be seen that the expectancy of the glass to fail is related not only with the scaled distance but also with the reflected impulse that can also change if the scaled distance is different. Therefore, a laminated glass pane designed can withstand, according to UFC [23], the charges showed in Table 26.

Table 26 - Values of charges the glass can withstand according to UFC [23]

Charge	Scaled Distance, Z ($m/(kg^{1/3})$)	Positive Phase Duration, t_0^+ (ms)	Peak Reflected Overpressure, P_{so} (kPa)	Reflected Impulse, I_r (kPa.ms)	Glass Response
5kg@12m	7.02	7.30	54.5	148.2	Doesn't Fail
6kg@13m	7.15	7.15	52.8	154.2	Doesn't Fail
7kg@14m	7.32	8.28	50.8	158.4	Doesn't Fail
10kg@17m	7.89	9.55	45.1	164.5	Doesn't Fail

For charges of the same mass but at closer distances, the glass will most certainly fail according to UFC [51]. The conclusion taken from this analysis is that the glass behavior to a blast load is very complex and should be taken carefully, however, as a reference and a guideline, the UFC chart can be helpful to understand which kind of loads will break, or not, the glass.

Chapter 5. Numerical Data Analysis

5.1. LS-Dyna Software Introduction

LS-Dyna is a software developed by Livermore Software Technology Corporation (LSTC). Nowadays for the resolution of several problems around the engineering fields of knowledge, a finite element method is often used to obtain results of non-linear analysis with a certain degree of precision. There are several software today that purposely made for non-linear analysis like IDEAS®, ABAQUS®, ANSYS®, LS-DYNA® and ADINA® [45], [46], [47].

LS-Dyna is a powerful software that is used around the industry for its capability of predicting the response of a collision of a car against a wall or another car, the damage in the human being inside the vehicle, the capability of modelling fluids mechanics, modelling infrastructures for impact resistance, and the possibility of reproducing a blast wave to simulate the pressure wave as well as the damage that it can cause [57]. LS-Dyna has the capacity of doing non-linear explicit analysis as well as implicit analysis. For the presented work, it was used the explicit analysis because of the type of problem that is analyzed, that is a fast contact problem, in which case, the explicit analysis has a much better precision for the results than the implicit analysis. Also, the choice of explicit analysis had a benefit of reducing drastically the time consumption as well as Central Processing Unit (CPU) power needed to run the model [56].

The advantage of using such software is that when the model is calibrated and equilibrated, the need for real experimental tests is reduced, saving money, time and resources [58].

5.2. Modeling Base Characteristics

5.2.1. Generic Mesh Specifications

To obtain good results in a finite element method analysis, the mesh specification must be chosen wisely to ensure that there is a logical convergence of the results, and also, the convergence of those results, when the mesh is changed. One way to ensure the results are good, is to define a small size for the mesh, even though it can cost more time to process the information as well as CPU power.

In the presented work it was required the utilization of different finite elements like shell quad elements, beam elements, solid cube elements. The formulation used by LS-Dyna on Beam, Shell and Solid Formulations depend on the Element Formulation choice for each individual model [59].

5.3. Energy Dissipation Device

The Energy Dissipation Device or Dissipator has the final objective of reducing the damage on the glass, to improve the behavior of the structure response to a blast load. For this problem, it was made a finite element method to extrapolate the behavior of the device, and the apply it to the final solution with the laminated glass.

5.3.1. Materials used and Mesh Specification

In the model used, the materials used were PETG and Steel. Both materials were used in the 3 models explained further in this MSc Dissertation, with differences according to the problem that was being solved.

For Steel, the material had the keyword MAT_003_PLASTIC_KINEMATIC with the following definitions.

Table 27 - MAT_003_PLASTIC_KINEMATIC Properties for Steel

Property	Value
Mass Density, RO (kg/m^3)	7850
Young's Modulus, E (GPa)	210
Poisson's Coefficient, PR	0.3
Yield Strength, SIGY (MPa)	275
Cowper-Simonds Parameter, C	40
Cowper-Simonds Parameter, P	5
Failure Strain	0.2

The keyword MAT_003_PLASTIC_KINEMATIC formulation, has the capacity of simulating the elastoplastic properties of a material, and as the problem is highly dynamic, the Cowper-Simonds strain-rate effects are considered. [54]

The PETG, the material used was the same as the steel, however, the properties were different. These properties were mentioned by Coutinho [14] when a numerical model was made to simulate an impact load on the same Energy Dissipation Device.

The boundary conditions were set so that the dissipator is fixed in the bottom by all nodes, setting the six degrees of freedom of each node to 1 which means that it is totally block in the keyword BOUNDARY_SPC_SET.

5.3.2. Replication Model

It was made a replication of Coutinho's [14] model to understand if the model reproduced the same results. In order to do that, the model was made using the same keywords referred in Coutinho [14]. To model the energy dissipator device, two elements were used. Solid elements and shell elements. The solid element formulation was set in the keyword SECTION_SOLID using the option ELFORM=1 which stands for "Constant stress solid element" and it is the default value of LS-Dyna, controlled after by the keyword HOURGLASS to ensure that the internal energy of the element is maintained. The HOURGLASS definition will not permit the strange deformation of an element, making it behave like it should, by applying the opposite force if the element starts to deform in an impossible way. The shell formulation was set in SECTION_SHELL using the option ELFORM=10 which stands for "Belytschko-Wong-Chiang" which is a formulation made to prevent the shell element to bend.

The materials used for the model were already introduced, but some differences were made. To model the steel ball (Figure *58*), the material chose was MAT_20_RIGID, to ensure that the time spent on the model was reduced, and the Mass Density was set differently so the ball would have a

weight of 4,853 kg as the laboratory experiment. The material used for PETG was MAT_003_PLASTIC_KINEMATIC only with the small change of the Cowper-Simonds parameters, that were set as 0, since the PETG was considered to stress-strain rate effects whatsoever.

The contact used between the steel ball and the energy dissipator device, was CONTACT_AUTOMATIC_SURFACE_TO_SURFACE which means that every contact between any node or shell of one surface and the other is taken into account, and between the shell elements and solid elements the contact was CONTACT_TIED_NODES_TO_SURFACE to simulate that the dissipator works as one, and so the shell is totally connected to the solid body, and to model the contact between the parts of the energy dissipator itself was, CONTACT_AUTOMATIC_SINGLE_SURFACE with the friction coefficients, static (FS) and dynamic (FD) according to Behalek et al. [60] set to 0,16 and 0,10 respectively.

The ball was modelled as having initial velocity, setting the keyword INITIAL_VELOCITY to a value of -2.04 m/s for the 1st series tests and -3.04 m/s for the 2nd series tests as described in Coutinho [14].

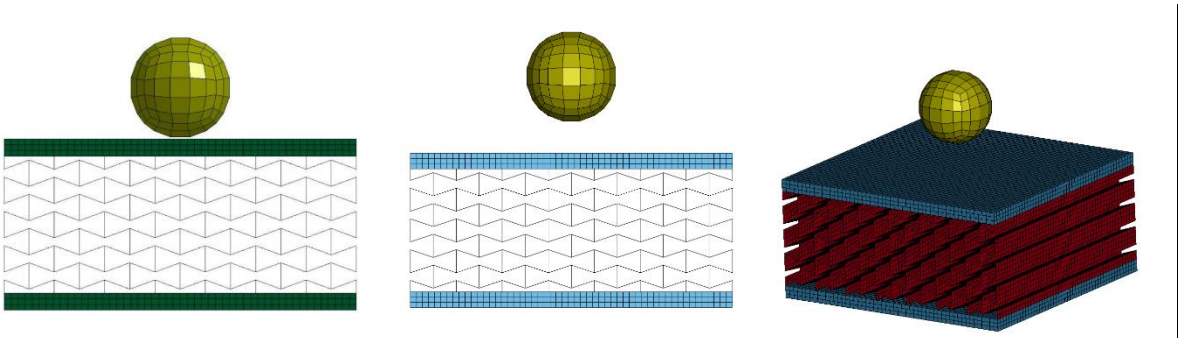

Figure 58 - Coutinho Model (Left) (Source: [14]), FE Model made (Middle), FE Model Made from perspective (Right)

The LS-Dyna results were very close to Coutinho's results and also close to the experimental results made by Coutinho [14] as it shown in Figure 59 and Figure 60.

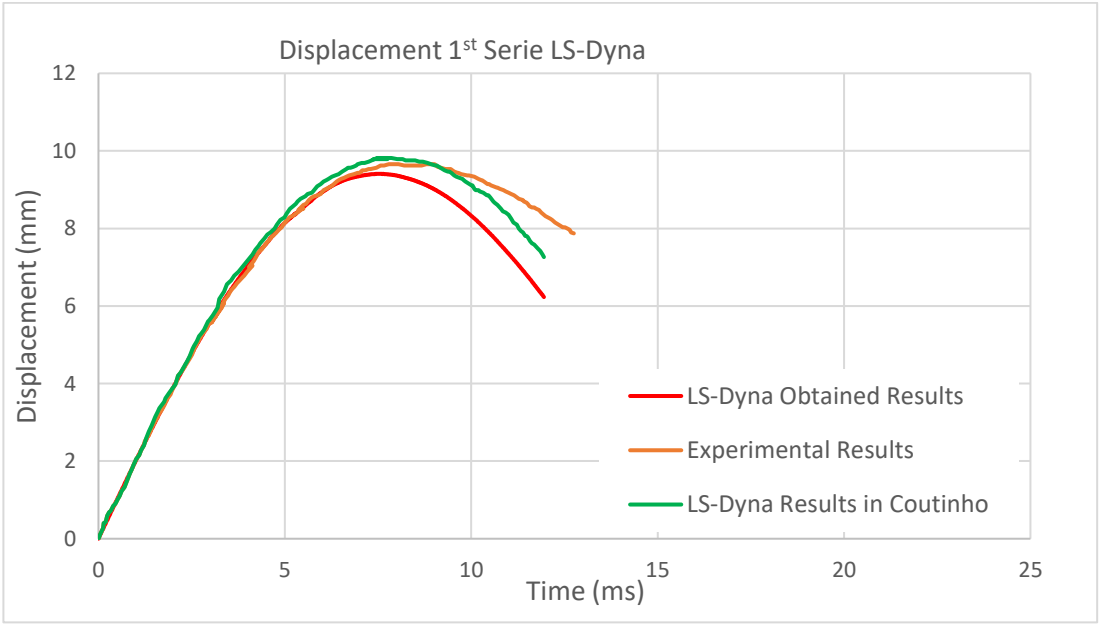

Figure 59 - Displacement of 1st Series Experiments and FE Model comparison

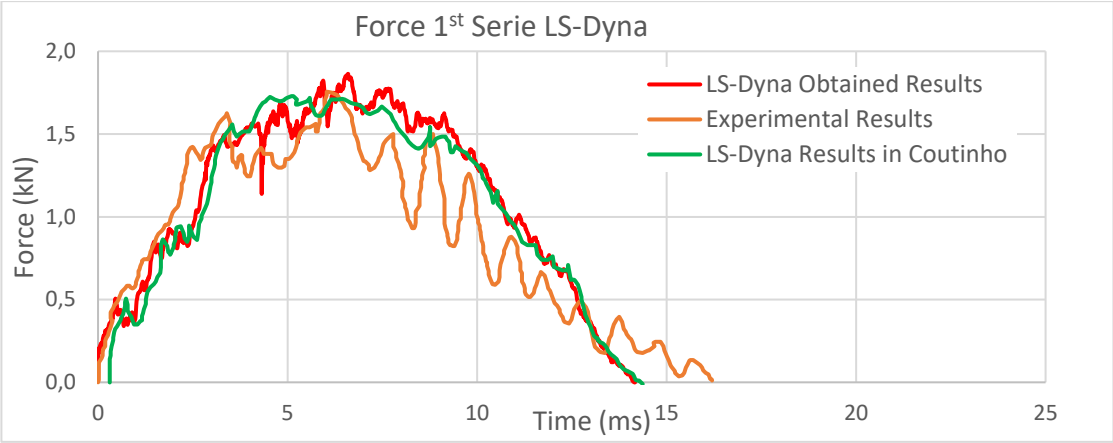

Figure 60 - Force for 1st Series Experiments and FE Model Comparison

The 2nd series results were also very close to Coutinho's Model, but with a small error compared to the experimental result. As it can be seen the replication model was made with success, meaning that, it was considered as validated.

5.3.3. Static Load Experiment

The same model was used but, the difference was, that the ball is now a steel plate also considered as rigid modelled as MAT_20_RIGID to simulate action of the Instron Static Hydraulic Press Machine. Then it was described a continuous motion to the plate using the keyword BOUNDARY_PRESCRIBED_MOTION_RIGID to a value of 2 mm/s and then the contact between the plate and the energy dissipator device used was CONTACT_AUTOMATIC_SURFACE_TO_SURFACE as it can be seen in Figure 61.

Also, to simulate the friction between the PETG and the hydraulic press, one lane of nodes of the top of the dissipator was blocked, using the keyword BOUNDARY_SPC_SET, since in the real experiment, no deviation was seen in the energy dissipator relatively to the hydraulic press.

The correct approach that should have been taken was an implicit analysis, since for long duration loads the implicit analysis is slightly better than the explicit analysis, however, the time that would take to run one model was too high, and it was a much more complex model, since some variables had to be added into the problem. Since the approximation of an explicit analysis was also good, the explicit analysis was used.

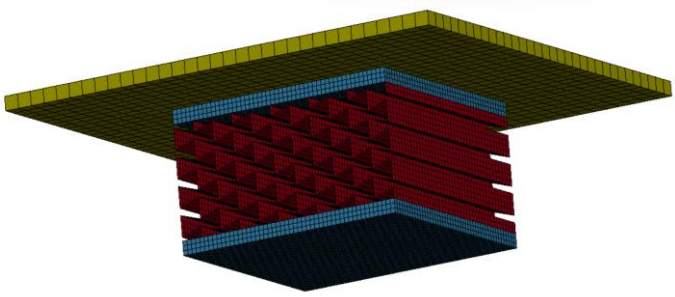

Figure 61 - FE Model of the Static Experiment

The results taken from LS-Dyna were compared to the ones obtained in the Experiment. The comparison is shown in Figure 62.

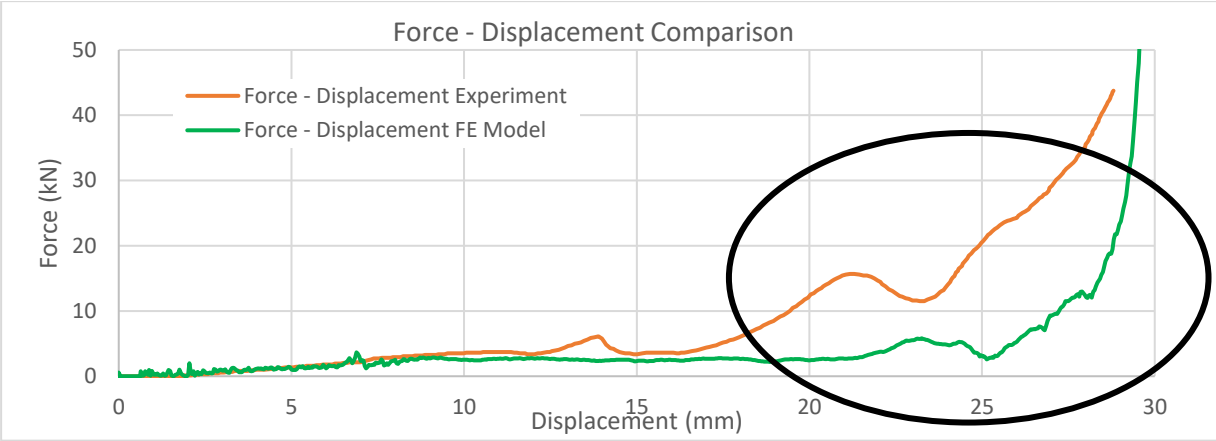

Figure 62 - Force - Displacement Comparison Graph

As it can be seen, after the 15 mm displacement is a larger error factor between the FE Model and the real experiment. The difference can be explained due to the fact of the cellular organization during the compression load. As it can be seen in Figure 63, the displacement is very different, which in the real experiment, for the observed organization, the force to compress the material is higher than the result in the FE Element as verified in Figure 62.

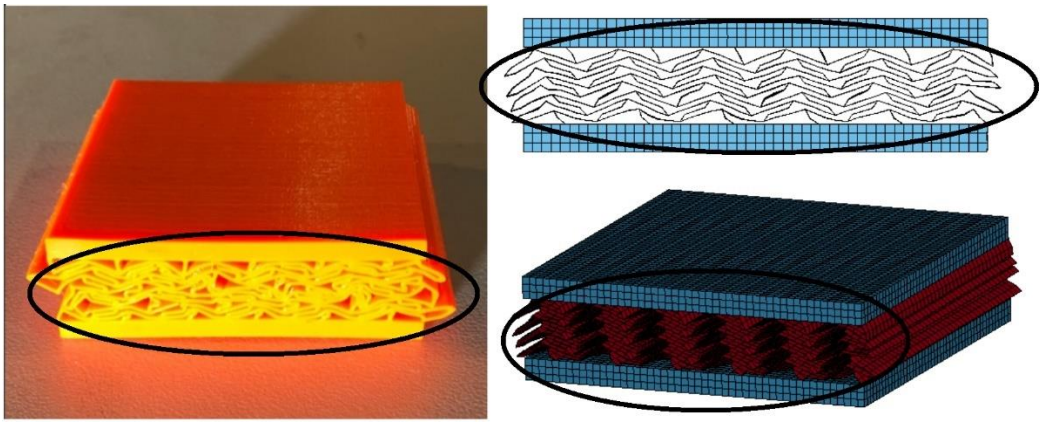

Figure 63 - Cellular organization difference between FE Model and Experiment

One factor that is not considered in LS-Dyna for the obtained response is the possibility of existing errors in the 3D printing process, that in some cases, there are zones with less resistance and zones with more resistance than normal that when the dissipator is compressed will behave differently than expected. Also, the FE Model in LS-Dyna is not taking into account the friction as it is in reality, and such an approximation could also explain some differences between the obtained results.

Even with a known error between the static behavior and the FE method, the model can be considered useful for further applications with different geometry and different size energy dissipator device.

5.3.4. Extrapolation to a Different Size Dissipator

To better apply the energy dissipation device to the case of study, it was chosen to change the size of the energy dissipation device to 125 mm long and 42 mm wide from 50 mm long by 50 mm wide. The 125 mm choice is based on being a multiple of a meter, to have easy and more real numbers to

work with. The 42 mm choice was made because of the distance between the threaded bolt and the margin of the steel profile.

To apply an impulse loading in the dissipator, the keyword used was LOAD_NODE_SET where the load is divided by the number of nodes and then applied. To define the impulse loading the keyword DEFINE_CURVE was used. The FE Model used is shown in Figure 64 along with the real test devices.

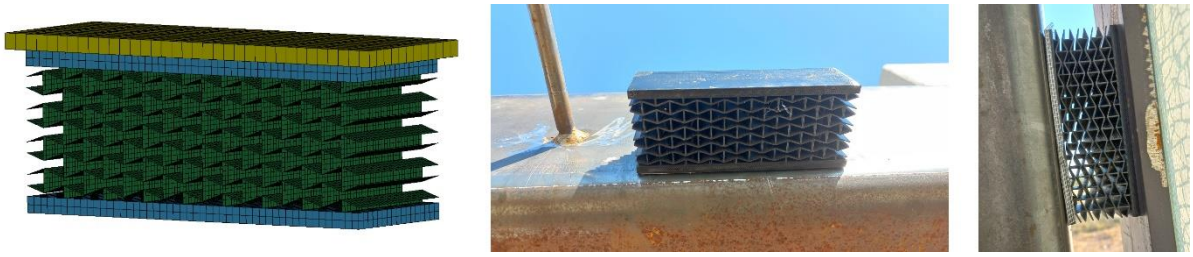

Figure 64 - FE Model of the dissipator (Left), Dissipator Glued to the Structure (Middle), Complete System of the structure (Right)

5.3.5. Dynamic Response of the Dissipator to Blast Load Effects (Impulse Loading)

To obtain the dynamic response of the energy dissipation device, it was made a model similar to the static load, with the final dissipation device with a rigid plate, which is now loaded with an impulse to analyze the behavior of the dissipator.

To be able to understand the dynamic response of the dissipator, 24 models were made with different impulsive loads. The impulsive loadings were tested to see if the dissipator would behave different to different impulse loading and to carefully establish the equation of the stress-strain relation. In Table 28 we can see the different loads applied.

Table 28 - Impulse Loads Applied

Load (kN)	Time (ms)	Load (kN)	Time (ms)	Load (kN)	Time (ms)
2.5	2.5	2.5	5	2.5	7.5
5	2.5	5	5	5	7.5
7.5	2.5	7.5	5	7.5	7.5
10	2.5	10	5	10	7.5
15	2.5	15	5	15	7.5
20	2.5	20	5	20	7.5
25	2.5	25	5	25	7.5
30	2.5	30	5	30	7.5

The reactions of obtained are presented in Figure 65, along with the equation chose for the stress-strain curve. In Figure 65, it is presented the response of the dissipator to an impulsive loading. Represented as orange the loads with duration of 7.5 ms, represent as blue, the loads of 5 ms and represented as green the loads of 2.5 ms. In black, the assumed medium response of the force-displacement function approximation of an energy dissipation device. The graph can be explained dividing it into three parts:

1) The first one, the elastic part, which corresponds to a displacement of around 2.5 mm, where the dissipator has the ability to return to its normal shape, behaving like a spring;
2) The second part, the plastic part, where is the maximum capacity of the device to dissipate energy due to the destruction of its cells until a displacement of around 30 mm, in which case the dissipator is no longer useful;
3) The last part, after 30 mm of displacement where the material is being totally crushed, represented by the force spike in the graph.

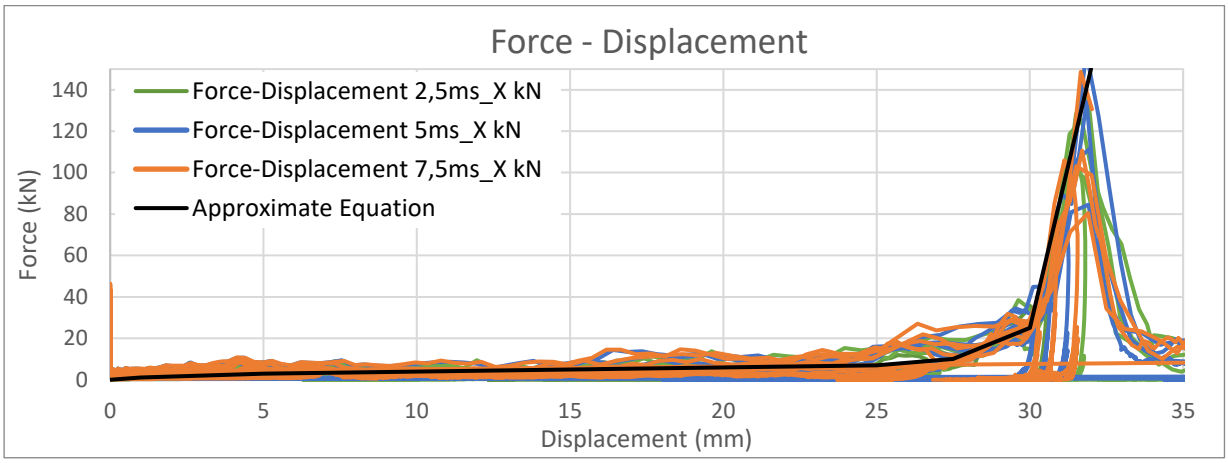

Figure 65 - Dynamic Response of the Energy Dissipation Device

After obtaining the medium equation for the force-displacement function, it was made the following calculations to transform the function into a stress-strain curve.

To obtain the strain curve, the displacement was divided by the total displacement possible, which means, if the device has 50 mm thickness in total, if at the value of 32 mm of displacement, is when the total crush of the material starts, then the strain can be calculated as:

$$\varepsilon = \frac{\Delta x}{x} = \frac{32\ \text{mm}}{50\ \text{mm}} = 0.64 \tag{5.1}$$

To obtain the values of stress, the force was divided by the area, considered as the area of the top surface of the dissipator which has the dimensions of 125x42 mm²:

$$\sigma = \frac{N}{A} = \frac{150\ \text{kN}}{5250\ \text{mm}^2} = 28.57\ \text{kPa} \tag{5.2}$$

Figure 66 shows the values for the stress-strain curve obtained.

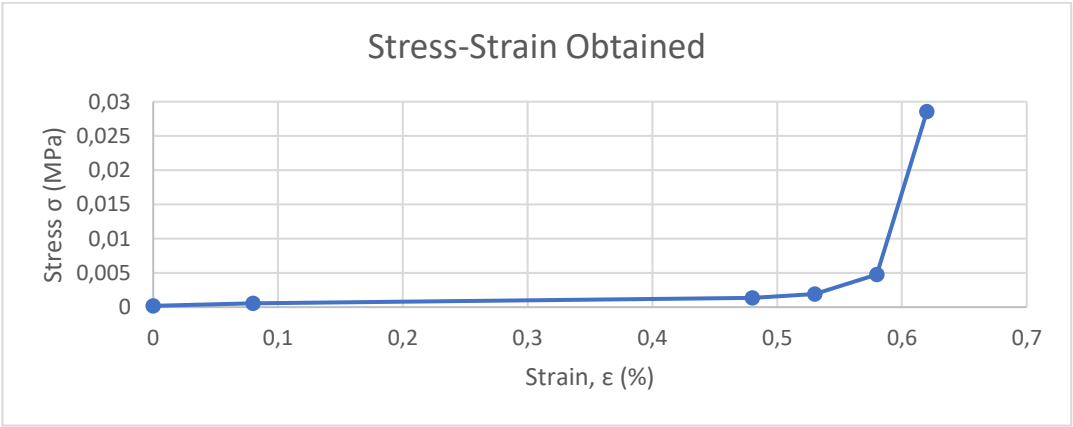

Figure 66 – Stress-Strain equation obtained

The next step was to apply the obtained equation in LS-Dyna to simulate an energy dissipation device. To do it, it was used a Beam element, using the element formulation in SECTION_BEAM as ELFORM=9 which is a spotweld beam formulation. This formulation forced the usage of the material keyword MAT_100_SPOTWELD where it was requested an area, and a rule for the plastic behavior of the material. The area was set to be an equivalent area of the dissipator as a circle calculated as:

$$A = \frac{\pi \times d^2}{4} = 5250\ \text{mm}^2 \tag{5.3}$$

And the value for the diameter is:

$$d = \sqrt{\frac{5250 \times 4}{\pi}} = 81.76\ \text{mm} \tag{5.4}$$

This approximation is rude, but is a simple way to approach the problem, and the results are good. [13] The rule for the plastic behavior was set in the keyword DEFINE_CURVE with the stress-strain function of Table 29. The value for 0 strain is explained by the fact that, when the dissipator starts entering the plastic zone, the plastic strain is equal to zero, while the stress is already above 0 from the elastic zone. This means that the elastic strain has reached is limit, and now, the plastic strain will start from 0.

Table 29 - Values for DEFINE_CURVE

Stress (MPa)	Strain
0.00019048	0
0.00038095	0.03
0.00057143	0.08
0.00133333	0.48
0.00190476	0.53
0.00476190	0.58
0.02857143	0.62

5.4. Obtained Results of the Glass Model

5.4.1. Materials Used and Mesh Specifications

To model the laminated glass, many different materials were tried. For the difference between shell and solid as explained in Hooper et al. [11] the difference between the shell formulation and the solid formulation was almost zero. And so, knowing that the solid element would cost more time and CPU power, a shell element was used for the glass. For the shell element different materials were tried. The materials tried were MAT_001_ELASTIC [11], [12] combined with the keyword ADD_MAT_EROSION [61], MAT_032_LAMINATED_GLASS [62] and MAT_280_GLASS [38], [63].

The different results showed that, the better material was MAT_001_ELASTIC with ADD_MAT_EROSION which is the complete elastic behavior of the glass and then when it reaches the value of the rupture stress, the element is eroded from the model. The material MAT_32_LAMINATED_GLASS gave bad results after applying the loads, and the material MAT_280_GLASS gave numerical errors and was very time consuming.

For the shell element formulation, in order to control the internal energy, the element formulation was defined in SECTION_SHELL as ELFORM=16 which is “Fully integrated shell element” in order to prevent the shell element from bending as distorting.

For the PVB, several materials were tried, some with solid elements, some with shell elements, and some with both approaches. The materials tried in the modelling were MAT_027_MOONEY_RIVLIN_RUBBER [61], MAT_76_GENERAL_VISCOELASTIC [38], and MAT_098_SIMPLIFIED_JOHNSON_COOK [64].

The best results came from two materials, MAT_027_MOONEY_RIVLIN but the HOURGLASS could not control the behavior of the elements, which meant that an error could be implied into the results, and the second material was MAT_098_SIMPLIFIED_JOHNSON_COOK which is a material that includes the Johnson-Cook equation without the parameters for temperature variation, which is not considered in the problem. [54], [64]

For the material MAT_76_GENERAL_VISCOELASTIC the model was not giving good results. This material uses the generalized Maxwell equations which explain the viscoelastic behavior and approach in some degree the behavior of the shear relaxation of the PVB, with the disadvantage of having to insert different values for the generalized Maxwell equations for different values of temperature.

For the PVB element, the shell formulation chosen in SECTION_SHELL was ELFORM=9 which stands for “Fully integrated Belytschko-Tsay membrane” where the shell element behaves only like a membrane, and the bending stiffness is ignored as it is observed in reality. The behavior of this shell element is controlled also by the keyword HOURGLASS to control strange variations of internal energy.

The contact used between the shells used was CONTACT_TIED_SURFACE_TO_SURFACE_OFFSET, where the PVB is considered to be totally bonded with the glass.

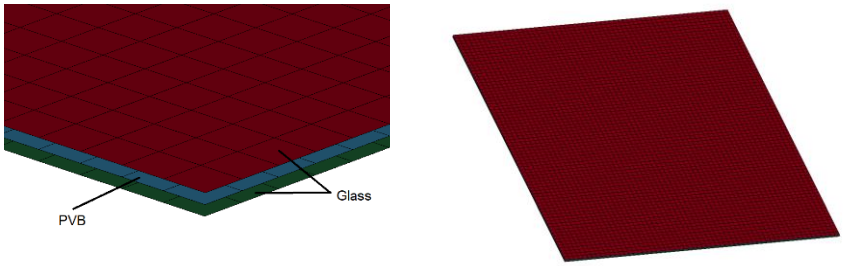

Figure 67 - FE Model of Laminated Glass

5.4.2. Model Specifications

To obtain the model validation the comparison was made between the finite element method and the real experiments. The results of real experiments were taken from two articles, Hooper et al. [11] and Zhang et al. [12].

For faster results, only a quarter of the panel used in the experiments was used, and then mirrored two times for visualization. The material used for the annealed glass was MAT_001_ELASTIC with the addition MAT_ADD_EROSION with the following specifications:

Table 30 – MAT_001_ELASTIC + ADD_MAT_EROSION Properties for Glass

Property	Value
Mass Density	2500 kg/m^3
Young's Modulus	72 GPa
Poisson's Coefficient	0.22
Rupture Stress (Annealed Glass)	80 MPa
Strain at Failure (Annealed Glass)	0.0011(1)
Rupture Stress (Tempered Glass)	120 MPa
Strain at Failure (Tempered Glass)	0.0016(6)

The strain at failure can be calculated as the division of the Rupture Stress by Young's Modulus:

$$\varepsilon = \frac{\sigma_{\text{Rupture}}}{\text{E}} = \frac{80}{72000} = 0.0011(1) \tag{5.5}$$

The element for the glass was chosen to be a shell with the element formulation as explained previously. For the PVB, the material used was MAT_098_SIMPLIFIED_JOHNSON_COOK with the following parameters:

Table 31 - MAT_098_SIMPLIFIED_JOHNSON_COOK Properties for PVB

Property/Parameter	Value
Mass Density	1100 kg/m^3
Young's Modulus	0.53 GPa
Poisson's Coefficient	0.485
A	6.72 MPa
B	10.6 MPa
C	0.248
n	0.303
Strain at Failure	2

The element for the PVB was chosen to be a shell with the element formulation as explained previously. To evaluate which load was better, two approaches were applied, the keyword LOAD_NODE_SET (LNS) and the keyword LOAD_BLAST_ENHANCED (LBE). Both offered close but different results, being the LOAD_NODE_SET closer to reality.

The keyword LOAD_NODE_SET applies a type of load defined by the keyword DEFINE_CURVE where each node selected has an applied a load, and the total load generated is defined to have the same impulse as the impulse generated by the positive phase duration of the Friedlander equation, as explained in Chapter 2. And the keyword LOAD_BLAST_ENHANCED will generate a blast load based on the theoretical formulations of Charles Kingery and Gerald Bulmash [45] where the only definitions are the location and the equivalent TNT weight of the explosive.

The difference between the two formulations has to do with the load applied on the panel. For LOAD_BLAST_ENHANCED the BLAST option card was set to 1 which means "hemispherical surface burst - charge is located on or very near the ground surface, initial shock wave is reflected and reinforced by the ground", the, meaning that, the wave will be reflected in the ground and then applied on the structure. In LODE_NODE_SET it is assumed that the load is planar, and it is used the positive phase

impulse from the Kingery and Bulmash [45] formulations and it is applied the load directly to the panel by a triangular equivalent load as explained in Chapter 2, where the maximum value is equal to the peak reflected overpressure with the necessary time duration until the total load applied is the impulse calculated from the expressions.

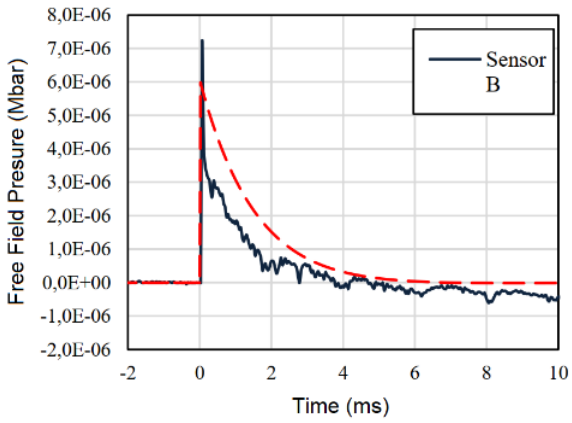

Figure 68 - Overpressure differences between LBE and measurement of a real blast wave (adapted from [56])

In literature, the blast loads used by LS-Dyna often underestimate the peak reflected overpressure that is seen in reality, what means that, when blast modelling is done, the peak reflected overpressure generated is lower than the real one as well but the impulse also often overestimated by blast methods in LS-Dyna [56]. In Figure 68 is presented the formulation used by LS-Dyna compared to a sensor capturing the pressure in a blast load.

Since every formulation has its flaws, it was decided to use the formulation LOAD_NODE_SET for being simple to perform and the results obtained were also better.

5.4.3. Comparison with Experimental tests described on “Hooper et al.” and “Zhang et. Al”

For comparison of the FE model and the real experiments, it was made the geometry of the elements, chosen to be square shells of 10 mm. The boundary conditions were considered fully clamped on the sides of the panel, but, in the reflection axis, the boundary condition was sliding clamped. The modelled panel had 600x750 mm^2. For each situations the shells were modelled as the medium line of the solid element, with 3 integration points across each shell so that that the evaluation of the stress in each could be measured. For the integration point, it was defined in the keyword INTEGRATION_SHELL where the points were divided as presented in the Figure 69.

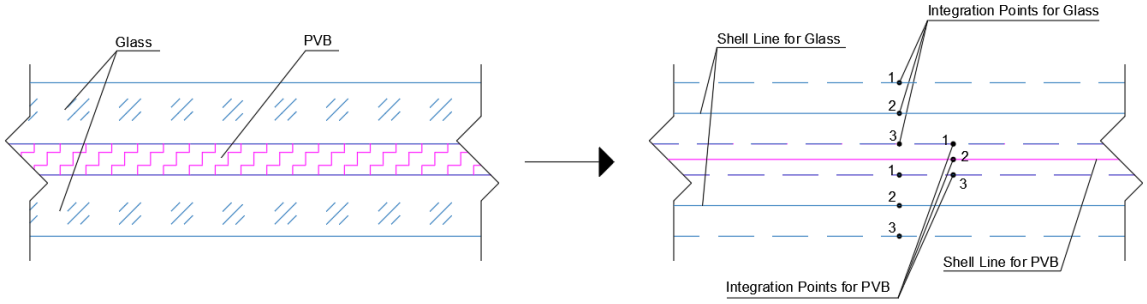

Figure 69 - Laminated Glass simplification and integration points location

The results of the experimental test present on literature are represented in Table 32, as well as the dimensions of the panel, as well as the load used to realize the experiment. The layout of the

glass gives the laminated glass dimensions. For example, a layout of 3/1.52/3 is a glass plie of 3 mm then the PVB interlayer with 1.52 mm and then another glass plie of 3 mm.

Table 32 - Field Experiments Results from Hooper et al. [11] and Zhang et al. [12]

Author	Dimensions (m)	Layout (mm)	Charge (TNT)	Scaled Distance (Z)	Maximum Displacement (mm)
Hooper et al.	1.5x1.2m	3/1.52/3	15kg@10m	4.05	349
	1.5x1.2m	3/1.52/3	15kg@13m	5.27	172
	1.5x1.2m	3/1.52/3	30kg@16m	5.15	202
	1.5x1.2m	3/1.52/3	30kg@14m	4.50	265
Zhang et al.	1.5x1.2m	3/1.52/3	10kg@10m	4.64	275
	1.5x1.2m	3/2.28/3	10kg@10m	4.64	280
	1.5x1.2m	3/1.52/3	10kg@9m	4.18	326
	1.5x1.2m	6/1.52/6	10kg@9m	4.18	230
	1.5x1.2m	3/1.52/3 (Tempered Glass)	10kg@12.3m	5.71	264

To apply the load, some calculations had to be made in order to accomplish a correct value. First it was calculated the area of the panel divided by four, since the model only contemplates a quarter of a plate.

$$A = \frac{1.8 \times 1.2}{4} = 0.45\ m^2 \tag{5.6}$$

Then the values for the peak reflected overpressure were calculated using the Kingery and Bulmash Equations [45], shown in Table *33*.

Table 33 - Overpressure values calculated by Kingery and Bulmash equations [45]

Author	Charge (TNT)	Scaled Distance (Z)	Peak Reflected Overpressure (kPa)	Positive Impulse (kPa.ms)
Hooper et al.	15kg@10m	4.05	157.3	395.1
	15kg@13m	5.27	90.8	292.1
	30kg@16m	5.15	95.0	377.7
	30kg@14m	4.50	124.8	438.1
Zhang et al.	10kg@10m	4.64	117.2	293.9
	10kg@10m	4.64	117.2	293.9
	10kg@9m	4.18	147.1	330.7
	10kg@9m	4.18	147.1	330.7
	10kg@12.3m (Tempered Glass)	5.71	78.1	233.7

After the calculation of the peak reflected overpressure, the value of equivalent time duration, t_d, could be calculated as it was explained in Chapter 2:

$$t_d = \frac{2 \times I_r^+}{P_{ro}} \tag{5.7}$$

Then to use the keyword LOAD_NODE_SET, the total load was multiplied by the area of the model and then divided by the number of nodes in the panel. The number of nodes were counted as 4636 nodes. The load in each node is presented in Table 34.

Table 34 - Values for transformation into an equivalent triangular load

Author	Charge (TNT)	Area (m^2)	Peak Reflected Overpressure (kPa)	Impulse (kPa.ms)	t_d (ms)	Load (kN)
Hooper et al.	15kg@10m	0.45	157.3	395.1	5.02	0.015269
	15kg@13m	0.45	90.8	292.1	6.44	0.008814
	30kg@16m	0.45	95	377.7	7.95	0.009221
	30kg@14m	0.45	124.8	438.1	7.02	0.012114
Zhang et al.	10kg@10m	0.45	117.2	293.9	5.02	0.011376
	10kg@10m	0.45	117.2	293.9	5.02	0.011376
	10kg@9m	0.45	147.1	330.7	4.50	0.014278
	10kg@9m	0.45	147.1	330.7	4.50	0.014278
	10kg@12.3m (Tempered Glass)	0.45	78.1	233.7	5.98	0.007581

For the keyword LOAD_BLAST_ENHANCED it was only needed to input the weight of the charge and the stand-off distance. The results are presented in Table 35, where it is shown the different results for LOAD_BLAST_ENHANCED and for LOAD_NODE_SET with the respective error associated.

Table 35 - Obtained Relative Error in the FE Model

Author	Charge (TNT)	Layout (mm)	Displacement Experiment (mm)	Displacement LBE (mm)	Displacement LNS (mm)	Error LBE (%)	Error LNS (%)
Hooper et al.	15kg@10m	3/1.52/3	349	310	329	11.17	5.73
	15kg@13m	3/1.52/3	172	224	236	30.23	37.21
	30kg@16m	3/1.52/3	202	165	193	18.32	4.46
	30kg@14m	3/1.52/3	265	200	225	24.53	15.09
Zhang et al.	10kg@10m	3/1.52/3	275	146	246	46.91	10.54
	10kg@10m	3/2.28/3	280	198	204	29.29	27.14
	10kg@9m	3/1.52/3	326	175	273	46.32	16.26
	10kg@9m	6/1.52/6	230	192	201	16.52	12.61
	10kg@12.3m	3/1.52/3 (Tempered Glass)	264	102	184	61.36	30.30

As it can be seen the model used with the formulation LNS obtained better result than LBE. The values marked as red is where the error was high, for instance, the charge of 15kg@13m of Hooper et al. [11]. Other authors tried to model the same field experiments and found that for the same experiment the FE model was giving them bad results, but close to what was verified in this Chapter [65]. LS-Dyna could not take into account the rebound behavior found on the field experiment.

For the field experiments realized by Zhang et al. [45] the values of error were higher in general, but two of them were a little off. One of them is related to higher PVB thickness and the second one, is related to the use of tempered glass. The tempered glass experiment can be considered strange

because, first, the charge has higher scaled distance which means, the impulse is lower, and second, the tempered glass is more resistance than an annealed glass. And only a 10 mm variation should not be considered normal since the impulse variation is around 20%. The total error for the keyword LODE_NODE_SET was 17.7% which was considered acceptable for a certain degree of certainty.

5.5. Experimental Set-Up Model

For the final model, the other two models obtained were joined along with the support structure to ensure that, the final goal of obtaining some degree of certainty, to then, extrapolate results to realize field experiments.

A simple model was made to save time and power of the processing unit. This model contained one laminated glass, with the continuous clamped fixing system, and behind it the energy dissipation device, or a rigid reaction, so that a comparison could be established between the response to a blast load without the energy dissipation device and with the energy dissipation device. In **Erro! A origem da r eferência não foi encontrada.** is shown a drawing of the system.

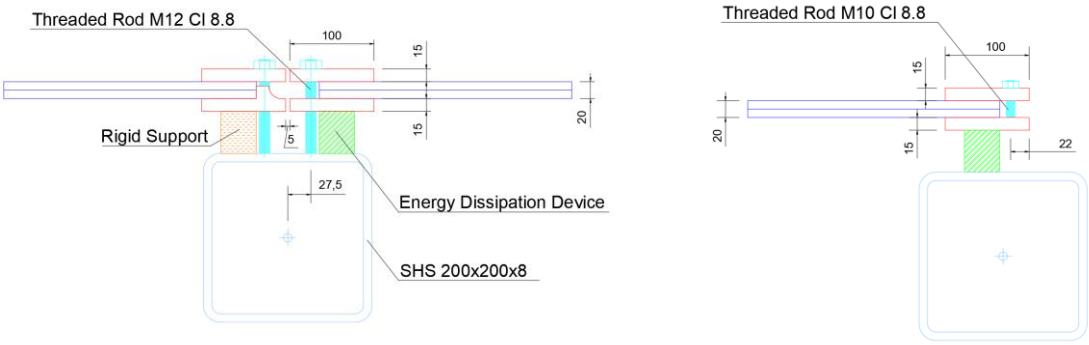

Figure 70 - AutoCAD design of the System

The FE contains some differences from the drawing since the M10 threaded bolts were modelled with the keyword MAT_100_SPOTWELD, and the M12 threaded bolts were not modelled since only the positive phase of the explosion is considered for the glass and the M12 bolts didn't represent any restrain to the movement of the panel having no differences in the final results. Also the support structure was considered rigid using the keyword MAT_20_RIGID. In Figure 71 are shown the differences between the design, the FE model and the real Set-Up.

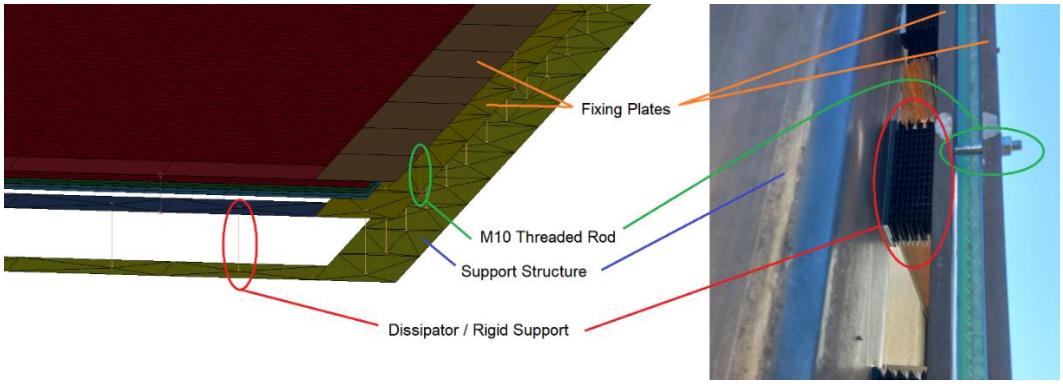

Figure 71 - FE Model in comparison with the experimental Set-Up

5.5.1. Materials Used and Mesh Specifications

The materials used in the finite element method, were already described. However, the threaded bolts were modelled as a beam element, with the element formulation in SECTION_BEAM, ELFORM=9 which is a spotweld beam. The characteristics for the threaded bolts were set in the keyword MAT_100_SPOTWELD with the values from Table 36 for M10 threaded bolts.

Table 36 - MAT_100_SPOTWELD Properties for a M10 Threaded Bolt

Property	Value
Mass Density	7850 kg/m3
Young's Modulus	210 GPa
Poisson's Coefficient	0.28
Yield Strength	355 MPa

In the keyword SECTION_SHELL, the value of the diameter was also set to 10 mm.

The M12 beams were not modelled in order to fasten up the run time, and also, it was considered that there was no influence of the M12 threaded bolt since all the panel could move through without any restrain.

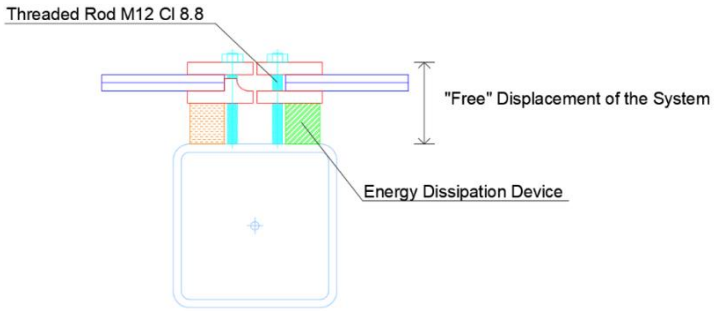

Figure 72 - Free Displacement of the glass panel in the threaded bolt

For the energy dissipation device, the parameters are presented in Table 37.

Table 37 - MAT_100_SPOTWELD Properties for the Energy Dissipation Device

Property	Value	Unit
Mass Density	285	kg/m3
Young's Modulus	0.04	GPa
Poisson's Coefficient	0.19	-
Yield Strength	Function	MPa

The function for the yield strength of the energy dissipator device is explained in the previous subchapter. To analyze the glass, only small size elements were modelled, as it was the final objective. All of the support structure was modelled to be an auxiliar to the glass, and dissipator modelling. The fixing plates were modelled as steel already explained previously using MAT_003_PLASTIC_KINEMATIC, and the support structure was modeled using the MAT_20_RIGID, since the SHS steel profile was considered rigid during the FE model.

The contact between the glass elements and the steel elements was made using the keyword CONTACT_AUTOMATIC_SURFACE_TO_SURFACE.

The model of the glass is the same to the one used in the validation of the model explained in the previous section.

5.5.2. Results and Dissipator Locations

To have a degree of certainty for the experimental field test, first, to see if the model gave good results, the Unified Facilities Criteria (UFC) [23] was used as a term of comparison. It was used the pressure-duration curves for a 19 mm tempered glass with 1.07 x 2.14 m^2. The expected result is to be better in the 20 mm laminated glass, since, when a laminated glass is resisting to a blast load, has the same behavior as monolithic glass of the same thickness, which means, in the case of study, a 20 mm laminated glass with tempered glass with the dimensions of 1 x 2 m^2 is considered to be a 20 mm thick tempered glass, and so it is expected that the FE model could withstand the blasts that a 19 mm tempered glass could too, since the glass panel has higher thickness, and it is also smaller.

The blast loads were applied using the keyword LOAD_NODE_SET with the same calculations as explained previously for the glass panel validation.

The loads used are presented in the next table along with the comparison with UFC.

Table 38 - Comparison between FE Model and UFC [23] Values

Load	UFC	FE Model
5kg@7m	Breaks	Breaks
5kg@9m	Breaks	Breaks
5kg@10m	Breaks	Breaks
5kg@11m	Breaks	Does not Break
5kg@12m	Does not Break	Does not Break
20kg@10m	Breaks	Breaks

The results obtained by using the FE model explain that the laminated glass will resist more than the 19 mm tempered glass as it was expected by the calculations made.

The next step for the calculation was to know what is the best location for the dissipator, since the panel will react has a body before the glass breaks, and it will apply a force in the dissipator.

Using the simply support slab approach observed in Bares [52], it is known that when a distributed force is applied, the force originated in the corners are negative, and so, for that reason, the corner dissipators were not considered to see which ones do resist the more.

After the analysis of the results, the glass with the dissipators did not break and obviously the tensions were lower in the glass with the dissipation system than the glass without the dissipation system as expected.

It was analyzed the axial force in the dissipators as well as its displacement represented by the SPOTWELD beams, and it was verified that the displacement was only around 6 mm and the axial force was about 3 kN in the best performing dissipator, which means that some dissipators were not doing much in terms of being activated to dissipate energy. To ensure a better response, some dissipators

were removed from the panel, and different combinations were tried until the “optimal” response was found. The best combination achieved is shown in Figure 73, where 6 dissipators are on the top and bottom surfaces and 3 in the lateral surfaces.

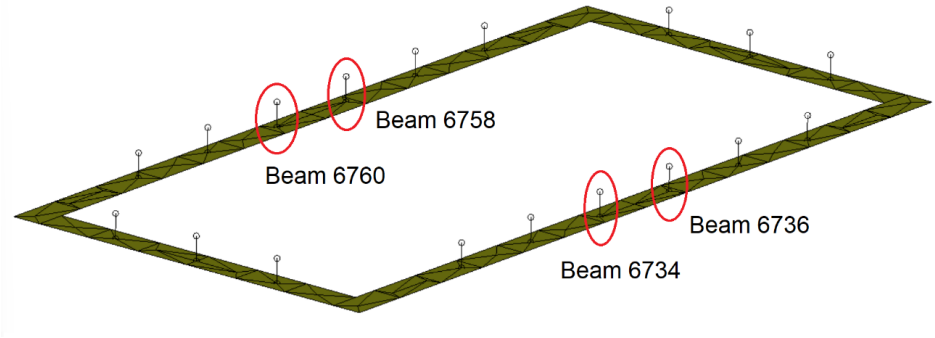

Figure 73 - Final dissipator configuration after the analysis and the identification of the best performing dissipators

For this combination, the glass withstood a charge of 5kg@9m without breaking and the best performing dissipators had a displacement of around 12.5 mm with an axial force of more than 4 kN.

In Figure 74 and Figure 75 is shown the graph of the axial force of the dissipators as well as its displacement.

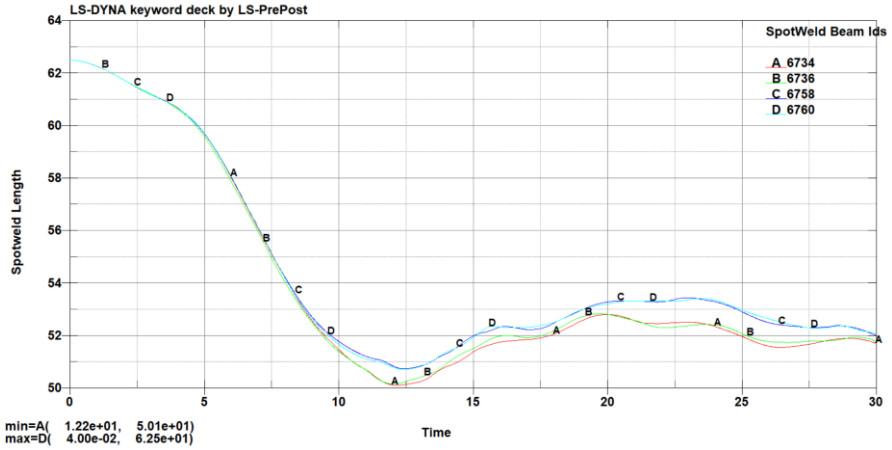

Figure 74 – SPOTWELD beams displacement measured

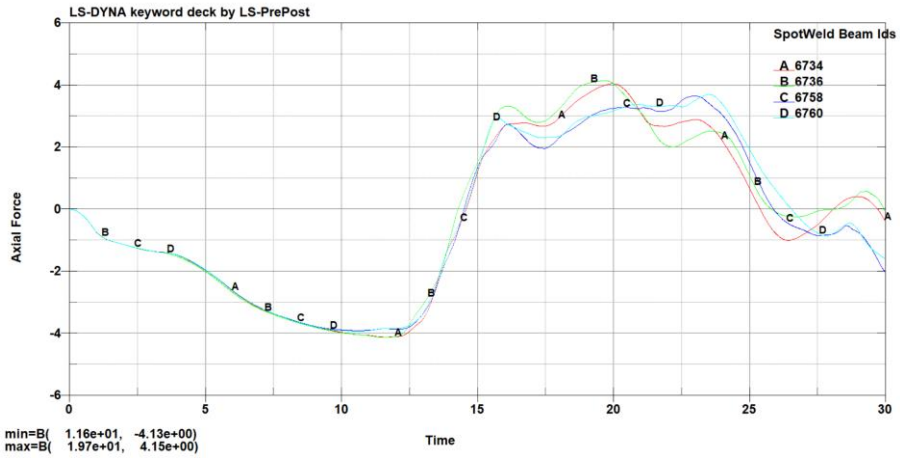

Figure 75 – SPOTWELD beams axial force measured

The disadvantage of using the beam element SPOTWELD for modelling the dissipator is that the compression is considered equal to the tension response but it was considered that, for time above 12 ms, the response of the SPOTWELD beams is not correct since the dissipator will not resist tension.

For a charge of 5kg@7m the results showed that, the dissipators did not work as good as for a load of 5kg@9m, which means that, it was found a range of response of the dissipator. For the charge of 5kg@7m the dissipators had less displacement, less axial force and the glass broke completely.

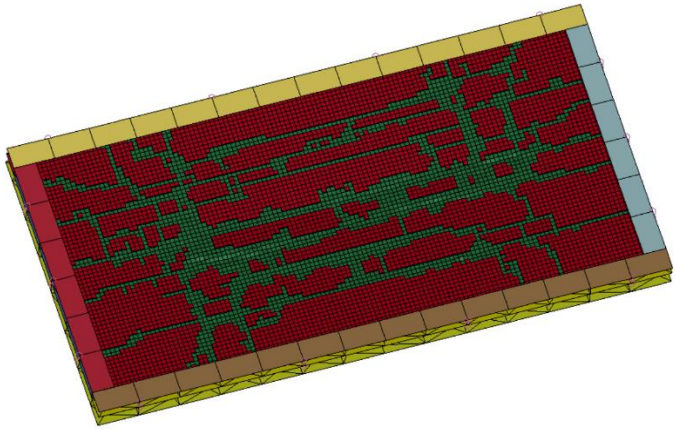

Figure 76 - Glass broken after a charge of 5kg@7m

It was also noted that the first glass plie to fail was the front one, and only an instant after the rear one. In Figure 77 it can be seen the instant before the back glass plie starts to fail.

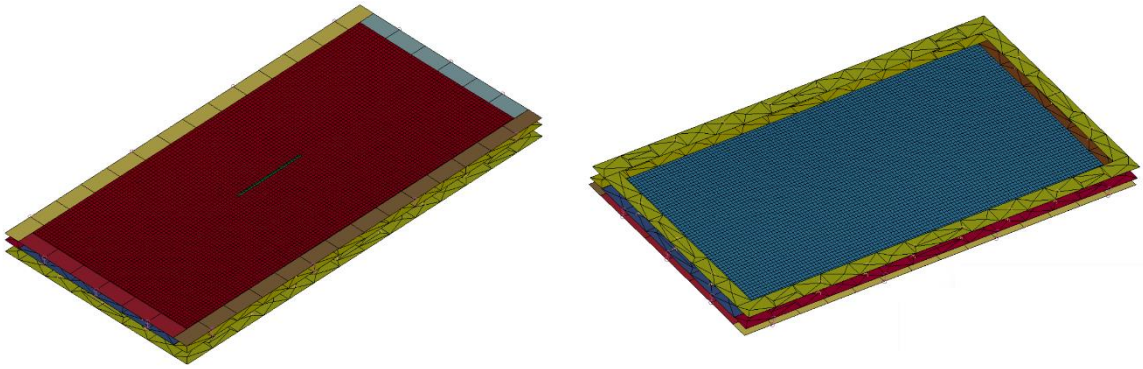

Figure 77 - Front glass plie (Left) failing at 4.42 ms before the rear plie (Right) failure

Chapter 6. Experimental Tests

6.1. Experimental Set-Up

Figure 78 - Accelerometer glued to the glass

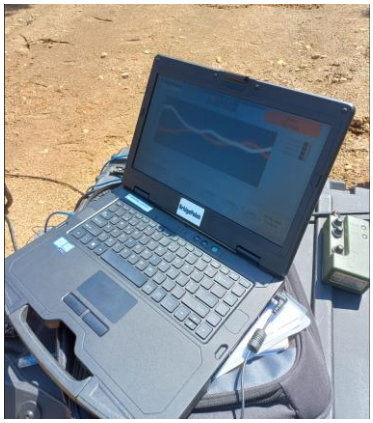

Figure 79 - Computer used for data gathering and analysis

The experimental set-up was assembled part by part. First the bottom glass was assembled, which is the one without the dissipation system. Then, the reflected pressure sensors were screwed into place, then the dissipators were glued into the steel frame on the top side, and only then the top glass was mounted as it can be seen in Figure 43 and Figure 47, and finally, the last reflected pressure sensor was assembled. The glass already had attached the accelerometers, so that the assembly of the structure was faster as it can be seen in Figure 78. Also, the incident pressure sensors were put into place in a way that the distance between the incident pressure sensor and the explosive is the same as the glass and the explosive. After all the cables were connected to a database and then to the computer for data gathering (Figure 79).

The final step consisted in applying the charge for the explosion. The cables were connected on one end to the detonator attached to the charge, and also connected on the other end to the blasting machine or shot exploder. Once the blasting machine is activated the explosion occurs. The charges were mounted 80 cm above ground level.

The charge used was 5 kg of TNT, composed by individual blocks of 1 kg of TNT, set at different distances from the laminated glass. According to the technical fact sheet [66], TNT has a yellow color and a melting temperature of 80.1 ºC, and it is used around the world by military mainly to its insensitivity to collision and friction. The charges used are presented in Table 39, along with the scaled distances, and theoretical values for reflected impulse, peak incident, and peak reflected overpressures.

Figure 80 - Explosive Charge (5 kg of TNT) (Left), Blasting Machine (Middle), Detonator (Marked in red) (right)

Table 39 - Charges used and theoretical values used in the Field Experiment

Charge	Scaled Distance, Z ($m/(kg^{1/3})$)	Incident Impulse, I_s (kPa.ms)	Reflected Impulse, I_r (kPa.ms)	Peak Incident Pressure, P_{so} (kPa)	Peak Reflected Pressure, P_r (kPa)
5kg@9m	5.26	96.8	202.9	39.5	91.0
5kg@7m	4.09	120.9	268.6	62.1	153.9
5kg@6m	3.51	138.3	320	83.8	221.3
5kg@5m	2.92	162.2	395.2	122.1	354.2

6.1.1. Sensor Settings

The incident pressures sensors used were the ICP® Model 137B24B and the measurement values taken into consideration according to the Operating Manual [67] represented in Table 40.

Table 40 - ICP® Model 137B24B Pressure Sensor Measurement Values (Adapted from [67])

Performance	Value	Unit
Sensitivity (± 15%)	2.90	mV/kPa
Measurement Range (for ± 5 V output)	1724	kPa
Measurement Range (for ± 10 V output)	3447	kPa
Maximum Pressure	34474	kPa
Rise Time (Incident)	≤ 6.5	µs

The incident pressure sensors were mounted according to the Operating Manual [67] facing the explosive and fixed to a solid structure to prevent movement in the moment when the shock wave is passing through the sensor as it is shown in Figure 81.

Figure 81 - Incident Pressure Sensor (Blue) and Explosive Charge (Red)

6.1.1.2. Reflected Pressure Sensors

The reflected pressure used were ICP® Model 113B24 and the measurement values taken into consideration according to the Operating Manual [68] represented in Table 41.

Table 41 - ICP® Model 113B24 Pressure Sensor Measurement Values (Adapted from [68])

Performance	Value	Unit
Sensitivity (± 10%)	0.725	mV/kPa
Measurement Range (for ± 5 V output)	6895	kPa
Maximum Pressure	68950	kPa
Rise Time	≤ 1	µs

The reflected pressure sensors were screwed to the structure according to the Operating Manual [68]. In Figure 82 it is shown the pressure sensor, and how it was assembled.

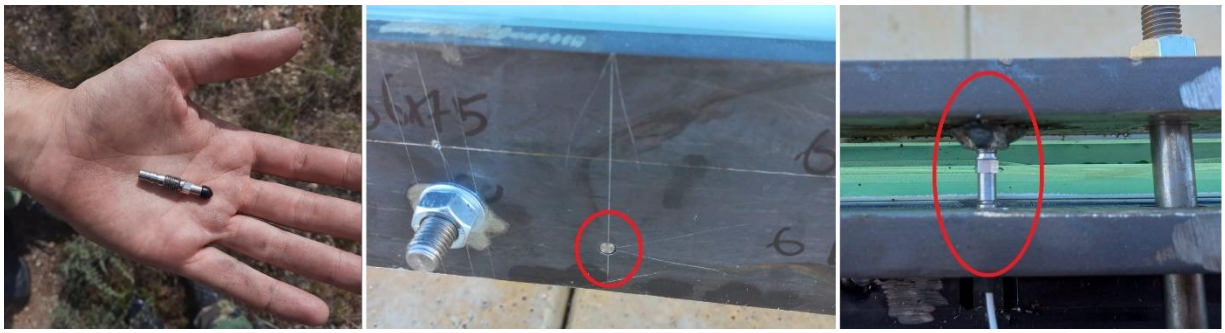

Figure 82 - Reflected Pressure Sensor

For the experimental set-up it was used three reflected pressure sensors in order to have better results. The locations of the reflected pressure sensors are presented in Figure 83.

Figure 83 - Reflected pressure Sensors Location (Red) (Not visible due to sensor size)

6.1.1.3. Accelerometer

The Accelerometer used were ICP® Model 350D02 and the measurement values taken into consideration according to the Operating Manual [69] represented in Table 42:

Table 42 - ICP® Model 350D02 Shock Accelerometer Measurement Values (Adapted from [69])

Performance	Value	Unit
Sensitivity (± 30%)	0.01	mV/m/s^2
Measurement Range	± 490000	m/s^2
Frequency Range (± 1 dB)	4 to 10000	Hz
Temperature Range	-23 to 66	ºC

The accelerometer was glued with a silicon component at the middle point of the glass panel on the opposite side of the explosive, according to the Operating Manual [69] instructions as it is presented

in Figure 78. In Figure 84 it can be seen the location of the accelerometers on the rear face of the laminated glass panel.

Figure 84 - Accelerometer location

6.2. Measured Values

After the data gathering, the values were stored in a computer to later be processed. It was verified that some measurements were wrong, due to graph analysis, which showed a measure error of the sensors in some cases. The analysis conclusion was that, for some values of pressure and acceleration the measurements were clearly wrong in comparison with theoretical values. Also, the comparison between each other was made, since they should match up in some degree, and in some cases, that was not the true.

6.2.1. Incident and Reflect Pressure

The values for incident pressure were taken and plotted into a graphic display to better analyze the data. After, it was made an approximation using the Friedlander equation (called the Friedlander's fit) only for the positive phase duration, since for the negative phase duration, the Friedlander equation is not as accurate as Rigby's equation, mentioned in its work [70]. For the reason mentioned, only the positive values of pressure were considered. The Friedlander's fit consists into making a Friedlander equation that is the closest possible to the experimental results. To do so, after registering the experimental data, it was made an optimization using the Solver analysis tool in Excel, so that the values of the peak overpressures, incident (P_{so}) and reflected (P_r), the values for the positive phase duration, t_0^+, and the values for the decay rate, b, had the least possible error between the experimental data and the Friedlander equation. As it can be seen in Figure 85, the incident pressure sensor measurement for the charge 5kg@9m in blue, and then, the Friedlander equation in red.

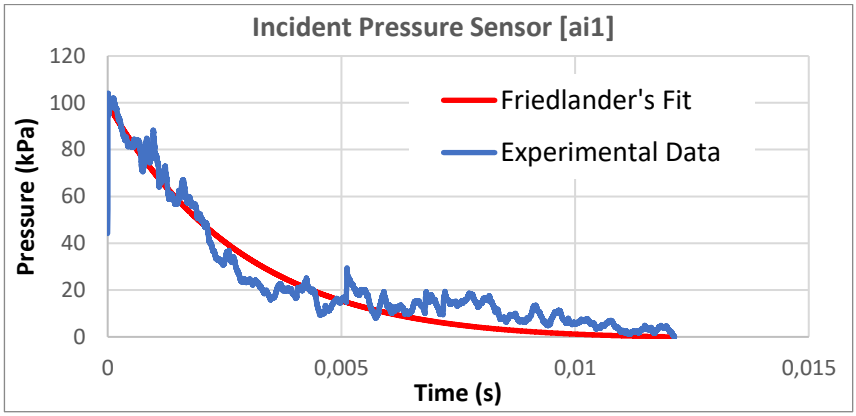

Figure 85 - Experimental data and Friedlander equation for 5kg@9m

After the Friedlander fit and adjustment, the values for P_{so}, t_0^+ and b were taken to calculate the values of impulse and to further comparison with theoretical values. In Table 43 is presented the obtained results for Friedlander's fit values either for the reflected pressure and the incident pressure.

Table 43 - Values for Friedlander's fit equation

Charge	Incident Pressure			Reflected Pressure		
	P_{so}	t_0^+	b	P_r	t_0^+	b
5kg@9m	99.53	12.05	3.20	126.62	7.67	0.86
5kg@7m	155.25	5.24	1.16	267.65	4.62	1.23
5kg@6m	140.37	5.93	2.42	107.23	1.00	0.70
5kg@5m	238.85	4.98	2.22	748.53	3.66	1.25

It was verified that, the results obtained for the overpressure values, either for incident or reflected, were higher than the theoretical values given by Kingery and Bulmash equations [45].

Also, it was verified that the values obtained in the charge of 5kg@6m, were considered to be wrong since the pressure should increase as the scaled distance is decreasing, which in the case of that charge was not true.

In Table 44 and Table 45 can be seen a comparison between the obtained values in the Friedlander fit equation and the theoretical values for pressure and impulse.

Table 44 - Pressure results and comparison

Charge	Z (m/(kg$^{1/3}$))	P_{so} (kPa.ms)	P_{so} Kingery (kPa.ms)	Error (%)	P_r (kPa.ms)	P_r Kingery (kPa.ms)	Error (%)
5kg@9m	5.26	99.53	39.5	151.40	126.62	91.0	39.14
5kg@7m	4.09	155.25	62.1	150.00	267.65	153.9	73.91
5kg@6m	3.51	140.37	83.8	-	107.23	221.3	-
5kg@5m	2.92	238.85	122.1	95.62	748.53	354.2	113.33

As it can be seen in Table 44, the values for peak reflected pressure and peak incident pressure presented (marked in red) for a charge of 5kg@6m are clearly wrong, because these values are lower than a pressure value for a closer scaled distance as explained before. Also, the peak reflected pressure

is lower than the theoretical pressure, which not obeys the pattern verified. The error was not therefore calculated and neither the impulse for those values as it can be seen in Table 45.

Table 45 - Impulse calculations and comparison

Charge	Z (m/(kg$^{1/3}$))	I_s (kPa.ms)	I_s Kingery (kPa.ms)	Error (%)	I_r (kPa.ms)	I_r Kingery (kPa.ms)	Error (%)
5kg@9m	5.26	261.35	96.8	169.99	370.10	202.9	82.41
5kg@7m	4.09	285.93	120.9	136.50	427.86	268.6	59.29
5kg@6m	3.51	-	138.3	-	-	320	-
5kg@5m	2.92	320.50	162.2	97.60	938.24	395.2	137.41

6.2.2. Acceleration

The values obtained for the acceleration values of the panel were plotted also into a graphic display. Then it was tried to obtain the displacement through the second derivation of the equation, but without success. It was verified that, the accelerations in the panels were very different when the dissipator did not break, which means there is a relationship between the acceleration of the panel and the dissipator response. When the dissipator did break, the acceleration of the panel with dissipator was about the same of the panel without dissipator. The measured values for the acceleration are presented in Table 46 along with the behavior of the dissipator.

Table 46 - Acceleration measured results

Charge	Acceleration		Dissipator Behavior
	Without Dissipator	With Dissipator	
5kg@9m	1418.04	842.18	Does not Break
5kg@7m	667.95	541.62	Breaks
5kg@6m	1543.05	1473.37	Breaks
5kg@5m	1730.58	752.01	Does not Break

As it can be seen in Table 46 the acceleration values for the charge of 5kg@7m are not correct, even though it can be verified a relationship between the two values. It was expected that the acceleration for that charge to be higher than 5kg@9m but lower than 5kg@6m. But, also, as it could be seen in the real experiment, since the dissipator broke it was expected that, the difference between the two accelerations were closer as it can be seen in the 5kg@6m experiment.

6.3. Analysis of the Results

6.3.1. Glass Response Analysis with and without dissipation System

Without the dissipator, the acceleration of the glass was very high which can be translated into a bigger displacement, as explained before. The first charge used in the experiment was the 5kg@9m, and according to the FE method, the rigid support glass was expected to fail, but the glass with the energy dissipation system was expected to not fail. The experiment showed a different result. Both of the front glass plies failed, but it was noted that, the break pattern gave indications of projectile impact

causing the glass to fail not to the shock wave but to impact of the projectiles originated from the explosion. As it can be seen in Figure 86, an example of broken glass due to projectile impact.

Figure 86 - Projectile impact on the glass with a charge of 5kg@9m

Even though the glass failed, as it can be seen in Figure 86, the dissipators did not break which meant it stayed in the elastic response spectrum, while on the FE method showed a displacement for the plastic plateau response. To try and solve the problem, it was used a geotextile fabric in the ground to prevent projectiles from hitting the glass. In Figure 88 it can be seen the geotextile solution. After, the charge of 5kg@7m was tested and both glasses were expected to fail completely, which also did not happen. Only the front glass plie failed, and the rear one stayed without damage in both laminated glass panels. The fracture pattern clearly differed from the previous charge as it can be seen in Figure 89.

Figure 87 - Dissipator after charge of 5kg@9m (Red) and front glass plie broken (Green)

Figure 88 - Geotextile solution to prevent impacts on glass

Figure 89 - Glass rupture pattern comparison, on the left failure due to impact, on the right failure due to shock wave damage

Figure 90 - Dissipator response to charge of 5kg@7m

Figure 91 - Glass displacement (Left), Punctual damage of the top dissipators (Middle), Glass displacement and no damage on the side dissipators (Right), Charge: 5kg@5m

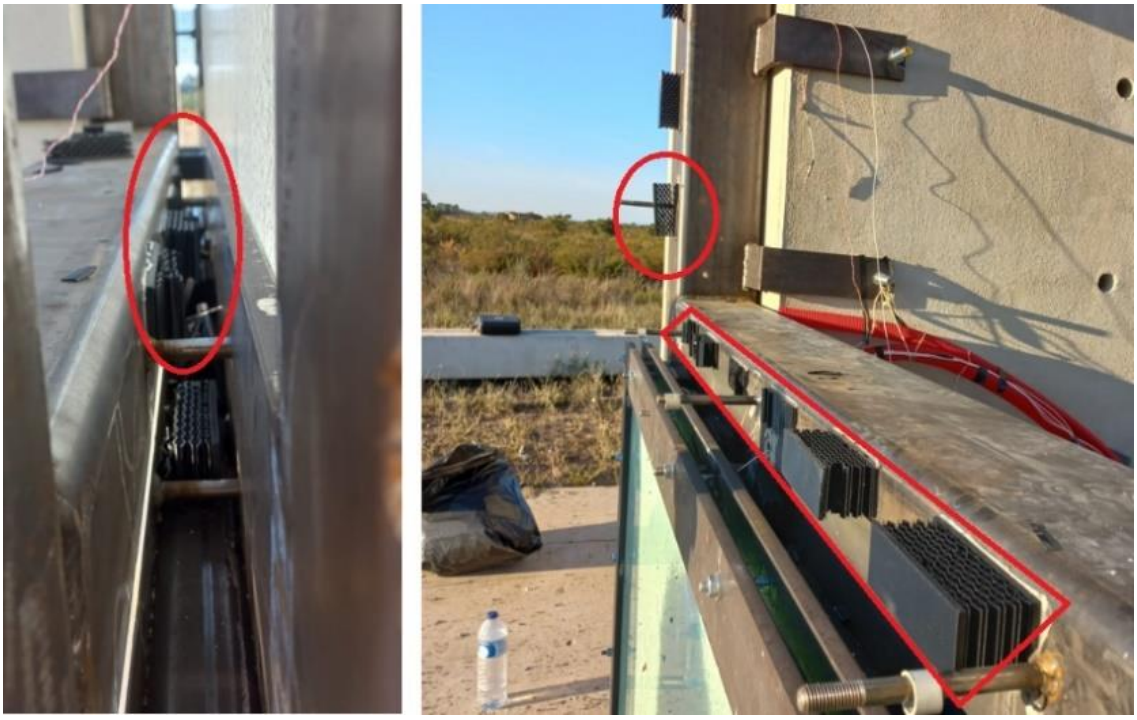

Figure 92 - Dissipator response to a charge of 5kg@6m

With this charge the dissipator was broken, meaning that some energy of the glass panel was dissipated by the system illustrated in Figure 90. To try and make the glass plies fail completely, the charge of 5kg@5m was tried. This charge made both of the glasses fail. But the dissipators did not work, and, as the charge of 5kg@9m, only stayed in the elastic range, which is not optimal for dissipating

energy. Visually, it was verified that the displacement of the rigid support glass was higher than the energy dissipation system glass. In Figure 91 is shown the overall result for the charge of 5kg@5m.

One small conclusion taken from the three experiments made, was that the dissipator had a range of values of scaled distance in which it is useful to dissipate energy and out of that range it is useful to reduce the displacement of the glass panel due to less acceleration compared to the rigid support panel, which can be translated in a certain way to less damage in the glass.

With this charge the dissipator was broken, meaning that some energy of the glass panel was dissipated by the system illustrated in Figure 90. To try and make the glass plies fail completely, the charge of 5kg@5m was tried. This charge made both of the glasses fail. But the dissipators did not work, and, as the charge of 5kg@9m, only stayed in the elastic range, which is not optimal for dissipating energy. Visually, it was verified that the displacement of the rigid support glass was higher than the energy dissipation system glass. In Figure 91 is shown the overall result for the charge of 5kg@5m.

The last experiment consisted in using the charge of 5kg@6m. In this experiment the front glass plie failed in both the laminated glasses, but the dissipators were almost completely broken, which meant that they worked in the plastic response spectrum, the optimal zone for dissipating energy (Figure 92).

To understand the response of the dissipator compared to a rigid support, a graphic was made using the obtained values for the acceleration presented in Table 46 without the values for the charge of 5kg@7m since they were considered wrong. Displayed in Figure 93, is the graphic of the accelerations measured in the dissipators.

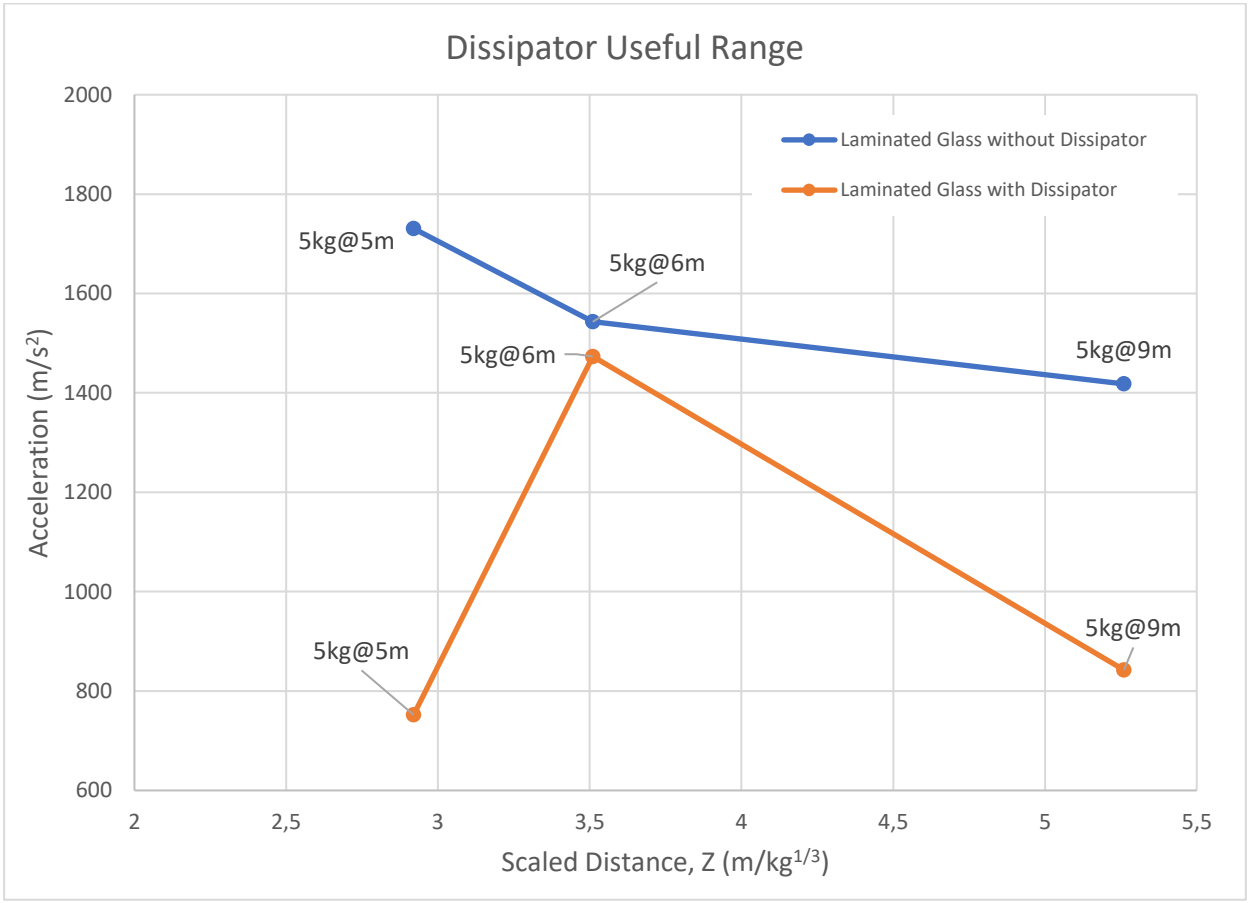

Figure 93 - Acceleration measurement differences

Also, it was calculated how much of a difference it is when the dissipator breaks and when it does not. In Table 47 is shown the differences between the elastic response and rigid support, and then, the difference of plastic response and rigid support.

Table 47 - Response Improvement Difference

Charge	Scaled Distance, Z ($m/(kg^{1/3})$)	Acceleration (m/s^2)		Plateau of Response	Improvement (%)
		Without Dissipator	With Dissipator		
5kg@5m	2.92	1730.58	752.01	Elastic	56.55
5kg@6m	3.51	1543.05	1473.37	Plastic	4.52
5kg@9m	5.26	1418.04	842.18	Elastic	40.61

As it can be seen, the improvements of the response to blast loads are significant but it can be better since experimentally, the damage on the tempered glass plies remained the same between the two laminated glass panels.

Chapter 7. Final Considerations

7.1. Main Conclusions

In the work developed it was verified that the use of an energy dissipating system improved the behavior of a laminated glass panel against a blast load.

It was concluded in the FE model that; the true scale blast tests on glass façades are very hard to reproduce with accuracy, from one side, it was extremely hard to characterize a complex material like the PVB and Tempered Glass for impulse loading in LS-Dyna. From the other, the use of LS-Dyna with the combination of many models, if not carefully validated, can result in the multiplication of the error, giving results very different form the experiments as it could be verified. In the FE model, the charge of 5kg@7m breaks both glass plies, which did not happen in the tests, meaning that the model does not reproduce well the tests.

It was also verified in the FE models that, when the load started to increase, the dissipators started to lose its capacity to dissipate energy, and only worked until a certain value for maximum performance. It was verified the same behavior in the field test but with differences in the glass behavior. In the FE Model when the dissipator started to lose capacity to dissipate energy, the glass already was failing, meaning that the laminated panel could continue to transfer load into the dissipating system. In the field experiments, is thought that, the dissipator only started to go back to the elastic response if the load applied in the glass is enough, so the glass fails completely, losing the capacity to distribute load to the dissipating system.

The conclusion taken for the behavior of the dissipating system is that there is a connection between the stiffness of the glass panel and the stiffness of the dissipator meaning that if the dissipator was less rigid, the range of response would probably been higher, since it allowed for more displacement along with less force applied for that displacement, which means that, for a small load applied in the dissipating system, it would start working sooner, preventing damage on the glass.

Other important conclusion is, in the normal environment, when a detonation occurs, the glass panels are subjected to projectiles, that sometimes can make the glass fail after the shock wave passes, meaning that, if a glazing solution is made for withstanding blast loads, the projectile impact must be considered.

In the field tests the control of the environment is only controllable to a certain degree, and it was verified that the higher pressures measured, and the impact of projectiles on the laminated glass panels were only few examples of how hard it is to control the environment.

In conclusion, it was verified that the laminated glass made of tempered glass plies is highly resistant to blast loads, and a glazing design for blast resistance is possible, however, improvements are required until implementing the dissipating system in practical applications.

7.2. Further Work

To improve the glazing solution façade there is still work a long work ahead. The suggested approach to improve the glass façade response is as follows:

1. Improvement of the Glass FE Models;
2. Scaling the geometry of the dissipator making it bigger so the stiffness to axial force is reduced, facilitating the displacement of the panel;
3. Applying mechanical linear motion guides to the steel panel in order to reduce the friction improving the capacity for displacement and the response of the dissipating system;
4. Applying a different location for the dissipators in order to obtain an even better solution;
5. Combining different scaled geometry dissipators to ensure a wider range of scaled distances for blast load resistance.

It can also be studied different combinations for Glass and PVB, for example:

- The same glass panel but with thicker PVB;
- The same glass panel with the same load twice at a higher distance, to understand that, even if the glass does not break, if it loses load capacity;
- The analysis of the same glass panel, also for the negative phase of the explosion.

References

[1] S. el Hajj, “Writing (from) the Rubble: Reflections on the August 4, 2020 Explosion in Beirut, Lebanon,” *Life Writing*, vol. 18, no. 1, pp. 7–23, 2021, doi: 10.1080/14484528.2020.1830736.

[2] “Ammonium nitrate that exploded in Beirut bought for mining, Mozambican firm says | CNN.” https://edition.cnn.com/2020/08/07/middleeast/beirut-lebanon-ammonium-nitrate-explosion/index.html (accessed Oct. 25, 2022).

[3] “1 American among 135 dead in massive Beirut explosion, officials say - ABC News.” https://abcnews.go.com/International/search-rescue-continues-beirut-wakes-effects-devastating-explosion/story?id=72185153 (accessed Oct. 25, 2022).

[4] W. Laqueur, *A history of terrorism*. 2017. doi: 10.4324/9781315083483.

[5] “NATO - Topic: NATO’s response to hybrid threats.” https://www.nato.int/cps/en/natohq/topics_156338.htm?selectedLocale=en (accessed Oct. 25, 2022).

[6] H. M. M. Fernandes, “As Novas Guerras: O Desafio da Guerra Híbrida,” *Revista de Ciências Militares*, vol. IV, no. 2, pp. 13–40, 2016, [Online]. Available: http://www.iesm.pt/cisdi/index.php/publicacoes/revista-de-ciencias-militares/edicoes.

[7] “Global Terrorism Index 2022,” *Institute for Economics & Peace*, pp. 1–99, 2021. doi: 10.4324/9780203731321.

[8] Ziad. O. Abu-Faraj, “Shattered Glass is Allegedly Blamable for Most of the Victims of Beirut’s Blast,” *LinkedIn Pulse*, no. August, pp. 1–15, 2020.

[9] “World Trade Center Lisboa concluído em junho – Forbes Portugal.” https://www.forbespt.com/world-trade-center-lisboa-concluido-em-junho/ (accessed Oct. 25, 2022).

[10] M. Kozłowski, A. Malewski, V. Akmadžić, and A. Vrdoljak, “Glass in structural applications,” *e-Zbornik: ELECTRONIC COLLECTION OF PAPERS OF THE FACULTY OF CIVIL ENGINEERING*, vol. 9, no. 18, pp. 47–55, 2019, [Online]. Available: https://e-zbornik.gf.sum.ba/en/235-glass-in-structural-applications

[11] P. A. Hooper, R. A. M. Sukhram, B. R. K. Blackman, and J. P. Dear, “On the blast resistance of laminated glass,” *Int J Solids Struct*, vol. 49, no. 6, pp. 899–918, 2012, doi: 10.1016/j.ijsolstr.2011.12.008.

[12] X. Zhang, H. Hao, and Z. Wang, “Experimental study of laminated glass window responses under impulsive and blast loading,” *Int J Impact Eng*, vol. 78, pp. 1–19, 2015, doi: 10.1016/j.ijimpeng.2014.11.020.

[13] F. da C. C. Martins, “Sistemas de Proteção de Fachadas Envidraçadas contra Explosões com Recurso a Tecnologias de Impressão 3D,” Academia Militar, 2021.

[14] M. Coutinho, “Mitigação de impactos com estruturas auxéticas impressas em 3-D”, Universidade de Lisboa, 2019.

[15] B. Hoffman, “Terrorist Targeting: Tactics, Trends, and Potentialities,” *Terrorism and Political Violence*, vol. 5, no. 2, pp. 12–29, 1993, doi: 10.1080/09546559308427205.

[16] J. Pinto, “Comportamento de Estruturas de Aço sob a Ação de Explosões - Conceção de dissipadores de energia,” Academia Militar, 2018.

[17] “Oklahoma City bombing: The day domestic terror shook America - BBC News.” https://www.bbc.com/news/world-us-canada-51735115 (accessed Oct. 25, 2022).

[18] U. S. A. M. C. Headquarters, *Engineering Design Handbook. Explosions in Air. Part 1*, AD/A-00381. Alexandria, Virginia: AMC Pamphlet AMCP 706-181, 1974.

[19] D. Cormie, G. Mays, and P. Smith, *Blast Effects on Buildings*, 3ª. Westminster, London: Institution of Civil Enginners, 2019. doi: 10.1680/beob.61477.

[20] P. Smith and J. Hetherington, *Blast and Ballistic Loading of Structures*, First Edit. Routledge, 2011. [Online]. Available: https://medium.com/@arifwicaksanaa/pengertian-use-case-a7e576e1b6bf

[21] H. Draganić and V. Sigmund, “Blast Loading on Structures,” *Technical Gazette*, vol. 19, pp. 643–652, 2012, doi: 10.1061/jsdeag.0000297.

[22] E. Yandzio and M. Gough, *Protection of Buildings Against Explosions.* Teh Steel Construction Institute, 1999.

[23] U.S. Department of Defense, “Unified Facilities Criteria (UFC) Structures To Resist the Effects of Accidental Explosions,” 2008.

[24] Gilbert F. Kinney and Kenneth J. Graham, *Explosive Shock in Air*, 2nd ed. New York: The Macmillan Company, 1985. [Online]. Available: https://mail.126.com/js6/main.jsp?sid=JBJVZRPPOKiuccygTRPPBHpZopcnIFff&df=mail126_letter%0Apapers3://publication/uuid/AAB230B2-1181-426C-AE51-1F62F1F0F6C1

[25] W. E. Baker, P. A. Cox, P. Westine, J. Kulesz, and R. A. Strehlow, “Explosion Hazards and Evaluation,” vol. 5, 1983, doi: 10.1016/0379-7112(84)90044-4.

[26] T.Ngo, P. Mendis, A. Gupta, and J. Ramsay, “Blast Loading and Blast Effects on Structures - An Overview,” *Electron. J. Struct. Eng*, pp. 76–91, 2007, doi: 10.1016/j.proeng.2017.09.432.

[27] D. O. Dusenberry, *Handbook for Blast-Resistant Design of Buildings*. John Wiley & Sons, Inc., 2010.

[28] Vasilis. Karlos and George. Solomos, *Calculation of Blast Loads for Application to Structural Components*. 2013. doi: 10.2788/61866.

[29] M. Patterson, *Structural Glass Facade and Enclosures*, vol. 53, no. 9. 2016.

[30] M. Haldimann, A. Luible, and M. Overend, *Structural use of Glass*. 2008. doi: 10.2749/sed010.

[31] C O’Regan, “Structural use of glass in buildings (Second edition),” no. 2nd Edition. 2014.

[32] J. Wurm, *Glass Structures: Design and Construction of Self-Supporting Skins*. Birkhauser, 2007.

[33] C. Schittich, G. Staib, D. Balkow, M. Schuler, and W. Sobek, *Glass Construction Manual*. Birkhäuser - Publishers for Architecture, 1999.

[34] “Industrial Glass - Properties of glass | Britannica.” https://www.britannica.com/topic/glass-properties-composition-and-industrial-production-234890/Properties-of-glass (accessed Oct. 25, 2022).

[35] C. Morison, “The Resistance Of Laminated Glass To Blast Pressure Loading And The Coefficients For Single Degree Of Freedom Analysis Of Laminated Glass,” Cranfields University, 2007.

[36] X. Zhang, H. Hao, Y. Shi, and J. Cui, “The mechanical properties of Polyvinyl Butyral (PVB) at high strain rates,” *Constr Build Mater*, vol. 93, pp. 404–415, 2015, doi: 10.1016/j.conbuildmat.2015.04.057.

[37] J. Wei and L. R. Dharani, “Fracture mechanics of laminated glass subjected to blast loading,” *Theoretical and Applied Fracture Mechanics*, vol. 44, no. 2, pp. 157–167, 2005, doi: 10.1016/j.tafmec.2005.06.004.

[38] A. Zemanová, P. Hála, P. Konrád, T. Janda, and R. Hlůžek, “The influence of interlayer properties on the response of laminated glass to low-velocity hard-object impact,” *Int J Impact Eng*, vol. 159, no. October 2021, 2022, doi: 10.1016/j.ijimpeng.2021.104036.

[39] R. J. L. Rita, “Comportamento de Fachadas Envidraçadas sob a Ação de Explosões,” 2020.

[40] Y. Liu and X. Zhang, “Metamaterials: A new frontier of science and technology,” *Chem Soc Rev*, vol. 40, no. 5, pp. 2494–2507, 2011, doi: 10.1039/c0cs00184h.

[41] T. Peng, “Analysis of Energy Utilization in 3D Printing Processes,” *Procedia CIRP*, vol. 40, pp. 62–67, 2016, doi: 10.1016/j.procir.2016.01.055.

[42] “What is FDM (fused deposition modeling) 3D printing? | Hubs.” https://www.hubs.com/knowledge-base/what-is-fdm-3d-printing/ (accessed Oct. 27, 2022).

[43] H. M. B. Rebelo, “Development and study of a high performance protective solution against blast loads,” 2020.

[44] CEN European Committee for Standardization, *EN 1993-1-1 Eurocode 3: Design of steel structures - Part 1-1: General rules and rules for buildings*. 2005.

[45] C. N. Kingery, “Air Blast Parameters from TNT Spherical Air Burst and Hemispherical Surface Burst,” 1984.

[46] J. M. Biggs, *Introduction to Structural Dynamics*. McGraw-Hill, 1964. doi: 10.1017/CBO9780511618086.

[47] Wessex Institute of Technology, “Short Course on Blast Effects and Analysis,” 2020, no. October.

[48] CEN European Committee for Standardization, *EN 1993-1-8 Eurocode 3: Design of steel structures - Part 1-8: Design for joints*. 2005.

[49] P. M. Mendes and J. O. Pedro, *Dimensionamento de estruturas de edifícios e estruturas especiais*. IST Press, 2020.

[50] CEN European Committee for Standardization, *EN 1991-1-4 Eurocode 1: Actions on structures - Part 1-4: General actions - Wind actions*. 2010.

[51] CEN European Committee for Standardization, *prEN 13474 Glass in building - Determination of the strength of glass panes*. Brussels, Belgium, 2009.

[52] R. Bares, *Tablas Para El Calculo De Placas Y Vigas Pared*. Barceloina: Editorial Gustavo Gili, S.A., 1970.

[53] CEN European Committee for Standardization, *EN1990 Eurocode - Basis of structural design*. 2002.

[54] Livermore Software Technology Corporation (LSTC), *LS-Dyna Theory Manual*. 2019.

[55] G. Dhatt, G. Touzot, and E. Lefrançois, *Finite Element Method*. John Wiley & Sons Inc., 2012.

[56] Z. S. Tabatabaei and J. S. Volz, “A Comparison between Three Different Blast Methods in LS-DYNA®: LBE, MM-ALE, Coupling of LBE and MM-ALE,” *12th International LS-DYNA Users Conference*, no. 3, pp. 1–10, 2012.

[57] T. P. Slavik, “A coupling of empirical explosive blast loads to ALE air domains in LS-DYNA®,” *IOP Conf Ser Mater Sci Eng*, vol. 10, no. 1, 2014, doi: 10.1088/1757-899X/10/1/012146.

[58] S. K. Hashemia and M. A. Bradford, “Numerical simulation of free-air explosion using LS-DYNA,” *Applied Mechanics and Materials*, vol. 553, no. May, pp. 780–785, 2014, doi: 10.4028/www.scientific.net/AMM.553.780.

[59] Livermore Software Technology Corporation (LSTC), *Keyword User’s Manual Volume I*, vol. I. 2019.

[60] L. Běhálek, P. Lenfeld, M. Seidl, J. Bobek, and A. Ausperger, “Friction properties of composites with natural fibres, synthetic and biodegradable polymer matrix,” in *NANOCON 2012 - 2nd International Conference, Conference Proceedings*, 2012.

[61] A. Jaware, S. Chandratre, M. Perez, and J. Narule, “An Advanced Methodology for Windscreen Modelling in LS-Dyna,” *International Journal of Mechanical Engineering and Technology*, vol. 10, no. 12, pp. 380–389, 2019.

[62] B. Feng, “Hybrid Laminated Glass: Material Characterisation and CAE Modelling,” pp. 1–4, 2017.

[63] R. Böhm, A. Haufe, and A. Erhart, “LS-DYNA Forum 2016 - A Novel Approach to Model Laminated Glass,” pp. 1–23, 2016.

[64] M. Eslami, K. M. Mosalam, V. Kodur, S. Marjanishvili, B. Katz, and H. N. Mahmoud, “Multi-performance blast pressure-duration curves of laminated glass panes,” *International Journal of Protective Structures*, vol. 12, no. 2, pp. 226–244, 2021, doi: 10.1177/2041419620968838.

[65] M. Larcher, G. Solomos, F. Casadei, and N. Gebbeken, “Experimental and numerical investigations of laminated glass subjected to blast loading,” *Int J Impact Eng*, vol. 39, no. 1, pp. 42–50, 2012, doi: 10.1016/j.ijimpeng.2011.09.006.

[66] United States Enviromental Protection Agency, “Technical Fact Sheet – 2,4,6-Trinitrotoluene (TNT),” *United States Environmental Protection Agency*, no. January, pp. 1–8, 2014, [Online]. Available: http://www2.epa.gov/sites/production/files/2014-03/documents/ffrrofactsheet_contaminant_tnt_january2014_final.pdf

[67] PCB Piezotronics, “Model 137B24B ICP® Pressure Sensor Installation and Operating Manual.” p. 9.

[68] PCB Piezotronics, “Model 113B24 ICP® Pressure Sensor Installation and Operating Manual.” p. 11.

[69] PCB Piezotronics, “Model 350D02 SHEAR ICP® Shock Accelerometer Installation and Operating Manual.” p. 16.

[70] S. D. Rigby, Sam E., Tyas, Andrew, Bennett, Terry, Clarke, Sam D., Fay, “The Negative Phase of the Blast Load,” *International Journal of Protective Structures*, vol. 5, no. 1, pp. 1–20, 2014.

Attachment A

Final Set Up Second Liutenant Machado
(Scale 1/50)

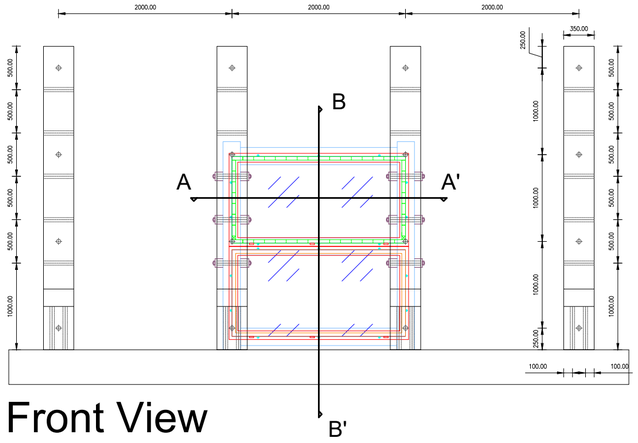

Front View

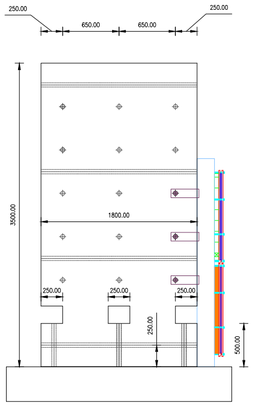

Left Side View

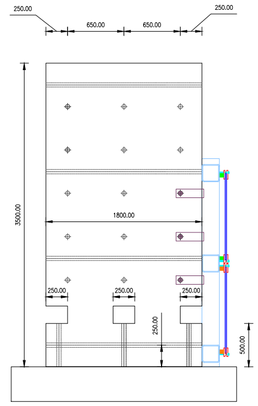

Left Side View
Cut BB'

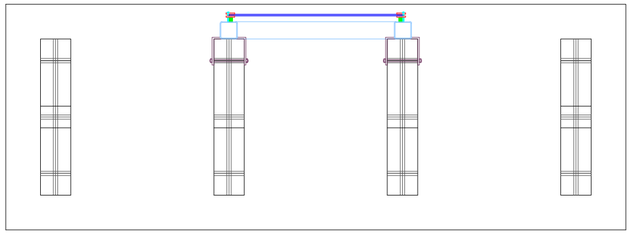

Top View

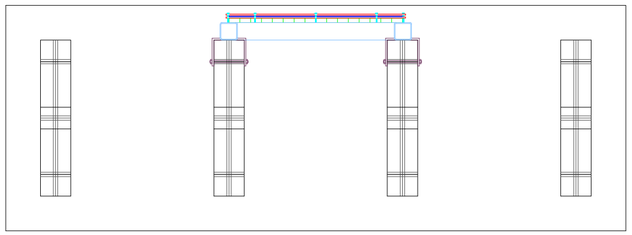

Top View Cut AA'

TÉCNICO LISBOA	Attachment A – Final Set–Up Drawing
	Date – October 2022
	Scale – 1:50
ACADEMIA MILITAR MILITARY ACADEMY	Author – José Machado
	Page number – 1

Details

Metallic Profile Detail (Scale 1/20)

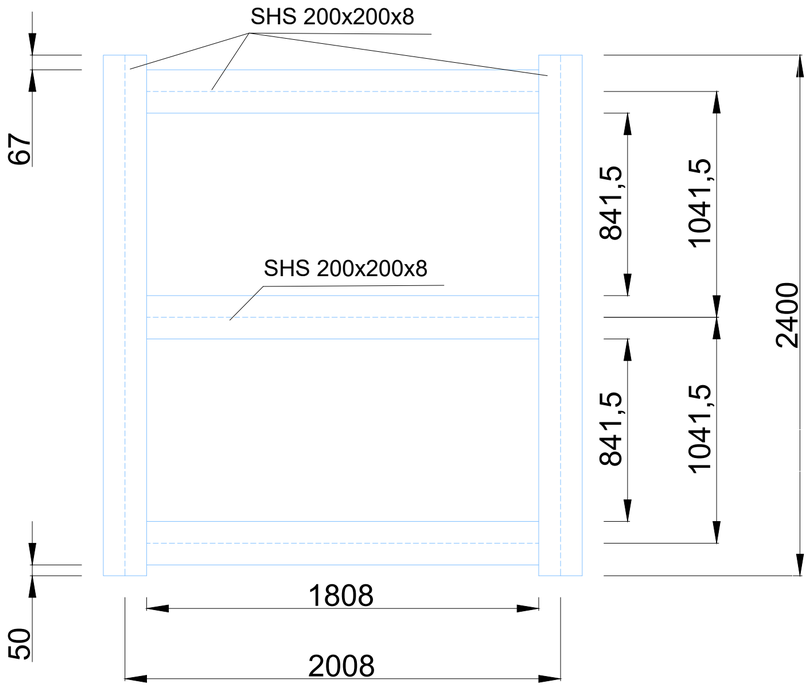

Fixing Plates Detail (Scale 1/5)

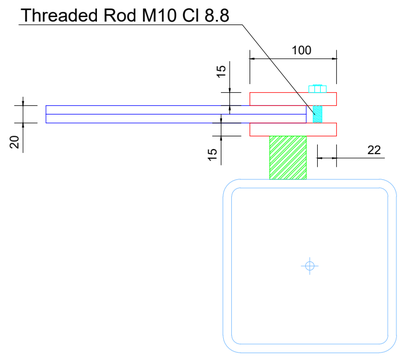

Profile SHS 200x200x8 Detail (Scale 1/5)

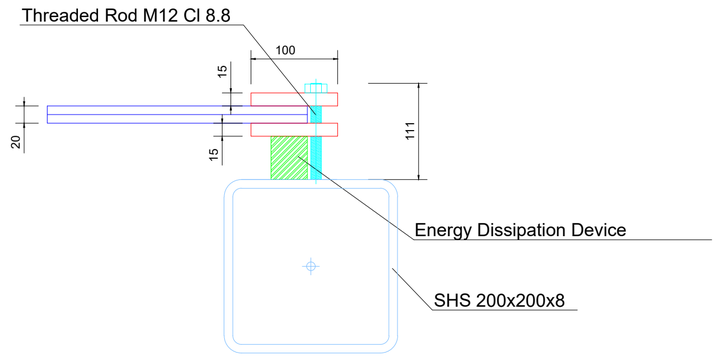

Profile SHS 200x200x8 Detail (Scale 1/5)

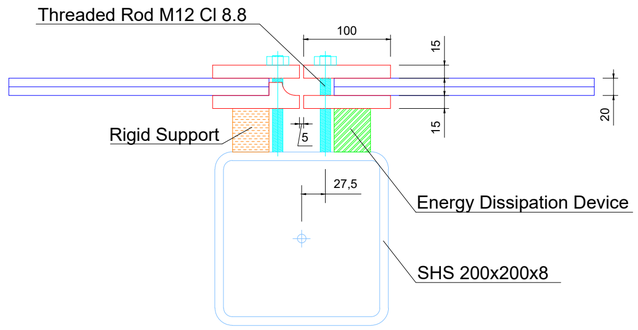

Fixing Plate Detail (Scale 1/2)

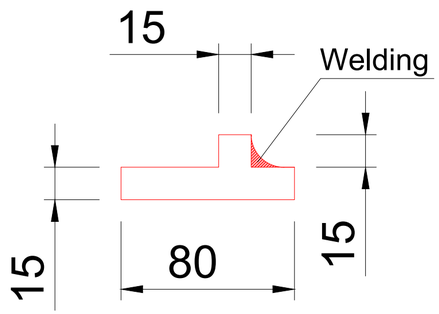

TÉCNICO LISBOA	Attachment A – Final Set-Up (Details)
	Date – October 2022
	Scale – Variable
ACADEMIA MILITAR MILITARY ACADEMY	Author – José Machado
	Page number – 2

Fixing Plates Detail (Scale 1/10)

Bottom Fixing Plate

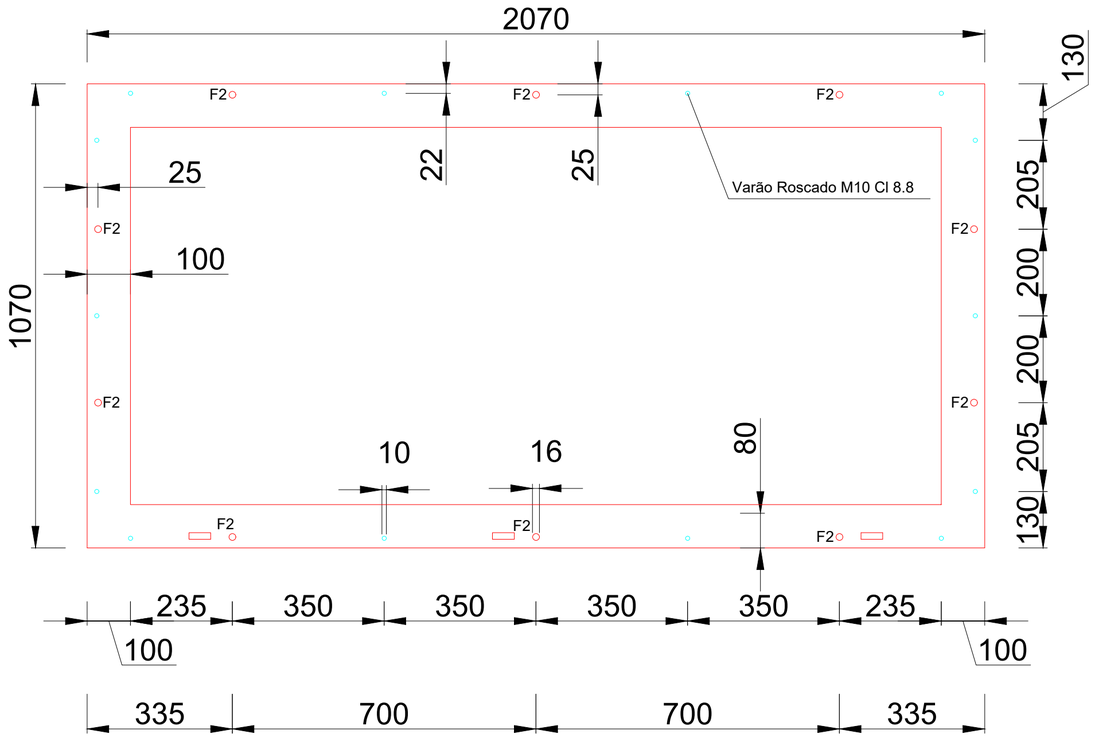

Top Fixing Plate

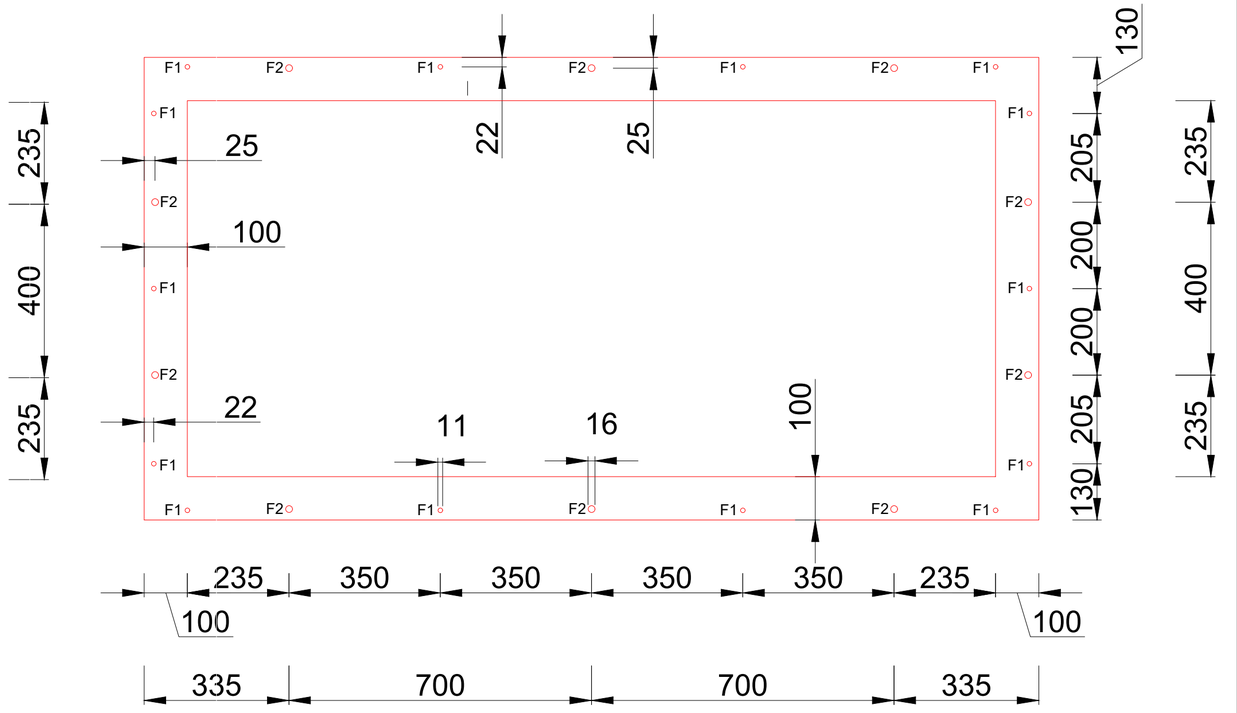

Glass Support Detail

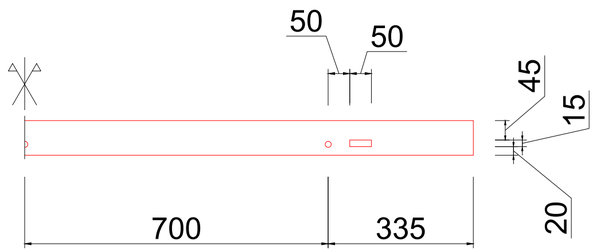

Fixing Plate Detail (Scale 1/2)

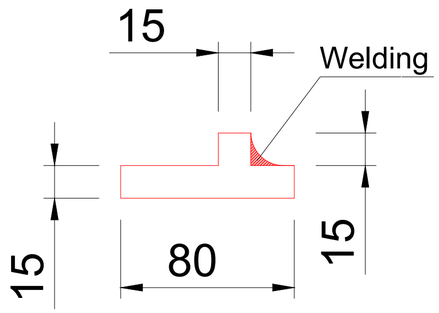

TÉCNICO LISBOA	Attachment A – Final Set-Up (Details)
	Date – October 2022
	Scale – Variable
ACADEMIA MILITAR MILITARY ACADEMY	Author – José Machado
	Page number – 3

SHS Profile - Wall Connection Detail
(Scale 1/10)

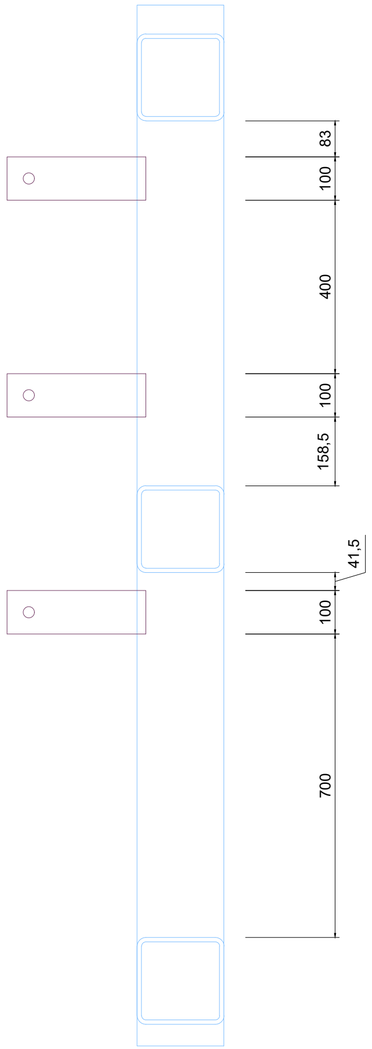

SHS Profile - Wall Connection Detail
(Scale 1/5)

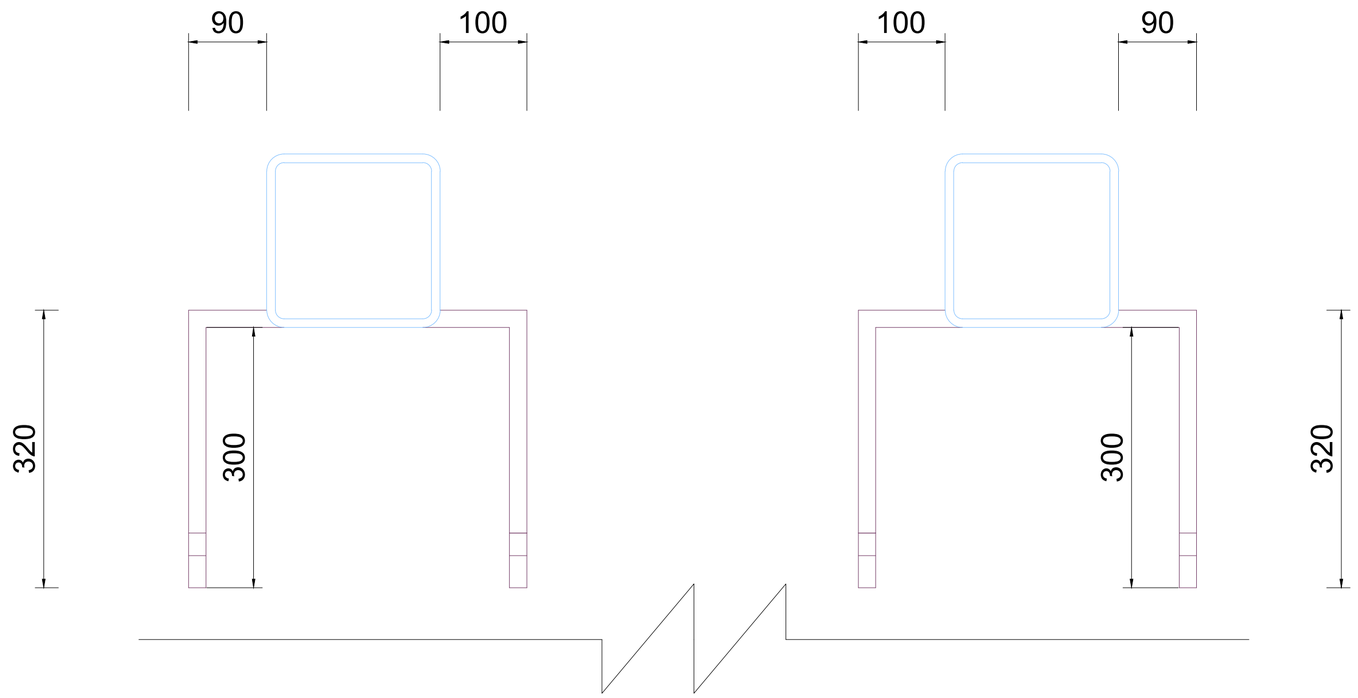

Wall Connection Plate Detail
(Scale1/5)

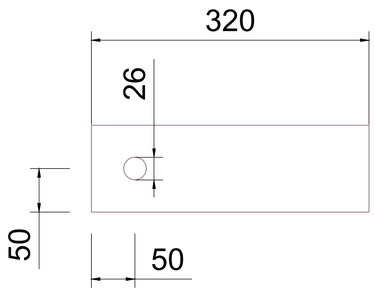

TÉCNICO LISBOA	Attachment A – Final Set–Up (Details)
	Date – October 2022
	Scale – Variable
ACADEMIA MILITAR MILITARY ACADEMY	Author – José Machado
	Page number – 4

Distance Details Threaded Rods (Scale 1/10)

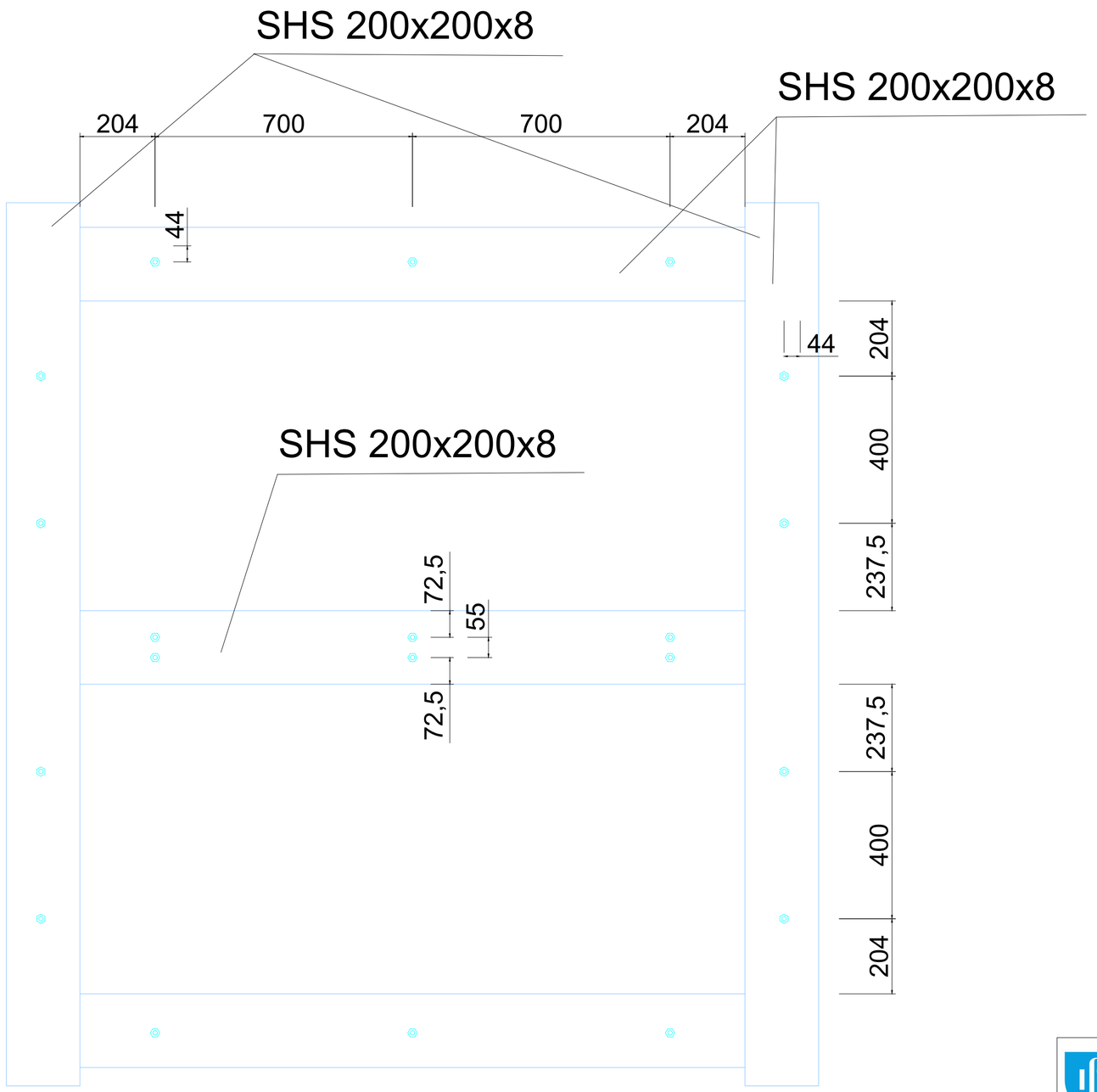

TÉCNICO LISBOA	Attachment A – Final Set-Up (Deteails)
	Date – October 2022
	Scale – 1:10
ACADEMIA MILITAR MILITARY ACADEMY	Author – José Machado
	Page number – 5

Attachment B

Experimental Set-Up

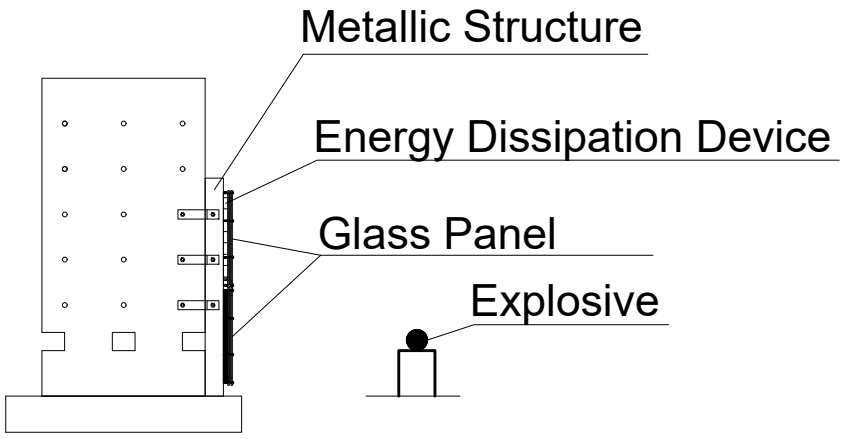

Left Side View

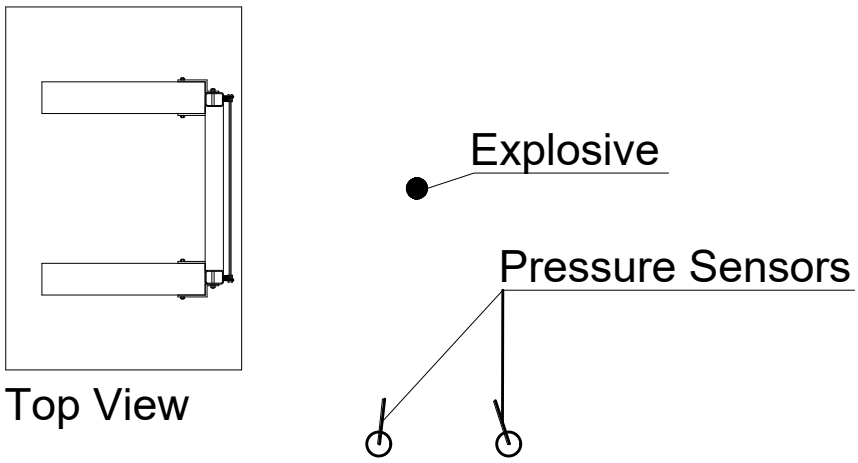

Top View

TÉCNICO LISBOA

ACADEMIA MILITAR
MILITARY ACADEMY

Attachment B – Experimental Set-Up
Date – October 2022
Scale – Without Scale (Sketch Draw)
Author – José Machado
Page number – B